

**On the Use of MODIS for Lake and Land Surface Temperature  
Investigations in the Regions of Great Bear Lake  
and Great Slave Lake, N.W.T.**

by

Homa Kheyrollah Pour

A thesis  
presented to the University of Waterloo  
in fulfillment of the  
thesis requirement for the degree of  
Master of Science  
in  
Geography

Waterloo, Ontario, Canada, 2011

© Homa Kheyrollah Pour 2011

## **AUTHOR'S DECLARATION**

I hereby declare that I am the sole author of this thesis. This is a true copy of the thesis, including any required final revisions, as accepted by my examiners.

I understand that my thesis may be made electronically available to the public.

## Abstract

Lake surface temperature ( $LST_{\text{lake}}$ ) can be obtained and studied in different ways: using *in situ* measurements, satellite imagery and modeling. Collecting spatially representative *in situ* data over lakes, especially for large and deep ones, is a real challenge. Satellite data products provide the opportunity to collect continuous data over very large geographic areas even in remote regions. Numerical modeling is also an approach to study the response and the role of lakes in the climate system. Satellite instruments provide spatial information unlike *in situ* measurements and one-dimensional (1-D) lake models that give vertical information at a single point or a few points in lakes. The advantage of remote sensing also applies to land where temperature measurements are usually taken at meteorological stations whose network is extremely sparse in northern regions. This thesis therefore examined the value of land/lake surface (skin) temperature ( $LST_{\text{land/lake}}$ ) measurements from satellites as a complement to *in situ* point measurements and numerical modeling.

The thesis is organized into two parts. The first part tested, two 1-D numerical models against *in situ* and satellite-derived LST measurements.  $LST_{\text{lake}}$  and ice phenology were simulated for various points at different depths on Great Slave Lake (GSL) and Great Bear Lake (GBL), two large lakes located in the Mackenzie River Basin in Canada's Northwest Territories, using the 1-D Freshwater Lake model (FLake) and the Canadian Lake Ice Model (CLIMo) over the 2002-2010 period. Input data from three weather stations (Yellowknife, Hay River and Deline) were used for model simulations.  $LST_{\text{lake}}$  model results are compared to those derived from the Moderate Resolution Imaging Spectroradiometer (MODIS) aboard the Earth Observing System Terra and Aqua satellite platforms. The main goal was to examine the performance of the FLake and CLIMo models in simulating  $LST_{\text{lake}}$  and ice-cover under different conditions against satellite data products. Both models reveal a good agreement with daily average MODIS  $LST_{\text{lake}}$  from GSL and GBL on an annual basis. CLIMo showed a generally better performance than FLake for both lakes, particularly during the ice-cover season.

Secondly, MODIS-derived lake and land surface temperature ( $LST_{\text{land/lake}}$ ) products are used to analyze land and lake surface temperature patterns during the open-water and snow/ice growth seasons for the same period of time in the regions of both GBL and GSL. Land and lake temperatures from MODIS were compared with near-surface air temperature measurements obtained from nearby weather stations and with *in situ* temperature moorings in GBL. Results show a good agreement between satellite and *in situ* observations. MODIS data were found to be very useful for investigating both the spatial and temporal (seasonal) evolution of  $LST_{\text{land/lake}}$  over lakes and land, and for improving our understanding of thermodynamic processes (heat gains and heat losses) of the lake/land systems. Among other findings, the MODIS satellite imagery showed that the surface temperature of lakes is colder in comparison to the surrounding land from April-August and warmer from September until spring thaw.

## Acknowledgements

This research was supported by European Space Agency (ESA-ESRIN) Contract No. 4000101296/10/I-LG (Support to Science Element, North Hydrology Project) and a Discovery Grant from the Natural Sciences and Engineering Research Council of Canada (NSERC) to C. Duguay.

In this project I got help from an enormous number of people who supported and encouraged me in making this work a success. I would like to express my heartfelt thanks to:

- Prof. *Claude Duguay*, who gave me the opportunity to work on a very interesting project in his group. I appreciate his scientific ideas which set this work on a firm basis. I would like to extend my heartfelt thanks for his continual support, his patience during times of struggle and frustration even in last minute work and his ability to ease the inherent stress of writing a thesis. He also created a unique and enjoyable working environment as I could not have asked for better supervisor. Thank you so much *Claude*.
- Prof. *Richard Kelly*, who always made himself available when necessary. His support and guidance throughout my graduate education is appreciated. He provided a friendly environment for discussion and interpretation through this research. Thanks *Richard*.
- Dr. *Ram Yerubandi* and Prof. *Roland Hall* who agreed to act as committee members on this thesis. Thanks.
- My colleagues in the department of Geography and Environmental Managements for their support and friendly atmosphere. And special thanks to *Kyung-Kuk (Kevin)Kang* for providing data at any time and fruitful discussions, *Laura Brown* to be a master of the CLIMo model and her time to run the model at any time, *Sonia Hachem* for her friendly support, guidance and time on answering my continuous questions. Thanks friends.
- *Fereidoun*, my wonderful husband, for his unflagging love and support throughout my life in the past years. He spares no effort to provide the best possible environment for me to study and his support during the stressful times. His advice throughout my education made my work much easier. *None of this could happen without you!*
- *Hooman*, my sweetie pie, for bringing exceptional joy and happiness to my life and the motivation of study. I love you *Hooman*.
- And last but not least, my *family* for their encouragements from so far away. Thank you.

## Table of Contents

<b>AUTHOR'S DECLARATION</b> .....	<b>ii</b>
<b>Abstract</b> .....	<b>iii</b>
<b>Acknowledgements</b> .....	<b>v</b>
<b>Table of Contents</b> .....	<b>vi</b>
<b>List of Figures</b> .....	<b>viii</b>
<b>List of Tables</b> .....	<b>xi</b>
<b>List of Abbreviations</b> .....	<b>xii</b>
<b>Chapter 1 General Introduction</b> .....	<b>1</b>
1.1 Introduction.....	1
1.2 Research Objectives.....	4
1.3 Thesis Overview .....	5
<b>Chapter 2 Review of Lake Thermodynamics and Research Methods</b> .....	<b>6</b>
2.1 Lake Thermodynamics.....	6
2.2 Lake Ice and Snow .....	7
2.3 Thermal Remote Sensing .....	10
2.3.1 Thermal Radiations .....	10
2.3.2 Moderate Resolution Imaging Spectrometer (MODIS) .....	11
2.4 Modeling .....	13
<b>Chapter 3 Simulation of surface temperature and ice-cover with 1-D models: A comparison with MODIS satellite data and <i>in situ</i> measurements</b> .....	<b>18</b>
Overview.....	18
3.1 Introduction.....	19
3.2 Study Area .....	21
3.3 Data and Methods .....	22
3.3.1 Moderate Resolution Imaging Spectroradiometer (MODIS).....	22
3.3.2 Canadian Ice Database (CID) .....	23
3.3.3 Canadian Lake Ice Model (CLIMo).....	24
3.3.4 Fresh Water Lake Model (FLake).....	25
3.4 Results and discussion .....	26

3.4.1 Lake Surface Temperature .....	27
3.4.2 Ice thickness and phenology (Back Bay, Great Slave Lake).....	37
3.5 Summary and Conclusion.....	40
<b>Chapter 4 Analysis of lake and land surface temperature patterns during the open-water and snow/ice growth seasons in the Great Bear and Great Slave Lake regions, Canada, from MODIS (2002-2010) .....</b>	<b>42</b>
Overview .....	42
4.1 Introduction .....	43
4.2 Data and Methods.....	45
4.2.1 Comparison of MODIS LST <sub>land</sub> with Near Surface Air Temperature.....	46
4.2.2 Comparison of MODIS LST <sub>lake</sub> with <i>In situ</i> Lake Temperature .....	46
4.2.3 Lake Depth versus Lake Surface Temperature.....	47
4.2.4 Lake and Land Surface Temperature Variations in the GSL Region.....	47
4.3 Result and Discussion.....	48
4.3.1 Comparison of MODIS LST <sub>land</sub> with Near Surface Air Temperature.....	48
4.3.2 Comparison of MODIS LST <sub>lake</sub> with In situ Lake Temperature .....	51
4.3.3 Lake Depth versus Lake Surface Temperature.....	53
4.3.4 Lake and Land Surface Temperature Variations in the GSL region .....	58
4.4 Summary and Conclusion.....	62
Acknowledgements .....	63
<b>Chapter 5 General Conclusion .....</b>	<b>64</b>
5.1 Summary .....	64
5.2 Limitations.....	66
5.3 Future Work .....	67
<b>References.....</b>	<b>69</b>
<b>Appendix I .....</b>	<b>75</b>
<b>Appendix II .....</b>	<b>76</b>
<b>Appendix III.....</b>	<b>77</b>
<b>Appendix IV.....</b>	<b>78</b>

## List of Figures

<b>Figure 2-1:</b> Schematic representation of typical dynamic lake behavior (Redrawn after Bluteau, 2006).....	7
<b>Figure 2-2:</b> The formation processes of congelation ice and snow ice (Redrawn after Alaska Lake Ice and Snow Observation Network).....	8
<b>Figure 2-3:</b> Cross sections of the snow cover on a lake (Imikpuk lake) in Alaska and on the nearby tundra. Light gray indicates snow; dark gray indicates ice or tundra (Source: Sturm and Liston, 2003). .....	10
<b>Figure 2-4:</b> Schematic representation of the lake ice model during winter. The layers with dashed lines represent ice and the gray layer above the ice is snow. The solid grey line indicates the temperature profile, which is computed using a finite-difference representation of the heat conservation Equation (2.3). The arrows along the top of the surface indicate the components of the surface heat budget included in the model (Source: Duguay <i>et al</i> , 2003).	15
<b>Figure 2-5:</b> Schematic representation of the temperature profile in the mixed layer, thermocline, and active layer of bottom sediments. The evolving temperature profile is specified by several time-dependent quantities (Source: Mironov, 2008). .....	16
<b>Figure 3-1:</b> Maps showing the location of GSL and GBL within the Mackenzie River Basin and meteorological stations.....	22
<b>Figure 3-2:</b> Comparison of modeled $LST_{lake}$ from CLIMo and FLake with MODIS-derived $LST_{lake}$ data during full year for 2002-2010 (a) Yellowknife (Back Bay), (b) Hay River, (c) GSL (Main Basin), (d) GBL (Deline).....	28
<b>Figure 3-3:</b> Comparison of modeled $LST_{lake}$ from CLIMo and FLake with MODIS-derived $LST_{lake}$ data during full year for 2002-2010 (a,b) Yellowknife (Back Bay) (c,d) Hay River, (e,f) GSL (Main Basin), (g,h) GBL (Deline).....	29
<b>Figure 3-4:</b> Comparison of modeled $LST_{lake}$ from CLIMo and FLake with MODIS-derived $LST_{lake}$ data during open-water season for 2002-2010 (a) Yellowknife (Back Bay), (b) Hay River, (c) GSL (Main Basin), (d) GBL (Deline). .....	32

<b>Figure 3-5:</b> Comparison of modeled $LST_{lake}$ from CLIMo and FLake with MODIS-derived $LST_{lake}$ data during open-water season for 2002-2010 (a,b) Yellowknife (Back Bay) (c,d) Hay River, (e,f) GSL (Main Basin), (g,h) GBL (Deline). .....	33
<b>Figure 3-6:</b> Comparison of modeled $LST_{lake}$ from CLIMo and FLake with MODIS-derived $LST_{lake}$ data during ice-cover season for 2002-2010 (a) Yellowknife (Back Bay), (b) Hay River, (c) GSL (Main Basin), (d) GBL (Deline). .....	35
<b>Figure 3-7:</b> Comparison of modeled $LST_{lake}$ from CLIMo and FLake with MODIS-derived $LST_{lake}$ data during ice-cover season for 2002-2010 (a,b) Yellowknife (Back Bay) (c,d) Hay River, (e,f) GSL (Main Basin), (g,h) GBL (Deline). .....	36
<b>Figure 3-8:</b> Comparison of observed (CID) and simulated (CLIMo and FLake) Ice thickness for Back Bay (1961-2008). .....	38
<b>Figure 3-9:</b> Comparison of observed (CID) and simulated Ice thickness for Back Bay (a) CLIMo, (b) FLake (1961-2008). .....	38
<b>Figure 3-10:</b> Comparison of observed (CID) and simulated (CLIMo and FLake) freeze-up and break-up dates for Back Bay (1961-1996). .....	39
<b>Figure 3-11:</b> Comparison of observed (CID) and simulated (CLIMo and FLake) (a,b) break-up, (c,d) freeze-up dates for Back Bay (1961-1996). .....	39
<b>Figure 4-1:</b> Bathymetry of GSL (Source: Schertzer <i>et al.</i> , 2000) and GBL (Source: Johnson 1994). Depth contours are in metre.....	44
<b>Figure 4-2:</b> Time series comparison (a) and the relation (b) between $LST_{land}$ -derived from MODIS and the air temperature at 2 m above the ground surface for Yellowknife weather station. ....	49
<b>Figure 4-3:</b> Time series comparison (a) and the relation (b) between $LST_{land}$ -derived from MODIS and the air temperature at 2 m above the ground surface for Hay River weather station. ....	50
<b>Figure 4-4:</b> Time series comparison (a) and the relation (b) between $LST_{land}$ -derived from MODIS and the air temperature at 2 m above the ground surface for Deline weather station. ....	51

**Figure 4-5:** Comparison of hourly MODIS  $LST_{lake}$  with hourly temperature mooring data over GBL on a) station 1, b) station 2, and c) station 3 (mid-July to September 2008). ..... 52

**Figure 4-6:** MODIS Land/Lake surface temperature in the Great Bear and Great Slave Lake region (January–December 2003). ..... 54

**Figure 4-7:** Monthly  $LST_{lake}$  average versus depth in GSL for July 2002-2010. .... 55

**Figure 4-8:** MODIS Land/Lake surface temperature in the Great Bear and Great Slave Lake region (July 2002-2010). ..... 56

**Figure 4-9:** Monthly  $LST_{lake}$  average versus depth in GSL for January 2002-2010. .... 57

**Figure 4-10:** MODIS Land/Lake surface temperature in the Great Bear and Great Slave Lake region (January 2002-2010). ..... 59

**Figure 4-11:** Monthly averaged  $LST_{land/lake}$  in GSL and Duncan (March-October, 2002-2010). ..... 60

**Figure 4-12:** Monthly averaged  $LST_{land/lake}$  in GSL and Duncan (July- May 2002-2010). .... 61

**Figure 4-13:**  $LST_{land/lake}$  differences ( $\Delta T = T_{land} - T_{lake}$ ) in GSL and Duncan Lake (January–December 2002-2010). ..... 61

### List of Tables

<b>Table 2-1:</b> MODIS data product inputs to the MODIS LST algorithm .....	13
<b>Table 3-1:</b> Physical characteristics of GSL and GBL: $Z_{ML}$ is the mixed layer depth, $Z_{Max}$ is the maximum depth, $Z_{Mean}$ is the average depth, V is lake volume and A is lake area. ....	21
<b>Table 3-2:</b> Comparison of observed and simulated lake surface temperature for Yellowknife (Back Bay), Hay River, GSL (Main Basin), and GBL (Deline) (2002-2010).....	27

## **List of Abbreviations**

AATSR	Advanced Along-Track Scanning Radiometer
AVHRR	Advanced Very High Resolution Radiometer
CLIMo	Canadian Lake Ice Model
ELCOM	Estuary and Lake COmputer Model
EOS	Earth Observation System
ESA	European Space Agency
FLake	Fresh Water Lake model
GBL	Great Bear lake
GSL	Great Slave Lake
$I_a$	Index of agreement
IFOV	Instantaneous Field Of View
$LST_{lake}$	Lake Surface temperature ( $^{\circ}C$ )
$LST_{land}$	Land Surface temperature ( $^{\circ}C$ )
MBE	Mean Bias Error
MODIS	Moderate Resolution Imaging Spectrometer
NOAA	National Oceanic and Atmospheric Administration
NWP	Numerical Weather Prediction
RMSE	Root Mean Square Error
SSM/I	Special Sensor Microwave Imager
SWE	Snow Water Equivalent
TIR	Thermal Infrared Radiation

## Preface

In addition to a general introduction, a background chapter and a general conclusion, the thesis contains two journal articles that examine the fundamental processes that govern the Lake Surface Temperature ( $LST_{\text{lake}}$ ) using satellite observations, *in situ* and simulation models. The first paper was submitted and accepted with revisions to the international journal *Tellus Series A: Dynamic Meteorology and Oceanography*. The paper discusses the simulation of  $LST_{\text{lake}}$  and ice-cover on large northern lakes with 1-D models and compares output with MODIS satellite data and *in situ* measurements. The second paper, being prepared for submission to the international journal of *Hydrological Processes*, contrasts land and lake surface temperature patterns observed from MODIS  $LST_{\text{land/lake}}$  during the open-water and snow/ice growth seasons.

The first article (Chapter 3) is the result of a direct collaboration with Professor Claude R. Duguay (University of Waterloo), Dr. Andrey Martynov (University of Quebec), and Laura Brown (University of Waterloo). Prof. Duguay aided a great deal with the initial proposal of the article, and provided continuous advice and comments throughout the duration of the study. Dr. Martynov's contributions included help in running the FLake model and provision of support through comments and advice before submission. Laura Brown contributed by providing the CLIMo model results and also support through comments and advice before submission.

The second article (Chapter 4) is the result of collaboration with Professor Duguay and Dr. Ram Yerubandi (Environment Canada). Prof. Duguay again provided a great deal of guidance and comments throughout the drafting of the article. Dr. Yerubandi provided the datasets necessary for this study, including *in situ* measurements of water temperature on Great Bear Lake. He will also provide comments and advice before submission of the paper to *Hydrological Processes*.

# Chapter 1

## General Introduction

### 1.1 Introduction

Lakes are a fundamental component of climate on the local and regional scale, functioning much as oceans do on the global scale (Schertzer, 1997). The heat transport and storage of lakes play an essential role in energy and water exchange with the atmosphere. The surface heat flux over lakes is strongly regulated by the Lake Surface Temperature ( $LST_{lake}$ ), which is a good indicator of the energy balance at the Earth's surface. It also influences regional heat, moisture content, and circulation of the atmosphere. At the same time that the  $LST_{lake}$  influences the sensible and latent heat fluxes, the  $LST_{lake}$  is itself affected by those same fluxes (Schertzer, 1997). The study of  $LST_{lake}$  is important because the entire process of energy exchange between a lake's surface and subsurface influences the static stability of the water column, which is essential in determining lake hydrodynamics (Lofgren and Zhu, 2000).

This kind of study is especially important for a country like Canada, in which there are more than two million lakes within five major drainage basins, covering 7.6 per cent of country's total area (Schertzer, 1997). The greater the water body size, the greater its effect on climate. In Mackenzie River Basin (MRB), located in northwestern Canada, the surface area of the lakes has been determined as  $\sim 144\,000\text{ km}^2$  by the Canada Centre for Remote Sensing (CCRS-2) land cover classification (Bussi eres, 2002). Lakes in the MRB provide essential transportation of energy and water into and through the basin by helping control the evaporation, runoff, and basin water storage (Oswald & Rouse, 2004). As lakes have a high heat capacity compared to land, they are able to store large quantities of heat, and their heat exchange with the atmosphere is heavily dependent on the heat storage and thermal characteristics of the lake (Schertzer, 1997).

Understanding these processes and the interactions of lakes with the atmosphere is an important issue, which allow for better climate modeling and weather forecasting. In most

Numerical Weather Prediction (NWP) and climate models, the effects of lakes have been ignored or treated in a simplistic way; because lakes are only regionally important compared to the land and sea that dominate the earth's surface. Improvement in predictions can be achieved by interactive coupling of the regional and global climate models with the lake models. To reach this goal, the first important step is to test and validate the performance of lake models using *in situ* and/or remote sensing observations. Satellite observations are increasingly used for this purpose. Thermal infrared data from satellite imaging systems can help to determine the spatial distribution of water body temperatures and their variation during the year, and are a powerful source of data for comparison with simulated  $LST_{lake}$  from numerical lake models.

One typical way of collecting lake properties is through *in situ* measurements where a person can use thermometer or buoys to measure the temperature of the lake. The advantage of remotely sensed data is that unlike much of the *in situ* measurements, it can be obtained over very large geographic areas rather than just at a single point or a few points. *In situ* data are often used in support of remotely sensed data, such as lake temperature at the same time as the remote sensor data are collected. It is vital to assess remotely sensed data as they are useful themselves for evaluating climate models and are a promising data source for assimilation into numerical weather forecasting models. The use of thermal data for estimation of  $LST_{lake}$  is a common operational application of satellite sensors, such as the Advanced Very High Resolution Radiometer (AVHRR) on the US National Oceanic and Atmospheric Administration (NOAA) polar orbiting satellites, Advanced Along-Track Scanning Radiometer (AATSR) onboard the European Space Agency (ESA) environmental satellite ENVISAT and the Moderate Resolution Imaging Spectroradiometer (MODIS) onboard the Terra and Aqua platforms that represents the imaging spectroradiometers able to retrieve surface temperature. MODIS Land and Lake Surface Temperature ( $LST_{land/lake}$ ) products have been compared and validated against ground-based temperature measurements over homogeneous areas such as lakes at mid-latitudes (Wan *et al.*, 2002a, b; Wan *et al.*, 2004; Oesch *et al.*, 2005; Hook *et al.*, 2007; Wan, 2008; Crosman and Horel, 2009) and rice

crops (Coll *et al.*, 2005, 2009; Wan *et al.*, 2004; Galve *et al.*, 2007). The 1 km products have been validated with the alternative radiance-based (R-based) method over a lake and rice crops (Wan and Li., 2008; Coll *et al.*, 2009) and dense forest (Coll *et al.*, 2009). Recently, Langer *et al.* (2010) and Westermann *et al.* (2011) compared summertime MODIS Land Surface Temperature ( $LST_{land}$ ) data with those obtained with a thermal imaging system installed on a mast 10 m above the ground at two permafrost sites. They reported differences of less than 2 K between the two sets of measurements under clear-sky conditions, with occasionally larger differences when clouds are not properly detected in the MODIS product.

Research on lake phenology has not only relied on using historical or satellite-derived data but also through the use of generalized hydrodynamic and thermodynamic models. There are both 1-D and 3-D lakes models available to simulate lake surface properties but 3-D models are seldom considered due to high computational cost (León *et al.*, 2005). Rouse *et al.* (1997) discussed the importance of understanding how mean depth relates to the thermal regime and water balance of lakes in subarctic and arctic North America and noted the significance of this information for modeling the responses of lakes to climate change. The Canadian Lake Ice Model (CLIMo), 1-D thermodynamic lake ice model, is well-tested and used for freshwater/ice-cover studies (e.g., Ménard *et al.*, 2002; Duguay *et al.*, 2003; Morris *et al.*, 2005). Simulated ice-growth processes using CLIMo on shallow lakes in arctic, subarctic, and high-boreal forest environments have been compared with field and satellite observations over several ice seasons (Duguay *et al.*, 2003). Ice-on dates have been simulated to within 2 days of observed values over the Churchill area, and the mean absolute error in ice-off dates varied from 1 to 8 days depending on the snow cover scenario used in the simulations. Ménard *et al.* (2002) studied ice phenology using CLIMo on GSL for a period of 1960 to 1991. Results are compared with *in situ* observations and those derived from the passive microwave the Special Sensor Microwave Imager (SSM/I) satellite imagery. Results demonstrated a very good agreement between observed and simulated ice thickness and freeze-up/break-up dates at this period of observations, particularly for the Back Bay (4 and 6 days overestimate for break-up and freeze-up respectively) and Hay River (4 days

underestimate and 5 days overestimate for break-up and freeze-up respectively). It has been shown that CLIMo is capable of reproducing the seasonal and inter-annual evolution of ice thickness and on-ice snow depth, as well as the inter-annual variations in freeze-up and break-up dates. León *et al.* (2007) validated the 3-D lake hydrodynamics model, Estuary and Lake COmputer Model (ELCOM), by using observed meteorological data and the output from the current RCM model as forcing input to compare the results with observed surface temperature on GSL. The result showed the temperature differences of 0.7 °C for the shallower western part of the basin and differences of -1.1°C in the deeper mid-lake. Recently, Martynov *et al.* (2010) showed the ability of two 1-D lake models (Hostetler and FLake models) to simulate  $LST_{lake}$  to typical temperate freezing lakes of North America. The authors found that the differences between the model results and observations increase with the average lake depth. CLIMo and FLake are the two models used in this thesis.

## 1.2 Research Objectives

The main goal of this research is to improve our knowledge and understanding of lake physical and hydrodynamic processes using spatial and temporal measurements of lake and land surface temperature in the Great Bear Lake (GBL) and Great Slave Lake (GSL) regions using MODIS satellite data. GBL and GSL are chosen as they are huge and their effect on regional climate is considerable. First, MODIS  $LST_{lake}$  observations are compared to numerical lake models to demonstrate the usefulness of MODIS  $LST_{lake}$  observations and models to climate science. Second, MODIS  $LST_{land/lake}$  are used to study the land and lake thermodynamics. To attain the above-mentioned goal four research objectives are pursued:

- 1- Evaluate the performance of two lake models, FLake and CLIMo, and compare the models estimated LSTs with those obtained from MODIS.
- 2- Identify the uncertainties and limitations of the numerical models and the MODIS satellite data products.

- 3- Compare and evaluate MODIS-derived LSTs over land and lakes with available meteorological station measurements and *in situ* observations.
- 4- Analyze the seasonal and inter-annual variations and spatial patterns in surface temperature over lakes and land.

### **1.3 Thesis Overview**

In Chapter 2, background information is provided on lake thermodynamics, lake ice, remote sensing, as well as modeling of  $LST_{lake}$ . Chapter 3 is the first appended paper, entitled “Simulation of surface temperature and ice-cover of large northern lakes with 1-D models: A comparison with MODIS satellite data and *in situ* measurements”. Chapter 4 is the second appended paper, entitled “Analysis of lake and land surface temperature patterns during the open-water and snow/ice growth seasons in the Great Bear and Great Slave Lake regions, Canada, from MODIS (2002-2010)”. Chapter 5 summarizes the main findings of the thesis and identifies some limitations of the study and directions for future research.

## Chapter 2

### Review of Lake Thermodynamics and Research Methods

This chapter contains three main components designed to provide a sufficient background before presenting results within the appended papers. In this chapter, a review of the thermodynamics of lakes, lake ice and snow is followed by a survey of remote sensing methods to obtain surface temperature and an overview of the two lake models used in the thesis.

#### 2.1 Lake Thermodynamics

Different elements affect the surface temperature of lakes. Daily and seasonal air temperature is the most obvious reason for temperature change in lakes. Lake depth (Balsamon *et al.*, 2010) and latitudinal locations (Schertzer, 1997) also influence the  $LST_{lake}$ . Lakes at high latitude present a challenge because the snow and ice have a high albedo that insulates the water from the atmosphere. Chen and Millero (1986) showed that water at the temperature of maximum density (3.98 °C) becomes lighter when it cools or warms. This behavior facilitates ice formation on freshwater lakes. In late spring, once the ice is melted, the upper layer of water warms until it reaches the temperature of maximum density. The denser layer of the surface sinks to the bottom of the lake and the new layer warms to 3.98 °C. This is repeated until the entire water column is at the temperature of maximum density (Figure 2.1, 2). The upper layer of water continues to warm in summer (>3.98 °C). The water column becomes stratified, with warmer (low density) water at the top and cool (high density) water on the bottom. Energy is transferred from the upper warm layer to the cool lower layer (Figure 2.1, 3). In the fall, the upper layer of water cools and sinks to the bottom of the lake. This process continues until the entire water column is at temperature of maximum density (Figure 2.1, 4). The upper layer continues to cool and ice forms once the surface of the water reaches 0°C, the freezing point of fresh water. In winter, the ice grows thicker as long as the air temperature is less than or equal to 0°C and heat is conducted upwards through the snow and ice into the atmosphere. As the ice grows, the upper layer of the water cools and the

entire water column becomes stratified, with the cool layer sitting on the lower layer of water that is at the temperature of maximum density (Figure 2.1, 1). In early spring, once the air temperature rises above 0°C, first the snow on the ice warms to 0°C and melts away, and then the ice absorbs solar radiation, warms to 0°C and melts. The ice-cover shrinks as it melts around the edges and also at the top and bottom.

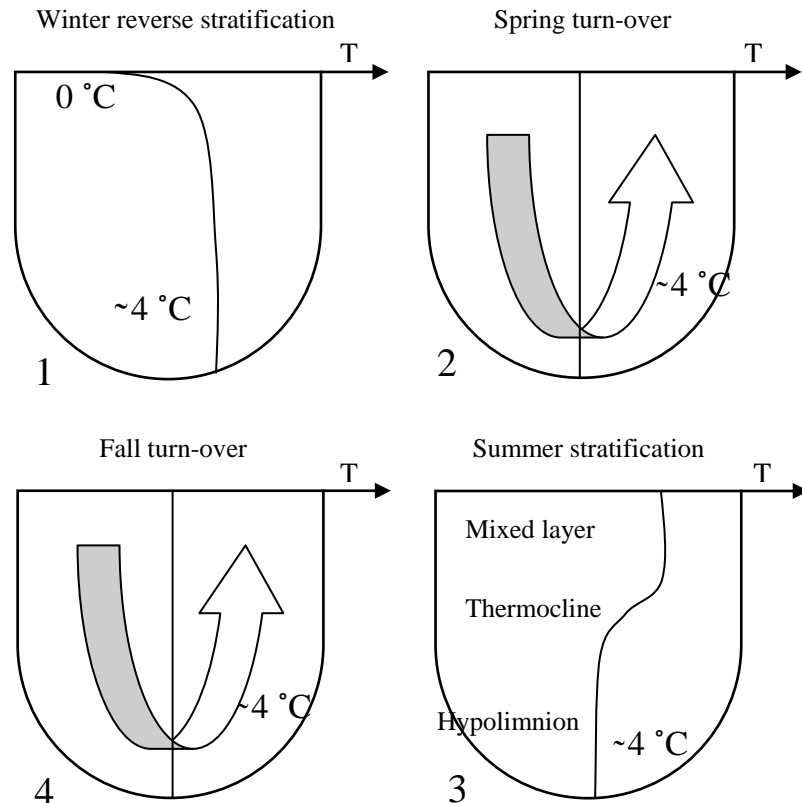


**Figure 2-1:** Schematic representation of typical dynamic lake behavior (Redrawn after Bluteau, 2006).

## 2.2 Lake Ice and Snow

Lake ice occurs where the average air temperature is below the freezing point. It happens at the higher latitudes of the Northern and Southern Hemisphere, which forms in the autumn,

thickens during the winter and melts in the spring. Air temperature is one of the main factors of the overall ice growth; however, snow and wind and hydrographic conditions such as currents and density stratification of the lake water forms ice (Bengtsson, 1986). There are two types of lake ice: congelation ice and snow ice. Congelation ice forms when the water freezes at the bottom of the ice-cover (Figure 2.2, 1 and 2) and freezing of slush at the top of the ice-cover creates snow ice (Figure 2.2, 4) (Adams, 1981). When the mass of snow is sufficient to depress the ice surface below the waterline, water flows up through fractures or gaps between ice and shore; as a result, slush occurs at the top of the ice-cover (Figure 2.2, 3). Congelation ice has high optical depth that allows light to pass right through to the underlying water, therefore is sometimes referred to as black ice. Snow ice is sometimes referred to as white ice because its high bubble content causes strong light scattering (Morris and Jeffries, 2006).

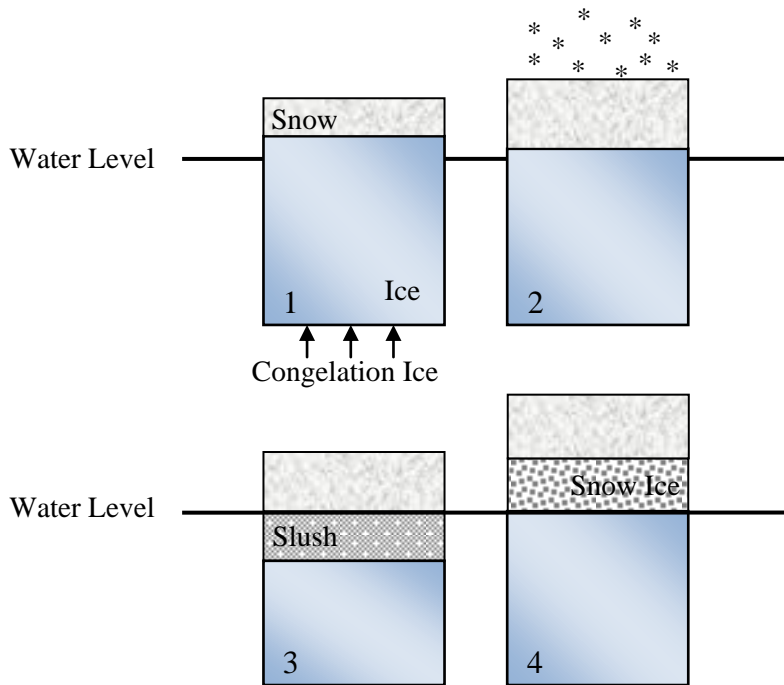


**Figure 2-2:** The formation processes of congelation ice and snow ice (Redrawn after Alaska Lake Ice and Snow Observation Network).

Overlying snow over the ice is a significant factor that affects the lake ice development. Snow insulates the lake ice from air temperature and decreases the process of thermal conductivity (Adams, 1976; Adams and Roulet, 1980; Bengtsson, 1986; Woo, 1989). As the temperature gradient at the ice/snow interface becomes warmer, the growing process of congelation ice decreases (Adams and Roulet, 1980). The magnitude at which the snow cover affects development of lake ice depends on the depth and density of the snowpack (Adams, 1976; Duguay *et al.*, 2002; Duguay *et al.*, 2003; Jeffries *et al.*, 2005). Wind is another important factor that redistributes snow and can affect both of these variables where it either strips snow from the surface or compacts it. Compacted snow possesses a higher thermal conductivity, allowing for a greater amount of heat loss at the snow/ice interface and increasing the congelation ice growth (Bengtsson, 1986). Wind-blown snow accumulation zones can also cause localized variations in ice thickness as a result of the variable insulation properties imposed on the ice (Adams, 1976).

The assumption has been that lake snow cover is essentially the same as that on the surrounding tundra, but field observations show that there are many important differences (Sturm and Liston, 2003). Previous studies showed that the snow cover on lakes is thinner, denser, and comprises less snow water equivalent (SWE) than the nearby land. Snow begins to fall in late August at some Arctic locations, but the lakes do not freeze until mid-September (Brewer, 1958; Jeffries *et al.*, 1996; Liston and Sturm, 2002). The early-season snow falls into the water and is not incorporated in the snow cover. This explains, in part, why there is less SWE on the lakes than on the tundra. Moreover, the snow layers on lakes are fewer than the ones on land and are harder.

The vertical temperature gradients across the lake snow cover are consistently greater than across tundra snow. The water under the ice provides a latent heat source that lasts throughout the winter, maintaining snow-ice interface temperatures several degrees higher than land snow-ground interface temperatures. On land, much of the latent heat associated with unfrozen soil moisture in the active layer is exhausted by mid-winter, so the interface temperatures drop as winter progresses (Sturm *et al.*, 1995; Jeffries *et al.*, 1999; Taras *et al.*,

2002). Figure 2.3 shows the distinctly different basal roughness of the ice vs. tundra in cross sections of the snow cover on Imikpuk Lake in Alaska and on the nearby tundra.

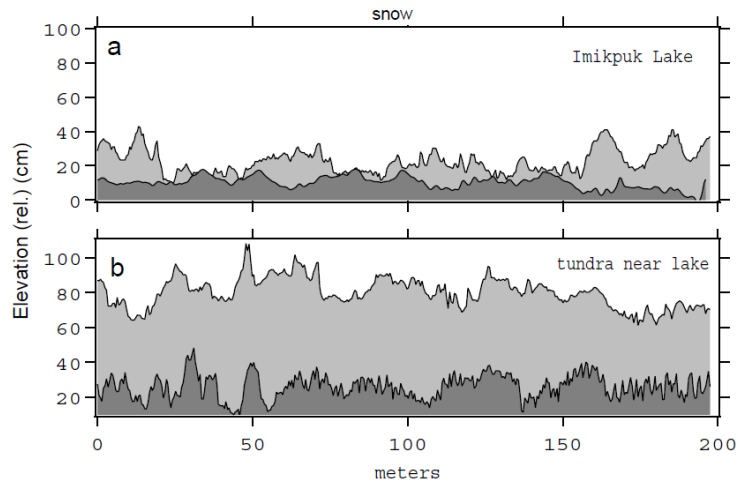


**Figure 2-3:** Cross sections of the snow cover on a lake (Imikpuk lake) in Alaska and on the nearby tundra. Light gray indicates snow; dark gray indicates ice or tundra (Source: Sturm and Liston, 2003).

## 2.3 Thermal Remote Sensing

### 2.3.1 Thermal Radiations

Thermal radiation is electromagnetic radiation that emits from any material at the given temperature, which is a function of temperature and wavelength. Based on Wien's Displacement Law, wavelength at which the largest portion of energy is emitted from a blackbody (blackbody absorbs all electromagnetic radiation incident upon it with zero reflectance) depends on temperature,

$$\lambda_m = \frac{A}{T} \quad (2.1)$$

where  $\lambda_m$  is the wavelength of maximum emittance ( $\mu\text{m}$ ),  $A$  is a constant ( $2898 \mu\text{m K}$ ), and  $T$  is temperature (K). The hotter objects emit more energy at shorter wavelengths than the cooler objects. For a blackbody, the total energy emitted from an object over all wavelengths varies as a function of the fourth power of surface temperature (Stefan-Boltzmann Law):

$$M = \sigma T^4 \quad (2.2)$$

where  $M$  is total radiant exitance from the surface of a material,  $\sigma$  is Stefan-Boltzmann constant ( $5.67 \times 10^{-8} \text{ Wm}^{-2}\text{K}^{-4}$ ), and  $T$  is absolute temperature of the emitting material (K).

Different factors influence the radiant temperature of surface such as emissivity, conductivity, capacity, diffusivity and inertia. External environmental conditions also affect the temperature radiance of the surface. Surface wind increases the convective heat transfer; rain and humidity make surface objects appear to be cooler; and clouds and fog will completely mask Thermal Infrared Radiation (TIR) emission. The best (TIR) images are acquired under clear skies with no surface wind and low humidity.

Convection is a primarily way of transfer energy in water bodies, which transfers heat to depths of 100 cm or more. As a result, water bodies acts as if it has a very high thermal inertia, and has a relatively uniform temperature both day and night. Consequently, water will be cooler than bounding land surfaces during the day heating period and warmer than the bounding land surfaces during the night cooling period. In solids, conduction is the primarily way of energy transfer, which cause relatively high daytime temperatures and relatively low nighttime temperature.

### **2.3.2 Moderate Resolution Imaging Spectrometer (MODIS)**

MODIS, the sensor from which the  $LST_{\text{land/lake}}$  data used in this thesis are derived from, is an EOS instrument on Terra and Aqua satellites in a 705 km sun-synchronous orbit, views the entire surface of the earth every 1 to 2 days. MODIS provides images of daylight reflection and day/night emission and scans  $\pm 55^\circ$  from nadir in 36 bands, with bands 1-19 and band 26 in the visible and near infrared range, and the remaining bands in the thermal infrared from 3-15  $\mu\text{m}$ . Specifically, bands 3-7, 13, and 16-19 are used to classify land-cover to infer emissivity, band 26 to detect cirrus clouds, and the thermal infrared bands 20, 22, 23, 29, 31, and 32 to correct for atmospheric effects and retrieve surface emissivity and temperature. The thermal infrared bands have an IFOV (instantaneous field-of-view) of approximately 1 km at

nadir. MODIS views cold space and a full-aperture blackbody before and after viewing the Earth scene in order to achieve calibration accuracy of better than 1% absolute for thermal infrared bands. MODIS is particularly useful because of its global coverage, radiometric resolution and dynamic ranges, and accurate calibration in multiple thermal infrared bands designed for retrievals of Sea Surface Temperature (SST),  $LST_{\text{land/lake}}$  (skin temperature) and atmospheric properties (Wan and Li, 1997). The thickness of the skin layer depends on the local energy flux of the molecular transport, which is usually less than 1 mm thick. The infrared wave can only penetrate water no deeper than  $\sim 500 \mu\text{m}$ . The MODIS instrument measures infrared radiances at two wavelengths around  $3.9 \mu\text{m}$  and  $11 \mu\text{m}$  where the penetration depths for these two bands are  $\sim 100 \mu\text{m}$  and  $\sim 10 \mu\text{m}$  (Yuan, 2009).

There are different MODIS surface temperature products: level 1B (L1B) product is a swath (scene) of MODIS data geolocated to latitude and longitude centers of 1 km resolution pixels; level 2 (L2) product is a geophysical product that remains in latitude and longitude orientation and has not been temporally or spatially manipulated; and level 3 (L3) product is a geophysical product which has been temporally and spatially manipulated, and is usually in a gridded map projection format referred to as tiles (Wan, 2007). The MOD11\_L2 LST product, which is used in this study, is generated by the generalized split-window LST algorithm. The split-window method corrects for atmospheric effects based on the differential absorption in adjacent infrared bands (Price, 1984). Different MODIS data product inputs to the MODIS LST algorithm are shown in Table 2.1. The generalized split-window algorithm applied to the MODIS brightness temperatures in channels 31 (10.78–11.28 $\mu\text{m}$ ) and 32 (11.77–12.27 $\mu\text{m}$ ), estimated from land cover types, atmospheric column water vapor and lower boundary air surface temperature are separated into tractable sub-ranges for optimal retrieval. The generalized split-window algorithm (Wan and Dozier, 1996) can be written as

$$LST = C + \left( A_1 + A_2 \frac{1-\varepsilon}{\varepsilon} + A_3 \frac{\Delta\varepsilon}{\varepsilon^2} \right) \frac{T_{31}+T_{32}}{2} + \left( B_1 + B_2 \frac{1-\varepsilon}{\varepsilon} + B_3 \frac{\Delta\varepsilon}{\varepsilon^2} \right) \frac{T_{31}+T_{32}}{2} \quad (2.3)$$

where  $\varepsilon = (\varepsilon_{31} + \varepsilon_{32})/2$  and  $\Delta\varepsilon = \varepsilon_{31} - \varepsilon_{32}$  are the mean emissivity and the emissivity difference in channels 31 and 32, respectively. Coefficients  $C$ ,  $A_i$  and  $B_i$  were obtained from linear regression of MODIS simulated data for wide ranges of surface and atmospheric conditions, and they depend on the view angle, the column water vapor content and the atmospheric lower boundary temperature.

**Table 2-1:** MODIS data product inputs to the MODIS LST algorithm for the MOD11\_L2 product (Source: Wan, 2007).

Earth Science Data Type (ESDT)	Long Name
MOD021KM	MODIS Level 1B Calibrated and Geolocated Radiances
MOD03	MODIS Geolocation
MOD35_L2	MODIS Cloud Mask
MOD07_L2	MODIS Atmospheric Profile
MOD12Q1	Land Cover
MOD10_L2	MODIS Snow Cover

## 2.4 Modeling

Numerical modeling is another approach to study lakes and, in this study, was used in addition to *in situ* and remote sensing measurements. Obviously, making *in situ* observations of large lakes, especially in cold regions that are covered with ice for several months, is a challenge. Satellite observations can give the wide spatial coverage of surface but are not able to provide direct measurements of the lake water below the surface (skin) such as the mixed layer depth or temperature profile. Therefore, numerical models become a useful tool to predict the mixing conditions and vertical temperature structure in lakes at different depths on various time scales.

The Canadian Lake Ice Model (CLIMo) (Duguay *et al.*, 2003) and Freshwater Lake (FLake) (Mironov 2008, Mironov *et al.*, 2010) are the two 1-D models used in this study, although many variations of such models have been developed. CLIMo is based on the 1-D

unsteady heat conduction equation, with penetrating solar radiation (Maykut and Untersteiner, 1971),

$$\rho C_P \frac{\partial T(z,t)}{\partial t} = \frac{\partial}{\partial z} k \frac{\partial T(z,t)}{\partial z} + F_{sw} I_0 (1 - \alpha) K e^{-Kz} \quad (2.4)$$

where  $T(z,t)$  is the temperature within the ice or snow (K),  $t$  is time (s) and  $z$  is depth measured positive downward from the upper surface (m).  $\rho$  is density ( $\text{kg m}^{-3}$ ),  $C_P$  specific heat capacity ( $\text{J kg}^{-1} \text{K}^{-1}$ ),  $k$  the thermal conductivity ( $\text{W M}^{-1} \text{K}^{-1}$ ),  $F_{sw}$  shows downwelling shortwave radiative energy flux ( $\text{W m}^{-2}$ ),  $I_0$  is the fraction of shortwave radiation flux that penetrates the surface (equal to 0.17 if snow depth  $\leq 0.01$  m, and equal to 0 if snow depth  $> 0.1$  m),  $\alpha$  is surface albedo, and  $K$  is bulk extinction coefficient for penetrating shortwave radiation, which is equal to  $1.5 \text{ m}^{-1}$ ). The model solves Equation (2.3) by arbitrary number of layers in both the ice and snow portions of the slab and is unconditionally stable (see Figure 2.4).

The freezing temperature of fresh water under the layer of ice plus snow is shown with  $T_f$  and the melting temperature at the surface with  $T_s$ . When melt is occurring at the upper surface, the boundary condition in that temperature is fixed at the melting point for fresh water and the heat flux offsets the latent heat of fusion of melting ice or snow. When ice melts away completely in summer, the model includes a fixed-depth mixed layer. When ice is present, the mixed layer is fixed at the freezing point, and when ice is absent, the mixed layer temperature is computed from the surface energy budget considering the fraction of shortwave radiation flux that penetrates the surface.

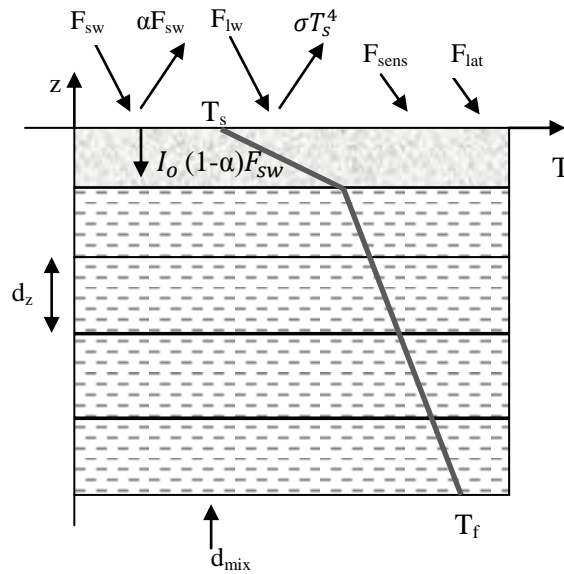


**Figure 2-4:** Schematic representation of the lake ice model during winter. The layers with dashed lines represent ice and the gray layer above the ice is snow. The solid grey line indicates the temperature profile, which is computed using a finite-difference representation of the heat conservation Equation (2.3). The arrows along the top of the surface indicate the components of the surface heat budget included in the model (Source: Duguay *et al.*, 2003).

CLIMo can be forced using hourly or daily mean values of air temperature ( $^{\circ}\text{C}$ ), wind speed (m/s), relative humidity (%), cloud cover (1/10), and snow depth (m). Snow density can be read as an input, whether as a constant, mean winter value or as a daily variable and the downward radiative terms either can be read directly or computed. The model produces outputs for different snow cover scenarios (0%, 25%, 50%, 75% and 100% of the on-shore snow cover depths) and mixed layer depths as well as all energy balance components, on-ice snow depth, annual break-up/freeze-up, ice thickness, and temperature profile in ice and snow.

FLake model is based on a self-similar parametric representation (assumed shape) of the evolving temperature profile. This concept originates from observations of oceanic mixed layer dynamics by Kitaigorodskii and Miropolsky (1970). Figure 2.5 illustrates the temperature profile in the mixed layer, thermocline, and active layer of bottom sediments for the model.

The mixed-layer temperature is shown with  $\theta_s(t)$  and its depth with  $h(t)$ .  $\theta_b(t)$  is the temperature at the water-bottom sediment interface and the temperature  $\theta_H(t)$  at the lower

boundary of the upper layer of bottom sediments penetrated by the thermal wave, and the depth  $H(t)$  of that layer. The temperature  $\theta_L$  at the outer edge  $z = L$  of the thermally active layer of bottom sediments is constant. In FLake, provision is made to model the evolution of snow cover above the lake ice, but it has not been sufficiently tested so far.

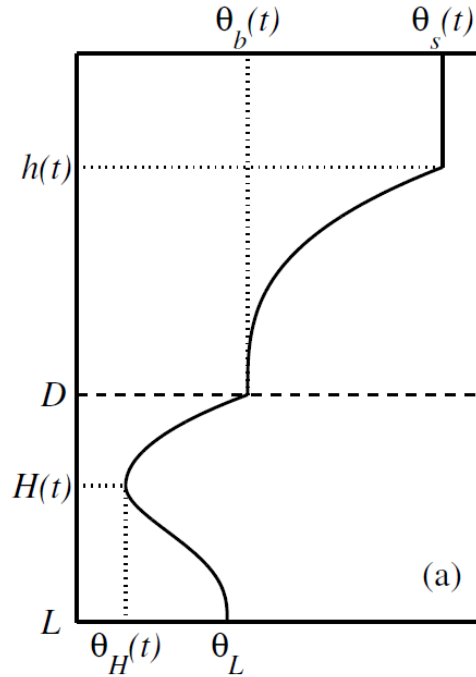


**Figure 2-5:** Schematic representation of the temperature profile in the mixed layer, thermocline, and active layer of bottom sediments. The evolving temperature profile is specified by several time-dependent quantities (Source: Mironov, 2008).

FLake can be forced with air temperature ( $^{\circ}\text{C}$ ), wind speed (m/s), air humidity (mb), incoming solar radiation ( $\text{W/m}^2$ ), and cloudiness (0-1) or incoming longwave radiation ( $\text{W/m}^2$ ). The model produces outputs as: lake surface temperature ( $^{\circ}\text{C}$ ), mean water temperature ( $^{\circ}\text{C}$ ), lake bottom temperature ( $^{\circ}\text{C}$ ), friction velocity in air (m/s), friction velocity in surface water (m/s), convective velocity scale (m/s), sensible and latent surface heat flux ( $\text{W/m}^2$ ), short-wave radiation ( $\text{W/m}^2$ ), longwave radiative flux from the atmosphere ( $\text{W/m}^2$ ), longwave radiative flux from the water ( $\text{W/m}^2$ ), mixed layer depth (m), depth of the thermal wave penetration in sediments (m), temperature at the crest of the thermal wave in sediments ( $^{\circ}\text{C}$ ), heat flux across the water-sediment boundary ( $\text{W/m}^2$ ), ice and snow

thickness (m), ice and snow temperature ( $^{\circ}\text{C}$ ). As indicated above, the snow module of FLake has not been sufficiently tested so far. Therefore, it has been set to zero in this study. In the next chapter, both CLIMo and FLake are used to simulate  $\text{LST}_{\text{lake}}$  and ice-cover over GBL and GSL. Results are compared to those obtained with MODIS during the open-water and snow/ice growth seasons.

One statistical measure used to compare the performance of models against observations is the relative index of agreement ( $I_a$ ) defined as (Wilmott and Wicks, 1980)

$$I_a = 1 - \left[ \frac{\sum_{i=1}^N (P_i - O_i)^2}{\sum_{i=1}^N (|P_i - O_m| + |O_i - O_m|)^2} \right] \quad (2.4)$$

where  $P_i$  and  $O_i$  are the predicted (modeled) and observed values, respectively.  $O_m$  is the average observed value, and  $N$  is the number of data points used. This index has values ranging from 0 (worst performance) to 1 (best possible performance).

The mean bias error (MBE), which provides a measure of systematic error is also calculated to examine the performance of models. The MBE indicates whether a model under-predicts or over-predicts a variable throughout a given period of time. If the error is completely random, the MBE value is equal to zero.

$$MBE = \frac{\sum_{i=1}^N [P_i - O_i]}{N} \quad (2.5)$$

The root mean square error (RMSE) is another useful statistical measure utilized in this thesis. It provides a measure of the nonsystematic error. The RMSE gives a measure of the total error and does not distinguish between under-prediction or over-prediction since the difference between the predicted and the observed value is squared. A RMSE of zero indicates that there is no deviation between the predicted and the observed values.

$$RMSE = \sqrt{\frac{\sum_{i=1}^N [P_i - O_i]^2}{N}} \quad (2.6)$$

## Chapter 3

### **Simulation of surface temperature and ice-cover with 1-D models: A comparison with MODIS satellite data and *in situ* measurements**

#### **Overview**

Lake Surface Temperature ( $LST_{lake}$ ) and ice phenology were simulated for various points differing in depth on Great Slave Lake (GSL) and Great Bear Lake (GBL), two large lakes located in the Mackenzie River Basin in Canada's Northwest Territories, using the one-dimensional (1-D) Freshwater Lake model (FLake) and Canadian Lake Ice Model (CLIMo) over the 2002-2010 period. Input data from three weather stations (Yellowknife, Hay River and Deline) were used for model simulations.  $LST_{lake}$  model results are compared to those derived from the Moderate Resolution Imaging Spectroradiometer (MODIS) aboard the Earth Observing System Terra and Aqua satellite platforms. The main goal was to examine the performance of the FLake and CLIMo models in simulating  $LST_{lake}$  and ice-cover under different conditions for the two large northern lakes and to identify the uncertainties of 1-D lake models and satellite data products. Both models reveal a good agreement with daily average MODIS  $LST_{lake}$  from GSL and GBL on an annual basis. CLIMo showed a generally better performance than FLake for both lakes, particularly during the ice-cover season. The absence of consideration of snow on lake ice in FLake was found to have a large impact on estimated ice thicknesses (26 cm thicker on average by the end of winter compared to *in situ* measurements; 9 cm for CLIMo) and break-up dates (5 days earlier in comparison with *in situ* measurements; 3 days later for CLIMo). The overall agreement between the two models and MODIS  $LST_{lake}$  products during both the open-water and ice-cover seasons indicates that the assimilation of satellite-retrieved  $LST_{lake}$  into numerical weather prediction (NWP) models merits to be explored.

### 3.1 Introduction

It has been recognized that large lakes have a considerable influence on local and regional climates (Eerola *et al.*, 2010). The influence of lakes on local temperature is important for a country like Canada where lakes are abundant. For example, it has been estimated that the Great Lakes of North America have a large influence by doubling the amount of local precipitation in winter and decreasing the amount of precipitation by 10% to 20% in summer (Ljungemyr *et al.*, 1996). The presence or absence of ice-cover on lakes during the winter months is also known to affect both regional climate and weather events (Rouse *et al.*, 2007a). If lakes are frozen, the physical properties of the lake surface such as surface temperature, albedo, and roughness are very different. Lake surface properties and the amount of lake surface area are major issues of interest when dealing with the lake-atmosphere interactions (Ljungemyr *et al.*, 1996). Understanding the process of the lake ice and its interactions with climate allow for better climate modeling and weather forecasting. In most numerical weather prediction (NWP) and climate models, however, the effect of lakes is often ignored or parameterized very roughly (Brown and Duguay, 2010). Improvement in numerical weather forecasting can be achieved by interactive coupling of NWP and regional climate models with lake models (Mironov *et al.*, 2010).

Samuelsson *et al.* (2010) investigated the impact of lakes on the European climate by coupling the Fresh-water Lake (FLake) model in the Rossby Centre Regional Climate Model (RCA3.1). Simulations where FLake is coupled to the RCM were compared to those in which all lakes in the model domain were replaced by land. Results showed that lakes have a warming effect on the European climate in all seasons, especially in fall and winter. Martynov *et al.* (2010) showed the ability of two 1-D lake models (Hostetler and FLake models) to simulate the surface temperature of typical temperate lakes in North America. Results showed a good performance of both models for shallow lakes, but larger differences were documented for deep lakes when comparing modeled and observed water temperature and ice-cover duration. Eerola *et al.* (2010) investigated the performance of the High Resolution Limited Area Model (HIRLAM) NWP model using the FLake model as a

parameterization scheme. The authors suggest that assimilation of lake surface temperature ( $LST_{lake}$ ) observations would likely produce more reliable forecasting results. The physical properties of the lake surface (surface temperature, albedo and roughness) are different with the presence of an ice-cover. Therefore, the ice-cover is also important for NWP models (Eerola *et al.*, 2010). An important step in this respect is to compare  $LST_{lake}$  and ice-cover obtained with lake models with those either measured *in situ* or retrieved from satellite remote sensing observations.

Remote sensing data are increasingly being used to derive  $LST_{lake}$ . Thermal infrared (TIR) satellite data (e.g. Terra and Aqua/MODIS data and Envisat/Advanced Along Track Scanning Radiometer (AATSR)) used to derive  $LST_{lake}$  have recently been validated against ground-based measurements for open-water conditions. Coll *et al.* (2009) compared *in situ* measured  $LST_{lake}$  (skin temperatures) with those derived from AATSR from Lake Tahoe, California, for the period July–December 2002 and July 2003. They showed an average bias (AATSR minus *in situ*) of  $-0.17^{\circ}\text{K}$ , a standard deviation of  $0.37^{\circ}\text{K}$ , and root mean square error of  $\pm 0.41^{\circ}\text{K}$ . For the same lake, Schneider *et al.* (2009) computed a bias (*in situ* minus satellite retrieval) and standard error of  $-0.007^{\circ}\text{C}$  and  $0.32^{\circ}\text{C}$ , respectively, for MODIS. The equivalent values for AATSR were reported to be  $-0.082^{\circ}\text{C}$  and  $0.30^{\circ}\text{C}$ , and for ATSR-2  $0.001^{\circ}\text{C}$  and  $0.19^{\circ}\text{C}$ . Coefficient of determination ( $R^2$ ) values greater than 0.99 were found for all three sensors. Also, Crosman and Horel (2009) found a bias of  $-1.5^{\circ}\text{C}$  between MODIS-derived  $LST_{lake}$  (L2) and *in situ* measurements from buoys deployed in Great Salt Lake, Utah.

In this paper, satellite-derived surface temperatures are analyzed against the CLIMo (Canadian Lake Ice Model) and FLake models in simulations of  $LST_{lake}$  and ice-cover for two large, deep, lakes of northern Canada. Uncertainties of the 1-D lake models and satellite data products are also identified. In particular,  $LST_{lake}$  simulated with the lake models are compared with those derived from MODIS on a daily basis annually and seasonally (open-water and ice-cover seasons) for the period 2002-2010. Simulated ice thickness and freeze-

up/break-up dates are compared to *in situ* observations for the periods 1961-1996 and 2002-2008.

### 3.2 Study Area

The study area encompasses Great Slave Lake (GSL) and Great Bear Lake (GBL), two lakes located in the Mackenzie River Basin in Canada's Northwest Territories (Figure 3.1). These lakes are deep, large, and cold. A previous study showed that the open-water period for GSL is longer with the warmer water surface temperature by an average of 2.7 °C compared to GBL (Rouse *et al.*, 2008). For this study, meteorological data used as forcing variables for the lake models were obtained from three weather stations located near the shore of GBL and GSL (Figure 3.1): the Deline station (65.10 °N, 123.30 °W), at an altitude of 213 m a.s.l, on the southwest shore of GBL; the Hay River station on the southwest shore of GSL (60.50 °N, 115.47 °W) at an altitude of 164 m a.s.l.; and the Yellowknife Airport weather station located close to the north shore of GSL (62.28 °N, 114.27 °W) at an altitude of 205 m a.s.l. The physical characteristics of the lake sites are shown in Table 3.1.

**Table 3-1:** Physical characteristics of GSL and GBL:  $Z_{ML}$  is the mixed layer depth,  $Z_{Max}$  is the maximum depth,  $Z_{Mean}$  is the average depth, V is lake volume and A is lake area.

Location	Lat (°N)	Lon (°W)	$Z_{ML}$ (m)	$Z_{Max}$ (m)	$Z_{Mean}$ (m)	V (km <sup>3</sup> )	A (km <sup>2</sup> )
<b>GSL</b>				614	41	1580	27,000
<i>Yellowknife station (Back Bay)</i>	62.28	114.27	10				
<i>Hay River station</i>	60.50	115.47	10				
<i>Main Basin</i>	61.50	114.6	40				
<b>GBL</b>				413	42	2240	31,000
<i>Deline station</i>	65.10	123.30	40				

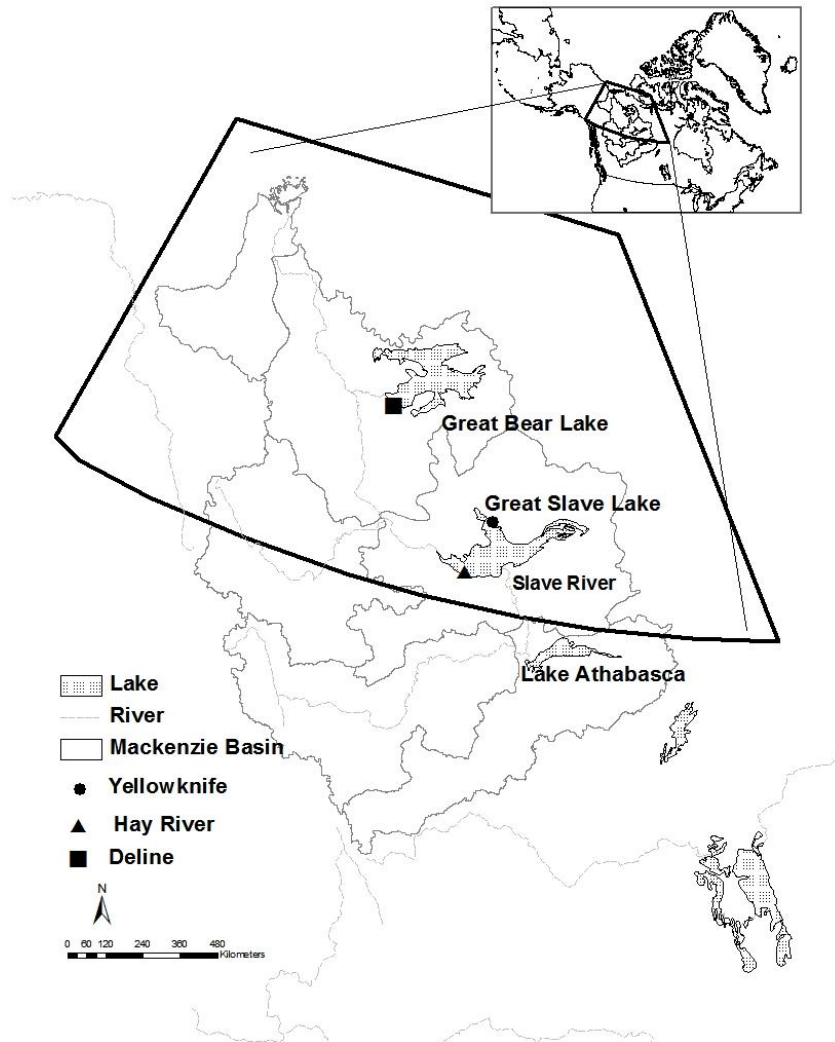


**Figure 3-1:** Maps showing the location of GSL and GBL within the Mackenzie River Basin and meteorological stations.

### 3.3 Data and Methods

#### 3.3.1 Moderate Resolution Imaging Spectroradiometer (MODIS)

The MODIS Terra and Aqua (L2, 1 km resolution, Version 5) day and night time  $LST_{lake}$  and emissivity products (MOD/MYD11\_L2) derived from the thermal-infrared channels 31 and 32 were acquired through the NASA Land Processes Distributed Active Archive Center (LP

DAAC) for the period 2002-2010. The products provide per-pixel temperature and emissivity values in a sequence of swath-based to grid-based global products and are produced daily at 5-minute increments.

The images were processed using a program written in the Interactive Data Language (IDL) to average Terra, Aqua, day, and night surface temperature L2 products into a new L3 product. In this program, first the section of the file intersecting the region of interest is read and then the latitude/longitude coordinates and time values are calculated for each pixel (cell). The file is split into approximately square tiles, which are re-projected to the Equal-Area Scalable Earth Grid (EASE-GRID) projection. This is done by calculating the projection coordinates of each observation and then using linear interpolation to calculate a value for the center of each EASE-GRID cell. Tiles are scaled to the desired output resolution (1 km in this study) by averaging all pixels that fall into the cell. For the entire file, two arrays are produced, one containing the average of all observations during the day and the other containing the observation during the night. The data from each array is added to an array containing the intermediate sum of all day/night observations for each pixel, respectively. After all files have been processed, an average is produced for each pixel of all observations during the day, and another is calculated for the night. These values are averaged together to produce the final surface temperature average with equal weighting between day and night values. These data, along with the day and night averages and the number of observations that went into producing each average, is output to a GEOTIFF file. The average (mean) daily values of pixels were extracted from the GEOTIFF files over the lake sites of Table 1 for comparison with the model simulations.

### **3.3.2 Canadian Ice Database (CID)**

Lake ice thickness measurements and freeze-up/break-up dates from Back Bay (GSL) for the periods 1961-1996 were extracted from Canadian Ice Database (CID) (Lenormand *et al.*, 2002) to evaluate the model results. No measurements are then available until the 2002-2008 period when ice thickness measurements resumed (not freeze-up/break-up observations). Ice thickness is measured about once a week, starting after freeze-up when the ice is safe to walk

on, and continues until break-up when the ice becomes unsafe. Freeze-up and break-up dates, as defined herein, correspond to complete freeze over (i.e. earliest date on which the lake is completely covered by ice) and water clear of ice (i.e. earliest date on which water is completely free of floating ice).

### **3.3.3 Canadian Lake Ice Model (CLIMo)**

CLIMo (Duguay *et al.*, 2003) has been developed to simulate ice phenology, thickness and ice composition on lakes of various depths. This 1-D thermodynamic ice model has been tested extensively to simulate ice-growth processes on shallow lakes in Arctic/sub-Arctic and high-boreal forest environments as well as on Great Slave Lake (e.g., Duguay *et al.*, 2003; Ménard *et al.*, 2002; Morris *et al.*, 2005). For shallow lakes in the Churchill region, Manitoba, ice-on dates have been simulated to within 2 days of *in situ* observations and within 1 to 8 days for break-up (ice-off) dates depending on the snow depth on ice scenario used in the simulations. Ménard *et al.* (2002) also studied ice phenology using CLIMo on GSL for the period 1960-1991. Freeze-up and break-up dates were compared with *in situ* observations and those derived from the passive microwave satellite imagery. Results showed a good agreement between observed and simulated ice thickness and freeze-up/break-up dates for this period, particularly for the Back Bay (4 and 6 days overestimate for break-up and freeze-up, respectively) and Hay River (4 days and 5 days overestimation for break-up and freeze-up, respectively). It was further demonstrated that CLIMo is capable of reproducing well the seasonal and inter-annual evolution of ice thickness and on-ice snow depth, as well as the inter-annual variations in freeze-up and break-up dates. However, to date, surface water and surface snow/ice temperatures generated by CLIMo have not been evaluated.

CLIMo performs a surface energy budget calculation to get net flux at ice, snow or open-water surfaces, solves the 1-D heat conduction problem using an implicit finite difference scheme with the ice/snow slab discretized into an arbitrary number of thickness layers. The surface energy budget is expressed as:

$$F_o = F_{lw} - \varepsilon \sigma T^4(0, t) + (1 - \alpha)(1 - I_o)F_{sw} + F_{lat} + F_{sens} \quad (3.1)$$

where  $F_o$  ( $\text{Wm}^{-2}$ ) is the net downward heat flux absorbed at the surface,  $F_{lw}$  ( $\text{Wm}^{-2}$ ) is the downwelling longwave radiative energy flux,  $\varepsilon$  is the surface emissivity,  $\sigma$  is the Stefan–Boltzmann constant ( $5.67 \times 10^{-8} \text{ Wm}^{-2} \text{ K}^{-4}$ ),  $T$  (K) is the temperature,  $t$  (s) is the time,  $\alpha$  is the surface albedo,  $I_o$  is the fraction of shortwave radiation flux that penetrates the surface (a fixed value dependent on snow depth),  $F_{sw}$  ( $\text{Wm}^{-2}$ ) is the downwelling shortwave radiative energy flux,  $F_{lat}$  ( $\text{Wm}^{-2}$ ) and  $F_{sens}$  ( $\text{Wm}^{-2}$ ) are the latent heat flux and sensible heat flux, respectively.

CLIMo includes a fixed-depth mixed layer in order to represent an annual cycle. When ice is present, the mixed layer is fixed at the freezing point; and when ice is absent, the mixed layer temperature is computed from the surface energy budget and hence represents a measure of the heat storage in the lake, namely

$$\rho_w C_{pw} d_{mix} \frac{\partial T_{mix}}{\partial t} = F_o + F_{sw} I_o (1 - \alpha) \quad (3.2)$$

where  $T_{mix}$  is the mixed layer temperature and  $d_{mix}$  is the effective mixed layer depth, and  $C_{pw}$  is the specific heat capacity of water (Duguay *et al.*, 2003).

The model can be forced with daily mean or hourly values of air temperature ( $^{\circ}\text{C}$ ), wind speed (m/s), relative humidity (%), cloud cover (in tenth), and snow depth (m). It produces outputs for different snow cover scenarios (0%, 25%, 50%, 75% and 100% of the on-shore snow cover depths) and mixed layer depths. In this study, mean daily values from the meteorological stations, a 50% snow cover scenario (50% less snow on ice surface than measured at the station on land), as well as 10 m (Back Bay and Hay River) and 40 m (GSL Main Basin and GBL near Deline) mixed layer depths were used in the simulations.

### 3.3.4 Fresh Water Lake Model (FLake)

The FLake model (Mironov 2008, Mironov *et al.*, 2010) is a fresh water lake model, which is based on a two-layer water temperature profile, mixed layer at the surface and the thermocline extending from the bottom of the mixed layer to the bottom of the lake. The model is able to predict the surface temperature in lakes of various depths on the time scales

from a few hours to a year. The structure of the stratified thermocline layer is described using the concept of self-similarity (assumed shape) of the temperature-depth curve. The same concept is used to describe the temperature structure of the thermally active upper layer of bottom sediments and of the ice and snow cover. The two-layer parameterization of the vertical temperature profile is:

$$\theta = \begin{cases} \theta_s(t), & \text{at } 0 \leq z \leq h \\ \theta_s(t) - (\theta_s(t) - \theta_b(t))\Phi_\theta(\xi), & \text{at } h \leq z \leq D \end{cases} \quad (3.3)$$

where  $\theta_s(t)$  is the temperature of the upper mix layer of depth  $h(t)$ ,  $\theta_b$  is the temperature at the water-bottom sediment interface ( $z = D$ ).  $\Phi_\theta(\xi) \equiv [\theta_s(t) - \theta(z, t)] / [\theta_s(t) - \theta_b(t)]$  is a dimensionless function of dimensionless depth  $\xi \equiv [z - h(t)] / [D - h(t)]$  that satisfied the boundary conditions  $\Phi_\theta(0) = 0$  and  $\Phi_\theta(1) = 1$ . The equation of heat budget of the mixed layer when  $z$  is between 0 and  $h$  is:

$$h \frac{\partial \theta_s}{\partial t} = \frac{1}{\rho_w c_w} [Q_s + I_s - Q_h - I_h] \quad (3.4)$$

where  $\rho_w$  is the water density,  $c_w$  is the specific heat of water,  $Q_s$  and  $I_s$  are the value of the vertical turbulent heat flux, and the heat flux due to solar radiation, respectively.  $Q_h$  and  $I_h$  are the heat fluxes at the bottom of the mixed layer (Mironov, 2008).

This model is very sensitive to the lake depth and it has been shown that using actual depth in deep lakes can lead to large errors. For the deep lakes, a virtual bottom depth usually at 40-60 m is used in simulations, instead of the real lake depth (Mironov, 2008). FLake does consider the snow cover over the lake ice surface but is not recommended to use. Therefore, the snow albedo is formally set equal to the ice albedo. As with CLIMo, mean daily values of atmospheric forcings were used for simulations with FLake.

### 3.4 Results and discussion

Results of surface temperature, ice thickness and freeze-up/break-up dates are compared between models, MODIS (Terra/Aqua) observation data, and *in situ* measurements from sites on GSL and GBL. The surface temperature results over the two large lakes are first plotted for the complete (full) years (Jan.-Dec.) and then separately for the open-water season (June-

Oct.) and ice-cover season (Nov.-May). Three statistical indices were calculated to assess the lake model results: the relative index of agreement ( $I_a$ ), the mean bias error (MBE), and the root mean square error (RMSE). These indices have been shown to be robust statistical measures for validating model performance (e.g. Wilmott and Wicks, 1980; Hinzman *et al.*, 1998). The  $I_a$  is a descriptive measure applied to make cross-comparisons between models or models and observations. Its value ranges from 0 (worst performance) to one (best possible performance) (Ménard *et al.*, 2002). The MBE was calculated as model minus MODIS results. Hence, a positive (negative) bias indicates that modeled values are warmer (colder) than satellite measurements.

### 3.4.1 Lake Surface Temperature

Modeled  $LST_{lake}$  from CLIMo and FLake are compared in Figure 3.2 with MODIS-derived  $LST_{lake}$  data for the four different sites (Yellowknife (Back Bay), Hay River, GSL (Main Basin), and GBL (Deline)) over the full year (Jan - Dec) from 2002 to 2010. As Figure 3.3 illustrates, both models show a good agreement compared to MODIS when data over the full year are considered ( $0.947 \leq I_a \leq 0.984$ ;  $0.43 \leq MBE \leq 4.46$ ;  $3.93 \leq RMSE \leq 6.56$ ). A complete summary of the statistical indices is presented in Table 3.2. The performance of the two models is not the same on a seasonal basis. Hence, results were also examined separately for the open-water and ice-cover seasons.

**Table 3-2:** Comparison of observed and simulated lake surface temperature for Yellowknife (Back Bay), Hay River, GSL (Main Basin), and GBL (Deline) (2002-2010).

		Back Bay		Hay River		GSL(Main Basin)		GBL (Deline)	
		CLIMo	FLake	CLIMo	FLake	CLIMo	FLake	CLIMo	FLake
Full year	$I_a$	0.984	0.962	0.956	0.949	0.981	0.954	0.975	0.947
	MBE	2.26	0.70	4.25	3.03	0.94	0.43	2.77	4.46
	RMSE	4.30	6.45	6.27	6.30	3.93	6.56	4.45	6.54
Open-water season	$I_a$	0.860	0.858	0.709	0.755	0.922	0.810	0.758	0.627
	MBE	3.10	0.85	5.10	3.47	0.96	2.73	3.49	5.76
	RMSE	4.20	3.53	6.86	6.65	2.78	4.26	4.06	6.20
Ice-cover season	$I_a$	0.948	0.798	0.948	0.873	0.924	0.787	0.929	0.840
	MBE	1.40	0.42	1.22	2.07	0.35	-2.76	1.97	3.25
	RMSE	4.71	9.02	5.11	7.84	5.14	8.76	5.01	7.28

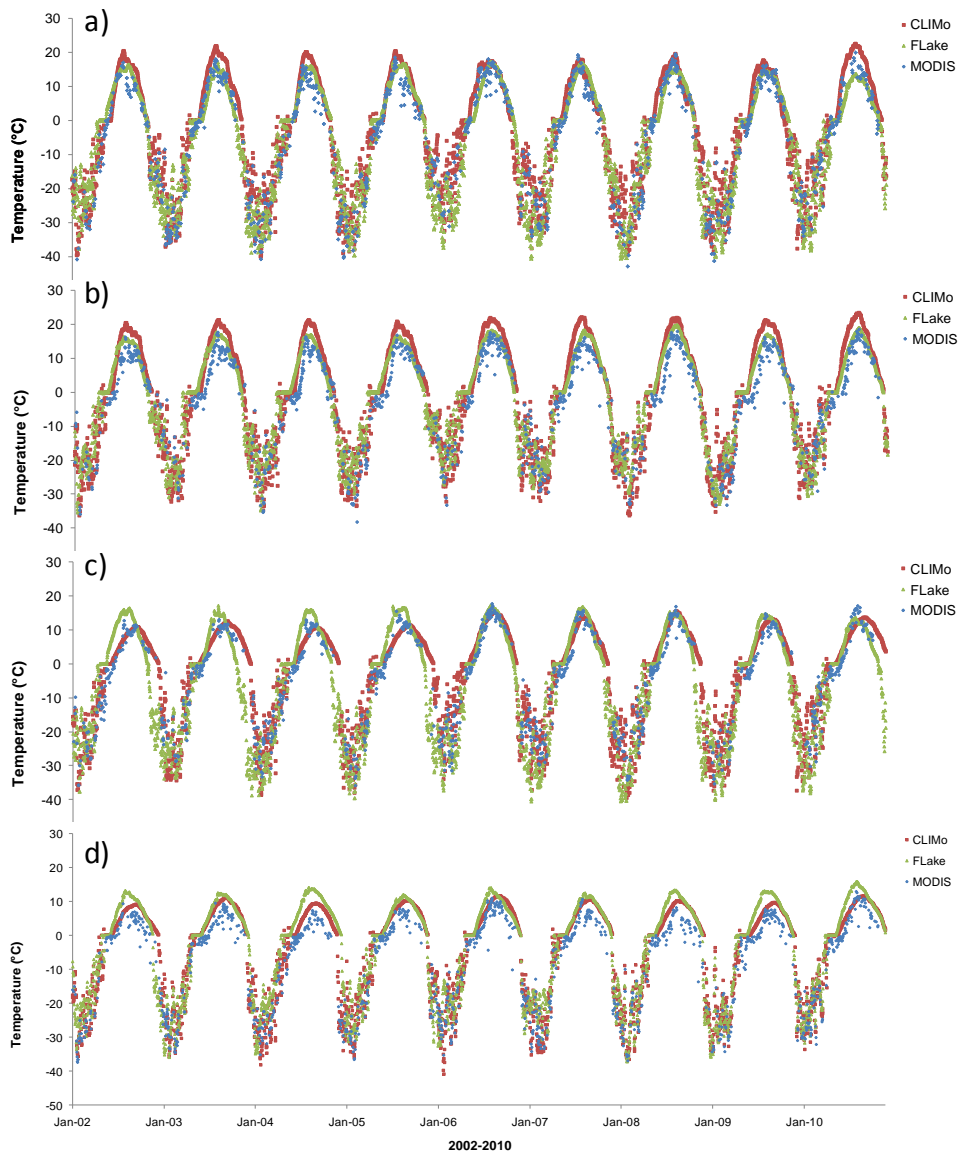


**Figure 3-2:** Comparison of modeled  $LST_{lake}$  from CLIMo and FLake with MODIS-derived  $LST_{lake}$  data during full year for 2002-2010 (a) Yellowknife (Back Bay), (b) Hay River, (c) GSL (Main Basin), (d) GBL (Deline).

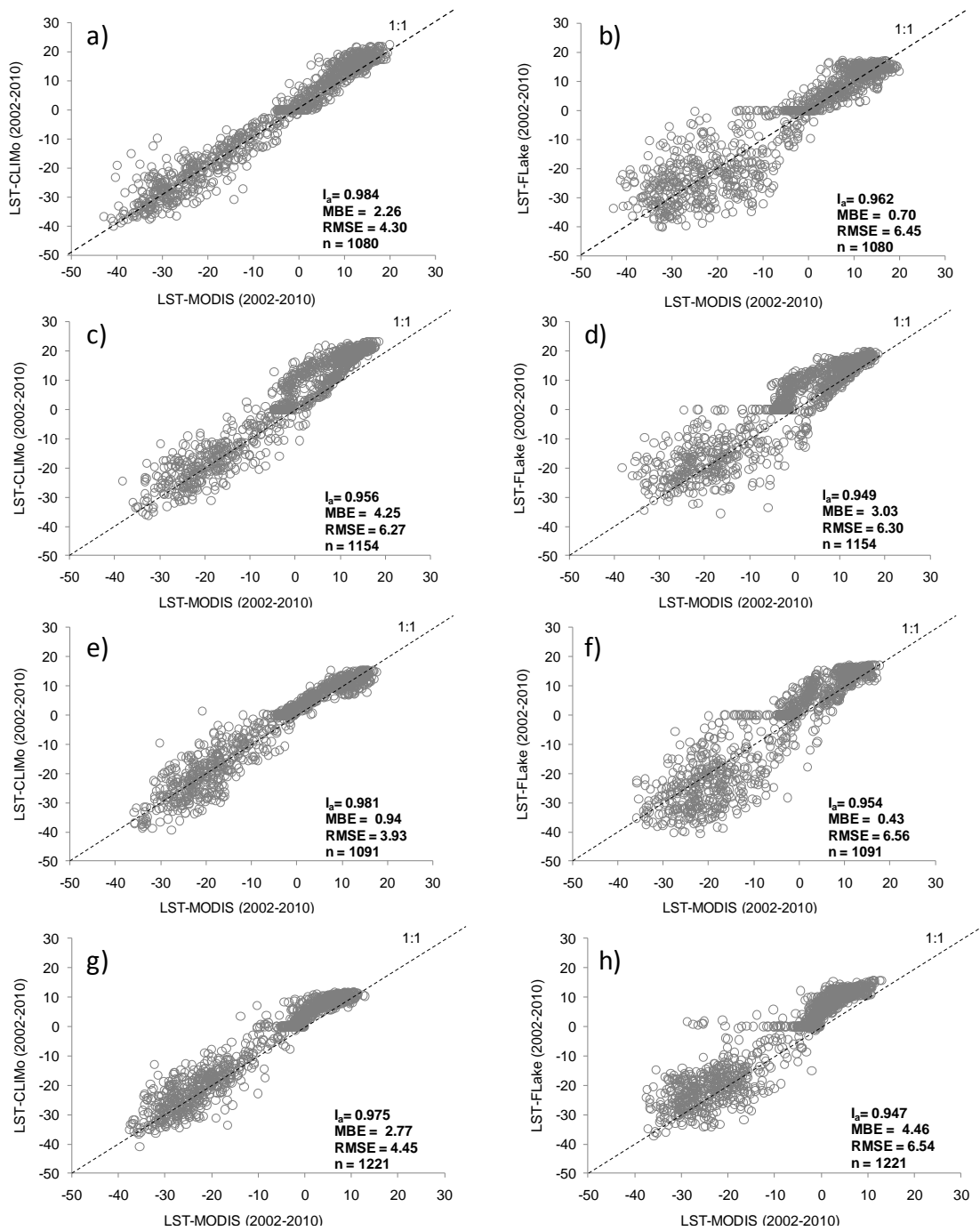


**Figure 3-3:** Comparison of modeled LST<sub>lake</sub> from CLIMo and FLake with MODIS-derived LST<sub>lake</sub> data during full year for 2002-2010 (a,b) Yellowknife (Back Bay) (c,d) Hay River, (e,f) GSL (Main Basin), (g,h) GBL (Deline).

### 3.4.1.1 Open-water Season

The open-water season  $LST_{lake}$  for the four study sites are shown in Figure 3.4. The results show that FLake fits better than CLIMo in Back Bay and Hay River sites with MBE of 0.85 and 3.47 and RMSE of 3.53 and 6.65, respectively (see Figure 3.5). In the model simulations, the lake depths and mixed layer depths (fixed for CLIMo) were chosen as 10 m for both sites. The results for the Hay River site show less agreement compared to Back Bay. As Hay River is located at lower latitude than the Back Bay site, higher surface temperature is observed over this region of the lake. MODIS  $LST_{lake}$  values are on average 3.8 °C higher for Hay River. Another reason for the warmer water temperature at the Hay River site is that the warmer water of the Slave River flows from the south into GSL from Lake Athabasca. The river water flows into the lake with a mean temperature of about 10-14°C above the temperature of maximum density, which increases the temperature of this part of the lake (Schertzer *et al.*, 2008). Howell *et al.* (2009) found that the break-up process of GSL starts first in this part of the lake due to discharge from Slave River. Also, León *et al.* (2007) validated a 3-D lake hydrodynamics model, the Estuary and Lake COmputer Model (ELCOM), by using observed meteorological data and the output from the current Canadian RCM as forcing input to compare the results with observed surface temperatures on GSL. They indicate that there are counter-clockwise dominant circulations patterns around the lake and a large central basin counter-clockwise gyre of the upper layer of this lake. This can at least partly explain the larger differences between simulated and observed  $LST_{lake}$  of Hay River compared to the Back Bay site, as FLake and CLIMo are 1-D models and therefore do not simulate lateral flow of warm water from a river which affects the Hay River site but not the Back Bay site.

CLIMo simulated  $LST_{lake}$  are about 2°C warmer for Back Bay and Hay River compared to those obtained with FLake. The lower agreement of CLIMo during summer may be explained by the fact that this model uses a constant (fixed) open-water season mixed layer depth in each simulation, while MODIS  $LST_{lake}$  capture the effect of the seasonally evolving mixed layer depth on the water surface temperature. The mixed layer depth is

greater in late fall/early winter than summer, and depends on the water density and wind (Schertzer *et al.*, 2008). The increased temperature during the summer period leads to more stable density stratification and reduces the penetration of wind-driven mixing. The lake water has the highest density just before freeze-up and leads to reduction in stability; therefore, the mixed layer increases in winter before an ice sheet is formed on the water body (Schertzer *et al.*, 2008). The thermocline layer in GSL deepens almost monotonically from June-July to the period of complete mixing achieved in late September-October as the temperature decreases due to increase of surface heat losses to the atmosphere (Rouse *et al.*, 2007a). On the other hand, the depth of the mixed layer is not equal year round. However, as alluded to earlier, the mixed layer is fixed in CLIMo during the whole open-water season. Obviously, this factor will have an impact on the seasonal evolution of open-water  $LST_{lake}$  calculated by this model compared to those either measured *in situ* or from MODIS.

Given the above, it is interesting to see that  $LST_{lake}$  from CLIMo agree better with MODIS than those obtained with FLake for the two deepest lake sites (40 m) (FLake -  $I_a$ : 0.810 and 0.627, MBE: 2.73 and 5.76, RMSE: 4.26 and 6.20; CLIMo -  $I_a$ : 0.922 and 0.758, MBE: 0.96 and 3.49, and RMSE: 2.78 and 4.06 for GSL Main Basin and GBL, respectively). This may be explained by the high sensitivity of FLake model to lake depth. The model does not allow for the hypolimnion layer between the thermocline and the lake bottom as it is based on two layer water temperatures. Martynov *et al.* (2010) showed that the Hostetler and FLake models perform well in small and shallow lakes, while strong differences are found between simulated and observed surface temperatures for the deeper Great Lakes of North America. CLIMo does not suffer from that similar problem as it has been shown to perform well for both shallow and deep lakes (Ménard *et al.*, 2002; Duguay *et al.*, 2003). However, one drawback, unlike FLake, is that the depth of the mixed layer must be specified and remains fixed for the entire open-water season.

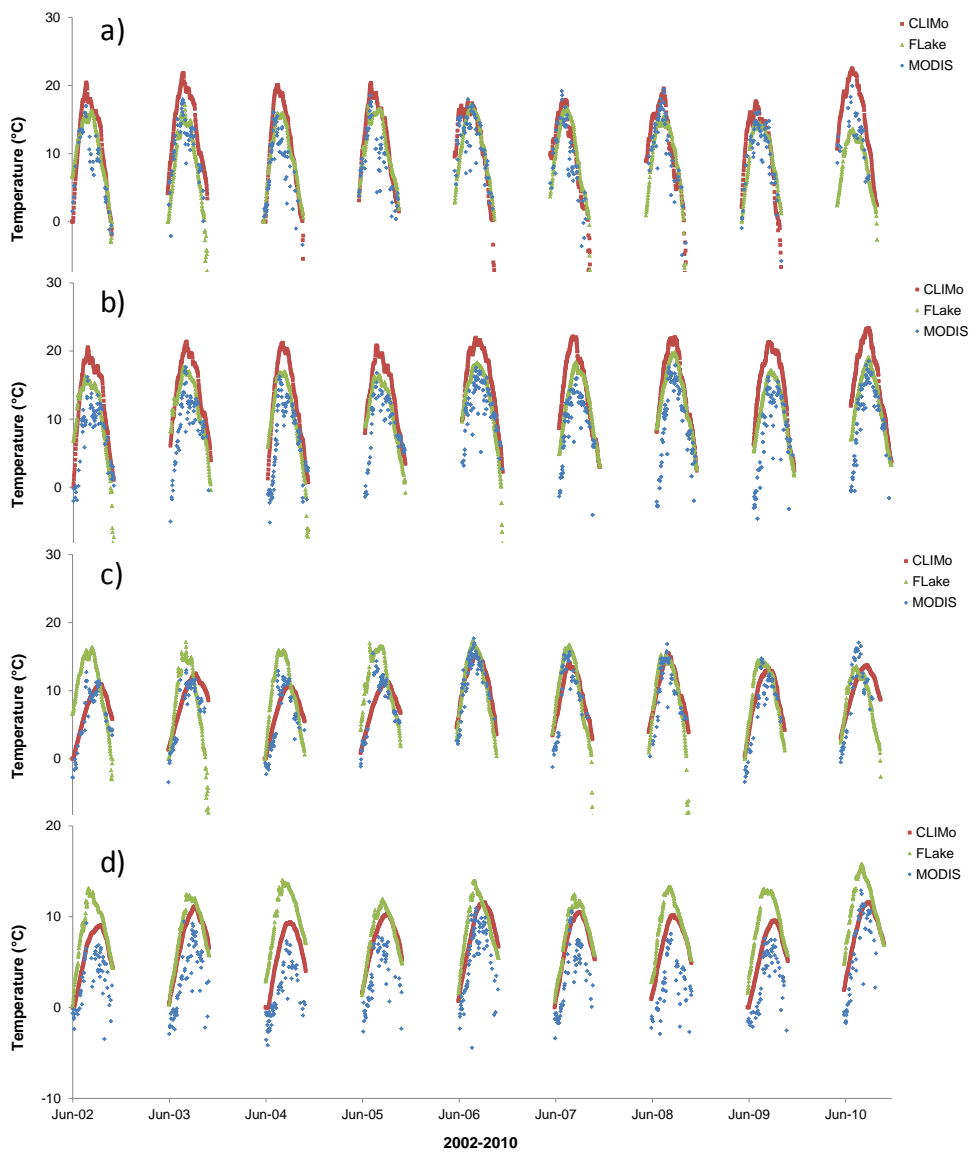


**Figure 3-4:** Comparison of modeled  $LST_{lake}$  from CLIMo and FLake with MODIS-derived  $LST_{lake}$  data during open-water season for 2002-2010 (a) Yellowknife (Back Bay), (b) Hay River, (c) GSL (Main Basin), (d) GBL (Deline).

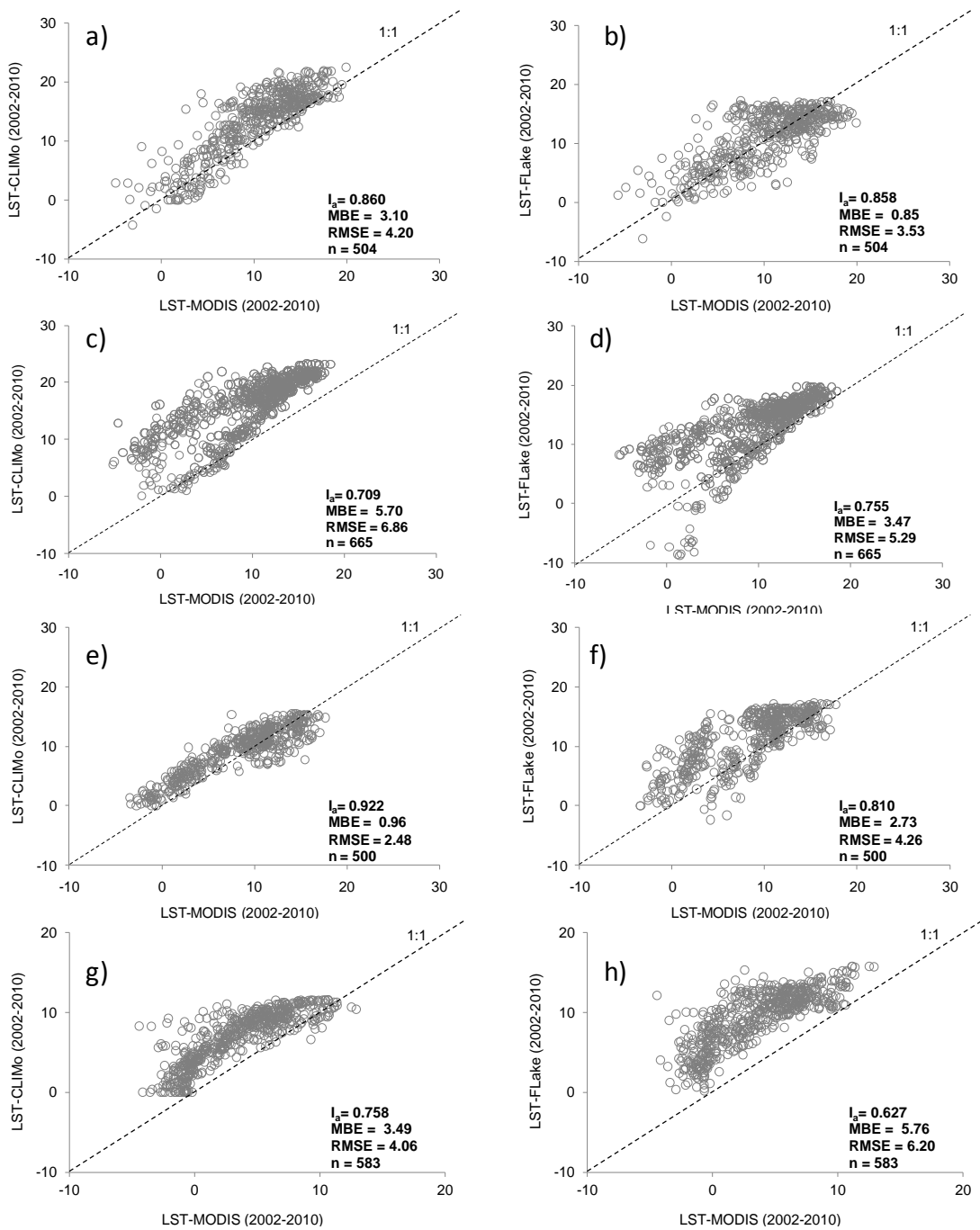
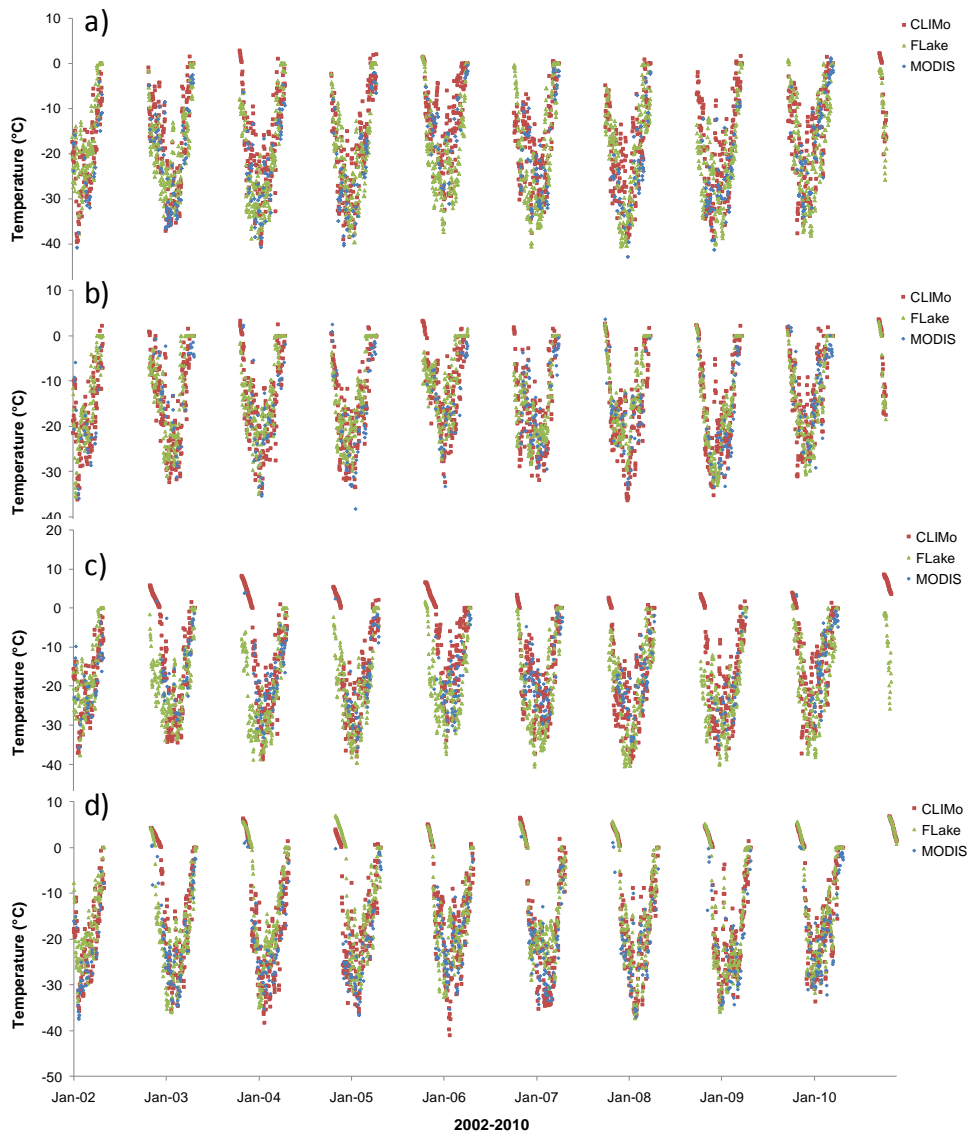


**Figure 3-5:** Comparison of modeled LST<sub>lake</sub> from CLIMo and FLake with MODIS-derived LST<sub>lake</sub> data during open-water season for 2002-2010 (a,b) Yellowknife (Back Bay) (c,d) Hay River, (e,f) GSL (Main Basin), (g,h) GBL (Deline).

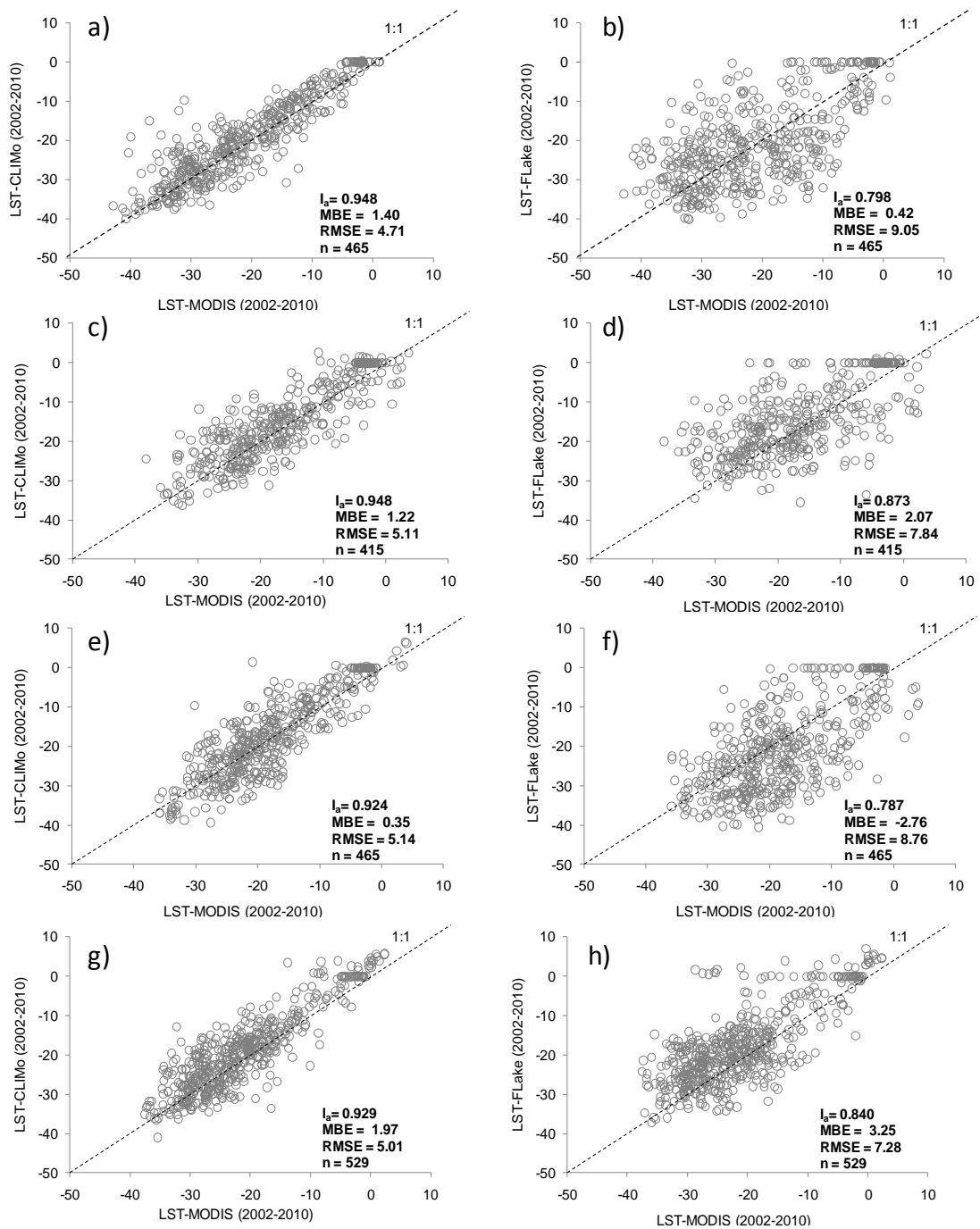
### 3.4.1.2 Ice-cover Season

Figure 3.6 shows simulated  $LST_{lake}$  values from models against MODIS-derived  $LST_{lake}$  during the ice-cover season. As apparent in this Figure, CLIMo  $LST_{lake}$  are closer than those of FLake with MODIS observations for all lake sites. As seen in Figure 3.7, the agreement between CLIMo simulated and MODIS  $LST_{lake}$  is strong with  $I_a$ /MBE/RMSE of 0.948/1.40/4.71 for Back Bay, 0.948/1.22/5.11 for Hay River, 0.924/0.35/5.14 for GSL (Main Basin), and 0.929/1.97/5.01 for GBL. MODIS shows relatively lower temperatures compared to the models, which can be partly explained by the time difference between the temperatures retrieved with MODIS and used to calculate daily averages in comparison with temperature measurements from weather stations that are used as input parameter in the models. Average daily air temperatures from meteorological stations are calculated from half hourly measurements but the crossing times for MODIS-Terra and MODIS-Aqua are at specific times at day and night, therefore not spread evenly over a full day. Average daily MODIS  $LST_{lake}$  are generated when there are at least one day and one night observation under clear-sky conditions. It is possible that the calculated average comes from colder daytime or night time acquisitions. Another reason for the colder MODIS  $LST_{lake}$  can be explained by the presence of undetected clouds. The standard MODIS cloudmask product is used to create the MODIS  $LST_{lake}$  L2 product. However, occasional undetected (cold) clouds exist in all cloudmask products. There is a 99% confidence for clear pixels but there is still some uncertainty, and it is possible that cloud top temperatures are measured rather than  $LST_{lake}$ . Langer *et al.* (2010) presented surface temperature measurements from a field-deployed thermal infrared camera to evaluate MODIS L2 data at a Siberian polygonal tundra site. They found several erroneous measurements occur in the MODIS  $LST_{lake}$  data during cloudy conditions (5 to 15 K colder temperatures from MODIS compared to those measured with the thermal camera).

Another important factor that has a direct impact on the models' simulated  $LST_{lake}$  is snow depth on the ice surface. As it was shown in section 3.3, FLake does not consider snow on ice, which is the primary reason for the weaker performance of this model (lower  $I_a$  and



**Figure 3-6:** Comparison of modeled  $LST_{lake}$  from CLIMo and FLake with MODIS-derived  $LST_{lake}$  data during ice-cover season for 2002-2010 (a) Yellowknife (Back Bay), (b) Hay River, (c) GSL (Main Basin), (d) GBL (Deline).



**Figure 3-7:** Comparison of modeled  $LST_{lake}$  from CLIMo and FLake with MODIS-derived  $LST_{lake}$  data during ice-cover season for 2002-2010 (a,b) Yellowknife (Back Bay) (c,d) Hay River, (e,f) GSL (Main Basin), (g,h) GBL (Deline).

higher RMSE values) during the winter season. In CLIMo, a 50% snow cover scenario was used in simulations during the ice-cover season. This explains its better performance as 50-70% of the snow measured at meteorological stations on land is generally a good average approximation of snow depth on open lake ice surfaces (Brown and Duguay, 2011). Snow depths vary within the 1 km pixels of MODIS and this is reflected in the satellite-retrieved  $LST_{lake}$ , as conductive heat flow through lake ice is a strong function of snow depth and density (Jeffries and Morris, 2006). Thicker snow results in lower conductive heat transfer from the ice/water interface to the air/snow interface. Consequently, snow cover will influence the surface temperature over the lake during the ice-cover season.

### **3.4.2 Ice thickness and phenology (Back Bay, Great Slave Lake)**

#### *3.4.2.1 Ice Thickness*

Figure 3.8 shows the simulated ice thickness from both models in comparison with *in situ* measurements for the period 1961-2008 at the Back Bay site. This is the only one of the four sites with a sufficiently long historical record for adequate comparison with model results, although there are missing data from 1996 to 2002. Results indicate a strong agreement between *in situ* measurements and CLIMo ( $I_a = 0.943$ , MBE = 9 cm, RMSE = 17 cm), and a lower agreement with FLake ( $I_a = 0.765$ , MBE = 26 cm, RMSE = 39 cm). As indicated earlier, FLake does not consider snow depth over lake ice. The accumulation of snow influences ice growth and thaw rates by adding an insulation layer. Previous results with CLIMo show that most of the variability in ice thickness and break-up dates is explained by snow on ice (Duguay *et al.*, 2003). In the FLake model, ice thickens more rapidly and also thaws faster compared to CLIMo and *in situ* measurements. The snow over the ice buffers the ice surface from the cold air above; consequently, temperature at the bottom of snow is higher and less variable than the air temperature, and therefore ice grows at a slower rate than in the absence of snow (Jeffries and Morris, 2006).

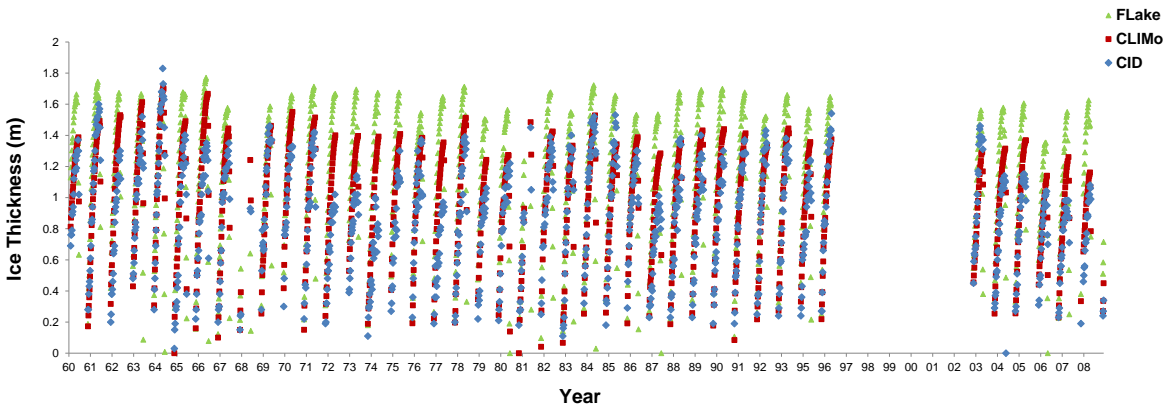


**Figure 3-8:** Comparison of observed (CID) and simulated (CLIMo and FLake) Ice thickness for Back Bay (1961-2008).

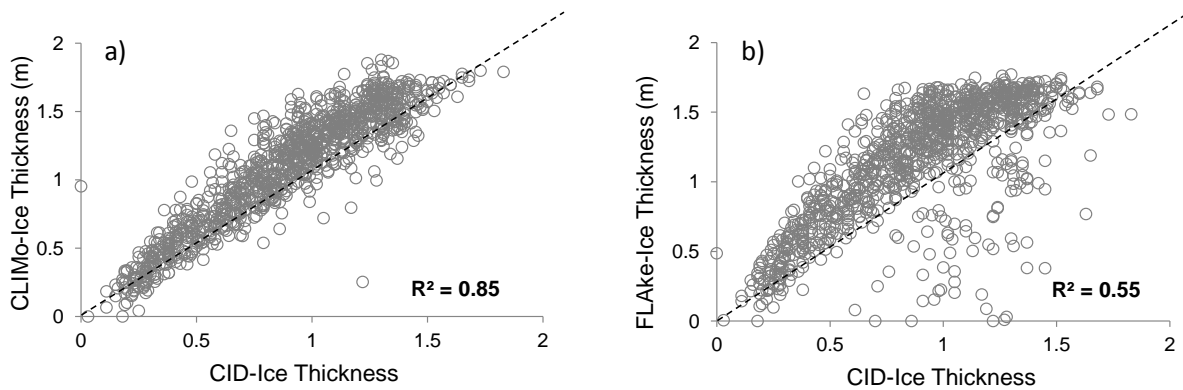


**Figure 3-9:** Comparison of observed (CID) and simulated Ice thickness for Back Bay (a) CLIMo, (b) FLake (1961-2008).

### 3.4.2.2 Freeze-up/break-up

Both lake models reproduce freeze-up and break-up dates very well for Back Bay over the entire time series of observations (Figures 3.10 and 3.11). As the FLake does not consider the insolation effect of snow, it grows ice faster but it also melts it faster. Break-up dates simulated with FLake model are therefore on average 5 days earlier (MBE = -5 days) compared with *in situ* observations, which is 3 days later in CLIMo. In the presence of snow, the absorbed solar radiation is lower due to a higher albedo. As a result, the absence of snow will lead to the absorption of more solar radiation, and result in earlier break-up. For freeze-up dates, results between FLake (MBE = 1 day, RMSE = 7 days) and CLIMo (MBE = 2

days, RMSE = 7 days) are very similar when compared to observations. An important factor on freeze-up dates is the lake depth (and depth of mixed layer). The greater the value, the longer it takes for the ice-cover to form. Ménard *et al.* (2002) showed that the best results with CLIMo are obtained with a mixed layer depth of 10 m for Back Bay, which is also the case for FLake.

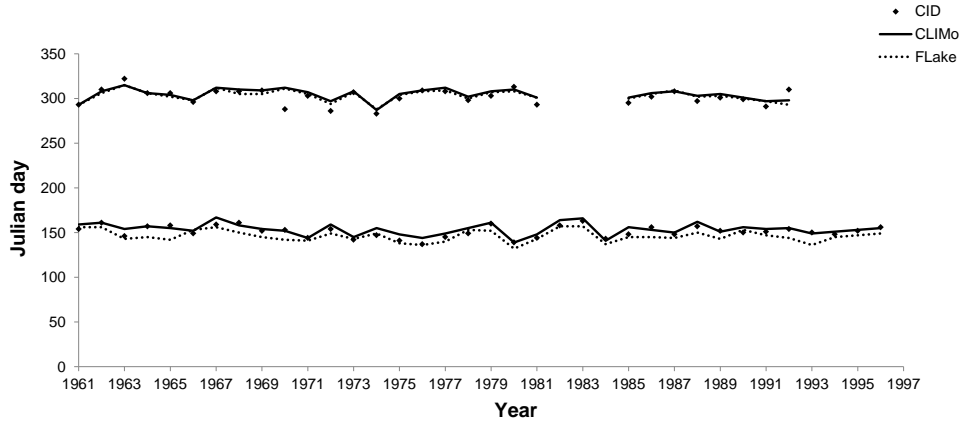


**Figure 3-10:** Comparison of observed (CID) and simulated (CLIMo and FLake) freeze-up and break-up dates for Back Bay (1961-1996).

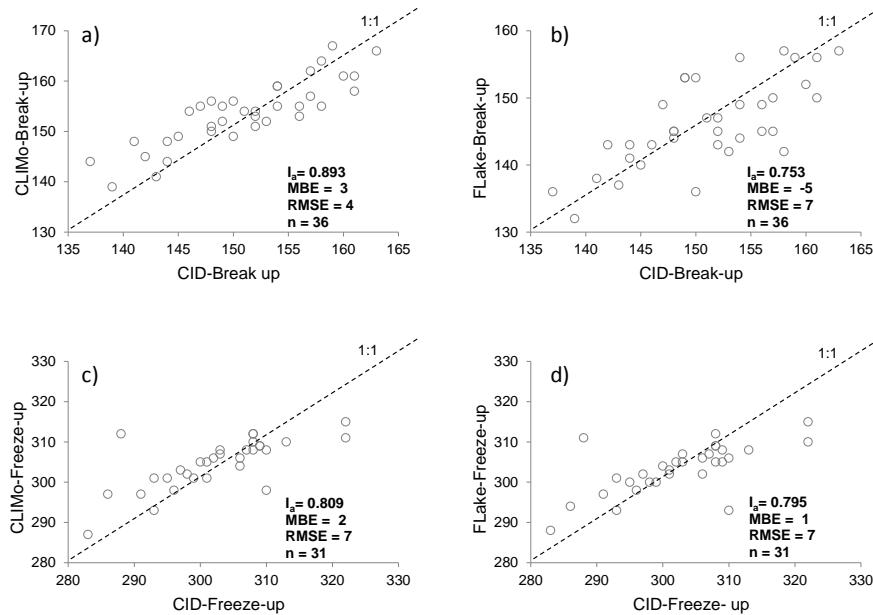


**Figure 3-11:** Comparison of observed (CID) and simulated (CLIMo and FLake) (a,b) break-up, (c,d) freeze-up dates for Back Bay (1961-1996).

### 3.5 Summary and Conclusion

Two 1-D lake models (CLIMo and FLake) were applied to simulate surface temperature, ice thickness and phenology on GSL and GBL. Data from three weather stations (Yellowknife, Hay River and Deline) were used as input for model simulations, and MODIS-Terra/Aqua  $LST_{lake}$  products as well as *in situ* ice observation sites on GSL were utilized to evaluate the model results. The simulations conducted for a nine-year period (2002-2010) have shown that both models are capable of reproducing the seasonal and inter-annual evolution of surface temperatures of the lakes as well as the inter-annual variations in ice thickness and freeze-up/ break-up dates.  $LST_{lake}$  over both lakes changes in different seasons during summer and winter seasons with the higher temperature in summer and colder temperature in winter. Both lakes are located at high latitude and are frozen for a considerable part of the year, so that the atmosphere does not always directly communicate with the lake water. Lake-atmosphere interactions occur for several months through the air-ice interface or, if snow is present, at the air-snow interface.

The CLIMo demonstrated a generally better performance than the FLake model in the case of GSL and GBL, especially for ice-cover season, when compared to MODIS and *in situ* measurements. The absence of snow in the FLake model had a large effect on ice growth and decay rates and thus, by extension, ice break-up dates. As the FLake model is based on two-layered structure, it does not allow for the formation of the hypolimnion layer in deep lakes. As a result, open-water temperature for the deepest lake sites (40 m) tended to be underestimated. MODIS data showed generally colder temperatures compared to models, which could be explained to some extent by undetected clouds (erroneous measurements during cloudy conditions) and the time differences of the MODIS  $LST_{lake}$  used to calculate clear-sky daily averages, compared to the daily air temperatures from weather stations used as forcing data in models. Cloud contamination has been identified as a source of occasional (low temperature) errors in MODIS products. To minimize this problem, averaging of  $LST_{lake}$  over longer time periods (weekly or monthly) merits to be further examined.

Overall, MODIS showed a very good agreement with the models when calculating statistics over a full annual cycle. Although biases were larger when years were broken down into the open-water and ice-cover seasons, results indicate that  $LST_{lake}$  data from MODIS or other thermal infrared satellite sensors such as AATSR are a promising data source for calibrating/evaluating lake models, as well as for data assimilation into NWP models. Evaluation of the accuracy of satellite-derived  $LST_{lake}$  is also needed for northern lakes as previous investigations have tended to focus on mid-latitude lakes during the open-water season only.

## Chapter 4

### **Analysis of lake and land surface temperature patterns during the open-water and snow/ice growth seasons in the Great Bear and Great Slave Lake regions, Canada, from MODIS (2002-2010)**

#### **Overview**

Lakes influence local and regional climates and circulation of the atmosphere. Air-water exchanges of heat and moisture have climatological implications for lakes and also the climate in the vicinity of the lakes. Temperature changes in lakes are strongly influenced by changes in seasonal air temperature. Daily temperature variations also affect the temperature of lakes, especially in the surface layers. The most practical way to obtain continuous measurements of surface temperature is by means of satellite remote sensing. In this study, satellite-derived lake/land surface temperature ( $LST_{\text{land/lake}}$ ) products from the Moderate Resolution Imaging Spectroradiometer (MODIS) aboard the Earth Observing System Terra and Aqua satellite platforms are used to analyze and contrast lake and land surface temperature patterns during the open-water and snow/ice growth seasons (2002-2010) in the Great Bear Lake (GBL) and Great Slave Lake (GSL) regions, Northwest Territories, Canada. Land and lake temperatures from MODIS are first compared with near-surface air temperature measurements obtained from three weather stations (Yellowknife, Hay River, and Deline) and from moorings installed in GBL.

Results show a strong agreement between satellite and station-based measurements. The analysis of spatiotemporal temperature patterns from MODIS reveals that the surface water temperature of lakes varies in a general way with depth and is colder than the surrounding land from April to August. It becomes equivalent to that of land in August and then becomes warmer starting in September until spring thaw. During the winter ice growth season, lakes lose heat by conduction through the upper ice/snow surface due to the gradient from the relatively warmer water below the ice to the colder air above the ice/snow interface. For this period, lakes remain warmer than land until spring break-up. For a few weeks,

between the onset of break-up until lakes become free of ice, land is warmer since spring melt proceeds more quickly on land than on lakes.

#### **4.1 Introduction**

Water temperature of large lakes is a good indicator of climate change (Livingstone, 2003) and has a significant impact on local water and energy balances (Long *et al.*, 2007). Water transports and stores heat, and plays an essential role in energy and water exchanges with the atmosphere. The linkages and feedbacks between lakes and surrounding terrestrial areas result in a dynamic coupled system and are sensitive to climatic changes (Blanken *et al.*, 2008). Lakes act as a heat sink during spring/summer when the land is a source of heat and inverse in fall/winter (Blanken *et al.*, 2008). They tend to reduce the fluxes of surface latent and sensible heat in summer and increase the latent and sensible heat fluxes in fall (Long *et al.*, 2007). The greater the size of the lake, the greater its effect is on climate.

The large number of lakes in the Mackenzie River Basin (MRB), Northwest Territories, Canada, plays an important role in the energy and water cycle. This study was carried out on three lakes located on subarctic continental climate in the MRB and contrasting their surface temperature evolution with that of the surrounding land. Two of the lakes are large and deep, Great Slave Lake (GSL; 60.50 °N, 114.60 °W) and Great Bear Lake (GBL; 65.10 °N, 123.30 °W) (Figure 4.1), while the third one, Duncan Lake (62.09 °N, 114 °W) is of medium size. From previous literature in this region, Rouse *et al.* (2007a) studied the sensitivity of energy and moisture exchanges between lakes and the atmosphere. They found that the presence of large lakes in the MRB region substantially decreases the inter-annual variability in evaporation totals. The cross-lake spatial variation in the bathymetry, water temperature, and meteorology of GSL was detailed by Schertzer *et al.* (2000) and followed by investigations of specific processes behind turbulent exchange (Blanken *et al.*, 2003), the inter-annual and seasonal variability of the surface energy balance (Rouse *et al.*, 2003a), and the lake's heat content and thermal mixing properties (Schertzer *et al.*, 2003). Blanken *et al.* (2008) also examined the influence of time scale on the magnitude and

controls of evaporation. However, much of this work has relied on *in situ* measurements which provide a good temporal resolution but a limited spatial coverage.

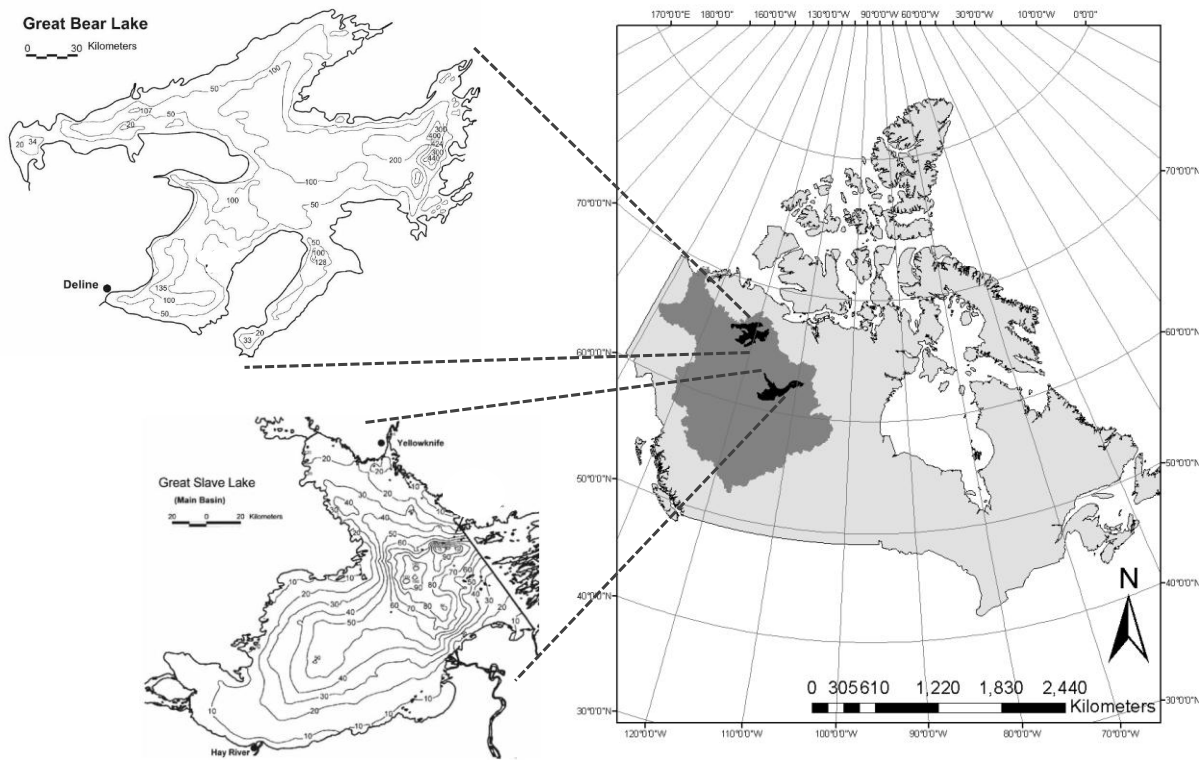


**Figure 4-1:** Bathymetry of GSL (Source: Schertzer *et al.*, 2000) and GBL (Source: Johnson 1994). Depth contours are in metre.

Remote sensing is becoming a promising data source for the study of lakes since it provides frequent data that can be used to estimate surface temperature and ice-cover over large and remote areas of the globe. Kheyrollah Pour *et al.* (accepted) investigated the agreements and differences between satellite-derived Lake Surface Temperature ( $LST_{lake}$ ) derived from the Moderate Resolution Imaging Spectroradiometer (MODIS) Terra and Aqua thermal infrared (TIR) data with surface water temperature simulated with the Canadian Lake Ice Model (CLIMo) and the Fresh-water Lake (FLake) model. MODIS-derived and simulated  $LST_{lake}$  for different lake depths in GSL and GBL (2002-2010) showed a good

agreement between when data were examined over a full annual cycle or broken down into open-water and ice-cover seasons. Results in the main basin of GSL showed a mean bias error of 0.94 °C and 0.43 °C for CLIMo and FLake, respectively, in comparison with MODIS. Crosman and Horel (2009) found a bias of -1.5 °C between MODIS-derived  $LST_{lake}$  (L2) and *in situ* measurements from buoys deployed in Great Salt Lake, Utah. Studies on Lake Tahoe, California, using Envisat/Advanced Along Track Scanning Radiometer (AATSR) also revealed an average bias (AATSR minus *in situ*) of -0.17 °K, a standard deviation of 0.37 °K, and root mean square error of  $\pm 0.41$  °K (Coll *et al.*, 2009), which was -0.007 °C and 0.32 °C (*in situ* minus satellite retrieval) using MODIS-Terra, and 0.001°C and 0.19°C ATSR-2 (Schneider *et al.*, 2009).

In this study, MODIS-derived surface temperature data are used to analyze lake and land surface temperature patterns during the open-water and snow/ice growth seasons in the GBL and GSL regions. The objectives are to: 1) evaluate and compare the MODIS L3  $LST_{land}$  with near-surface air temperature obtained from three weather stations; 2) evaluate and compare the MODIS L2  $LST_{lake}$  with *in situ* observations obtained from temperature moorings; 3) examine the value of MODIS for studying lake surface temperature dynamics and factors that influence the variation of surface temperature at different depths of the lakes, especially over GSL and GBL; and 4) analyze and contrast surface temperature differences between lakes and land annually and seasonally.

## 4.2 Data and Methods

MODIS Terra and Aqua Land Surface Temperature and Emissivity (MOD11\_L2, collection 5, 1 km) data were acquired from the NASA Land Processes Distributed Active Archive Center (LP DAAC) for the period 2002-2010. These data were produced using the generalized split window approach (Wan & Dozier, 1996) and the MODIS sensor radiance data product (MOD021KM), the geolocation product (MOD03), the atmospheric temperature and water profile (MOD07\_L2), the cloud mask (MOD35\_L2), the quarterly land cover (MOD12Q1), and snow product (MOD10\_L2). The  $LST_{land/lake}$  retrieval in a MODIS swath is

made by using L1B radiance data in bands 31 and 32 on land or inland water under clear-sky conditions with a confidence  $\geq 95\%$  over land  $\leq 2000$  m or  $\geq 66\%$  over land  $> 2000$  m, and at a confidence of  $\geq 66\%$  over lakes (Wan, 2005).

MODIS L3 LST<sub>land/lake</sub> daily, weekly, and monthly average Terra and Aqua products were generated over all territories above 55°N from MODIS L2. For a more detailed explanation of the methodology, the reader is referred to Kheyrollah Pour *et al.* (accepted). The new L3 products were first evaluated and compared with *in situ* temperature measurements (daily; L2 data for hourly), and then used to analyze seasonal (monthly) surface patterns for lakes and land. Occasionally, MODIS products deviate strongly from *in situ* measurements, which can be due to the presence of clouds undetected by MODIS. In such situation cloud top temperatures are measured rather than land surface temperatures (Langer *et al.*, 2010). Appendix I presents a suite of MODIS images acquired over GBL at times when clouds were undetected by the algorithm used to produce cloud masks. For this reason, care was taken to filter as much as possible MODIS LST data from undetected cloudy days prior to analysis.

#### **4.2.1 Comparison of MODIS LST<sub>land</sub> with Near Surface Air Temperature**

The MODIS LST<sub>land</sub> products were evaluated against 2-m screen height mean daily air temperature measurements from weather stations located near the shore of GSL and GBL: the Yellowknife Airport weather station located close to the north shore of GSL (62.28 °N, 114.27 °W); the Hay River station on the southwest shore of GSL (60.50 °N, 115.47 °W); and the Deline station situated on the southwest shore of GBL (near Keith Arm of GBL). In this evaluation, five MODIS pixels (1 km) were chosen close to the weather stations in open shrubland, as classified in the MODIS Terra land cover type product (MOD12Q1), and daily LST<sub>land</sub> were calculated by averaging these five pixels.

#### **4.2.2 Comparison of MODIS LST<sub>lake</sub> with *In situ* Lake Temperature**

The MODIS retrieved LST<sub>lake</sub> products were also evaluated against *in situ* measurements from three temperature moorings in GBL, which were deployed in Keith Arm (southwest

arm of GBL). Since the *in situ* water temperature measurements were made on an hourly basis, MODIS L2 LST<sub>lake</sub> data from daytime and nighttime overpasses acquired within the hour of these measurements were compared. Comparison took place when the moorings data were available from mid-July to September 2008. The *in situ* temperature measurements were obtained at different water depths in the lake from 0.5 m to 100 m (station 1 at 65 11' 25" °N, 122 37' 39" °W; station 2 at 65 10' 00" °N, 121 52' 03" °W; and station 3 at 65 24' 31" °N, 122 12' 26" °W). In this study, temperatures taken at a depth of 0.5 m were used as MODIS provides surface “skin” temperatures of the lake. Unfortunately, no *in situ* measurements were available for comparison at GSL at the time of writing of this thesis.

#### **4.2.3 Lake Depth versus Lake Surface Temperature**

The MODIS-derived mean monthly LST<sub>lake</sub> product was analyzed over GSL to determine if a general relation existed between lake depth and lake surface temperature. To examine this, pixels were selected in different areas of the lake (one pixel per different depth from 10 to 120 m) based on known bathymetry (Rouse *et al.*, 2008). Monthly LST<sub>lake</sub> maps were generated first for January-December 2003 to study LST<sub>land/lake</sub> variations in different seasons and then maps were produced for the months of July and January 2002-2010 to compare the LST<sub>lake</sub> variations in specific seasons, summer and winter, in various years, where the variation between LST<sub>lake</sub> at different depths. It was hypothesized that July (mid-summer) lake temperatures would show the largest differences between depths, and that this relation would also be visible during the early ice season (January) when the ice is still thin enough to show the influence of depth via conductive heat flow through the ice/snow interface. CLIMo (Duguay *et al.*, 2003), a 1-D thermodynamic ice model, was used to help interpret LST<sub>lake</sub> with variations in thermal conductivity during the ice-cover season.

#### **4.2.4 Lake and Land Surface Temperature Variations in the GSL Region**

Lake and surrounding land surface temperatures were analyzed and contrasted for the GSL region using the MODIS monthly average product. One medium size lake (Duncan Lake) and GSL were chosen. The pixels over Duncan Lake were taken in an area of ~23 m depth

and pixels over GSL were from an area with depth of ~70 m in the main lake basin. Land pixels were chosen from the open shrubland around the two lakes. The purpose of this analysis was to investigate differences (annually at a monthly time step) in the surface thermal regime of lakes of different sizes/depths and the surrounding land.

### **4.3 Result and Discussion**

#### **4.3.1 Comparison of MODIS $LST_{land}$ with Near Surface Air Temperature**

MODIS-derived daily  $LST_{land}$  versus daily averaged air temperature obtained from the Yellowknife, Hay River and Deline weather stations for the period 2002-2010 are shown in Figures 4.2a, 4.3a, and 4.4a. The MODIS temperatures shown in these Figures correspond to 1343, 1381 and 1437 average daily values calculated from day/night observations over the 9-year period for the Yellowknife, Hay River, and Deline stations, respectively. Comparison between satellite and station data shows a mean bias error (MBE) of  $-2.34$  °C,  $-2.22$  °C, and  $-0.91$  °C with the root mean square error (RMSE) of  $\pm 3.42$  °C,  $\pm 3.31$  °C, and  $\pm 2.7$  °C for Yellowknife, Hay River, and Deline stations, respectively. The negative bias indicates that the satellite measurements tend to be colder than air temperature measured at the stations. The relative index of agreement between satellite and *in situ* data ( $I_a$ , a descriptive measure applied to make cross-comparisons between two observations methods and varying between 0 and 1, e.g. Wilmott and Wicks, 1980; Hinzman *et al.*, 1998) shows a value close to the best possible performance with 0.991 for Yellowknife, 0.990 for Hay River, and 0.993 for Deline (see Figures 4.2b, 4.3b, and 4.4b). These high values are indicative of a high degree of synchrony between the two sets of measurements.

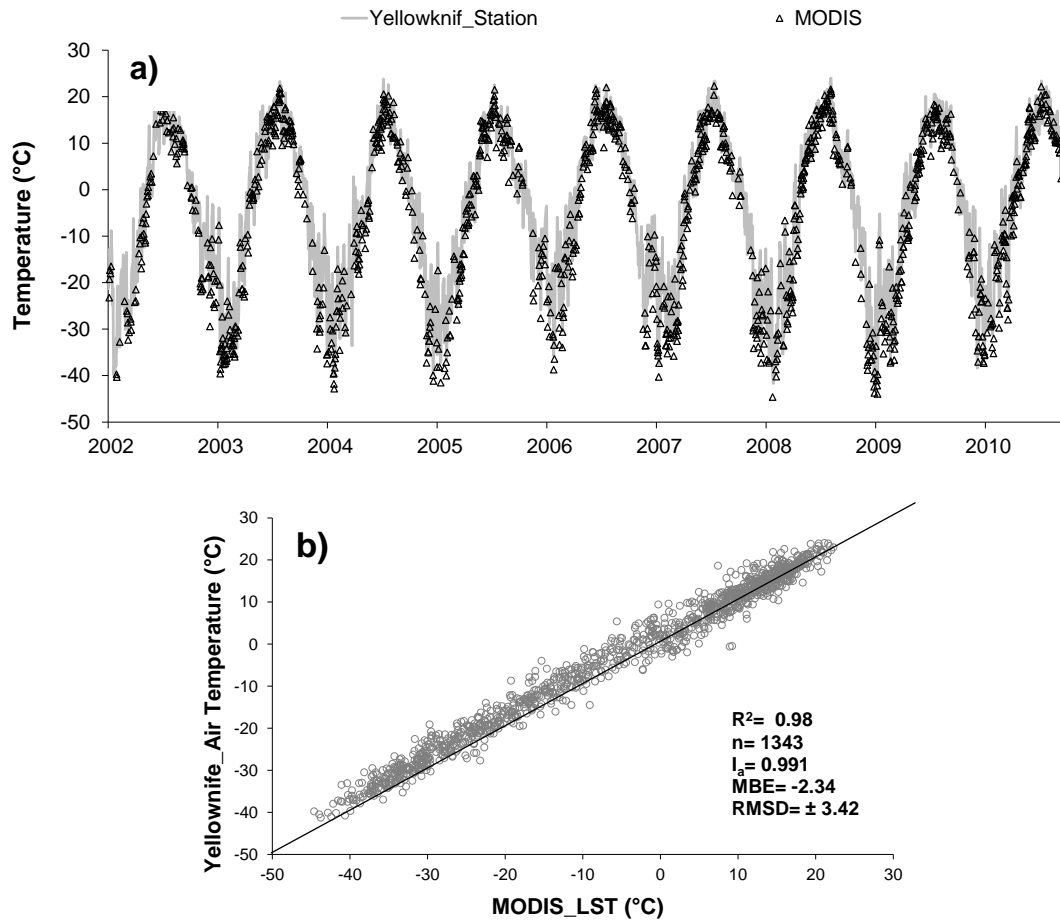


**Figure 4-2:** Time series comparison (a) and the relation (b) between  $LST_{land}$  -derived from MODIS and the air temperature at 2 m above the ground surface for Yellowknife weather station.

The reason that satellite data show colder temperatures over land is that MODIS measures a skin temperature in comparison to stations that measure temperature at about 2 m above the ground. The land surface cools and warms faster compared to the air. Results show a better fit when the temperature is above zero (MBE = -1.48 °C, RMSE =  $\pm 2.48$  °C for Yellowknife, MBE = -1.64 °C, RMSE =  $\pm 2.76$  °C for Hay River, and MBE = -0.17 °C, RMSE =  $\pm 2.45$  °C for Deline). In winter, land is covered by snow and ice. Consequently, MODIS shows a larger bias compared to the stations (MBE = -3.35 °C, RMSE =  $\pm 3.96$  °C

for Yellowknife, MBE = -3.03 °C, RMSE = ±3.71 °C for Hay River, and MBE = -3.01 °C, RMSE = ±3.56 °C for Deline).

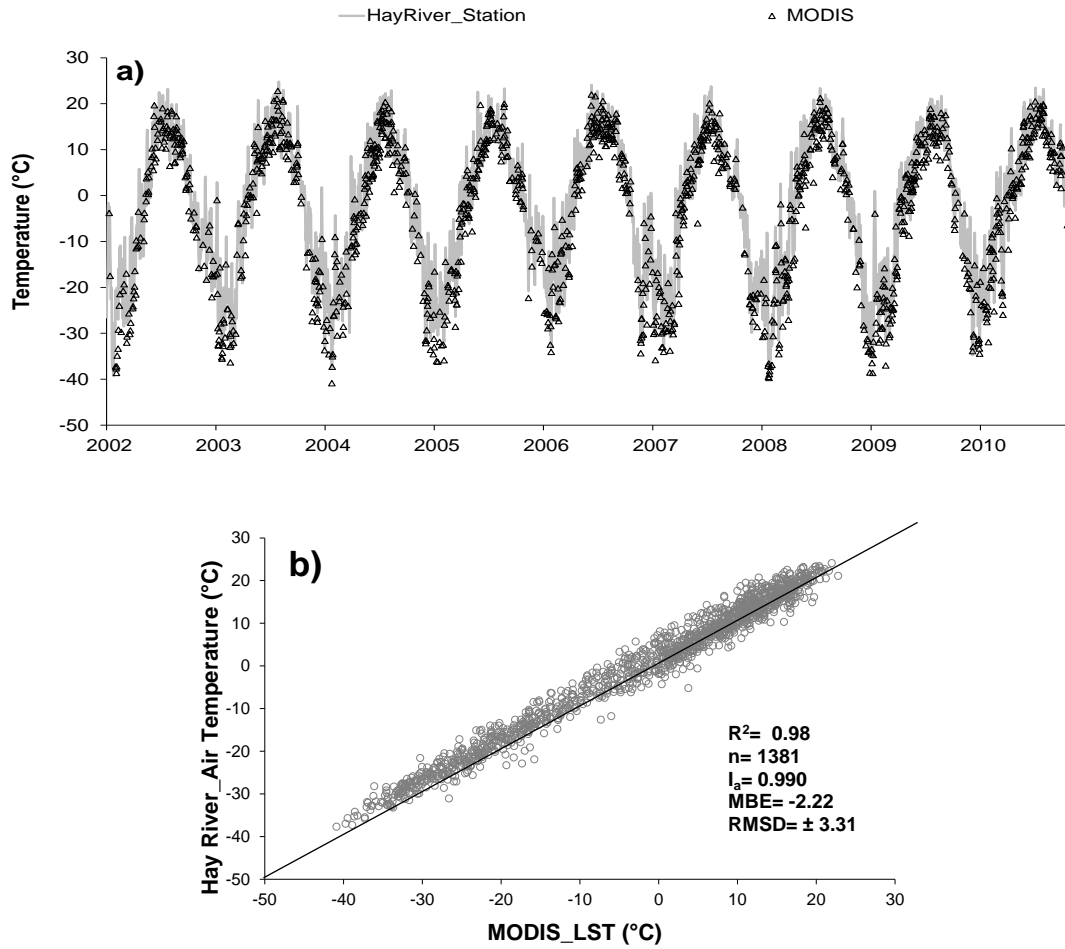


**Figure 4-3:** Time series comparison (a) and the relation (b) between  $LST_{land}$  -derived from MODIS and the air temperature at 2 m above the ground surface for Hay River weather station.

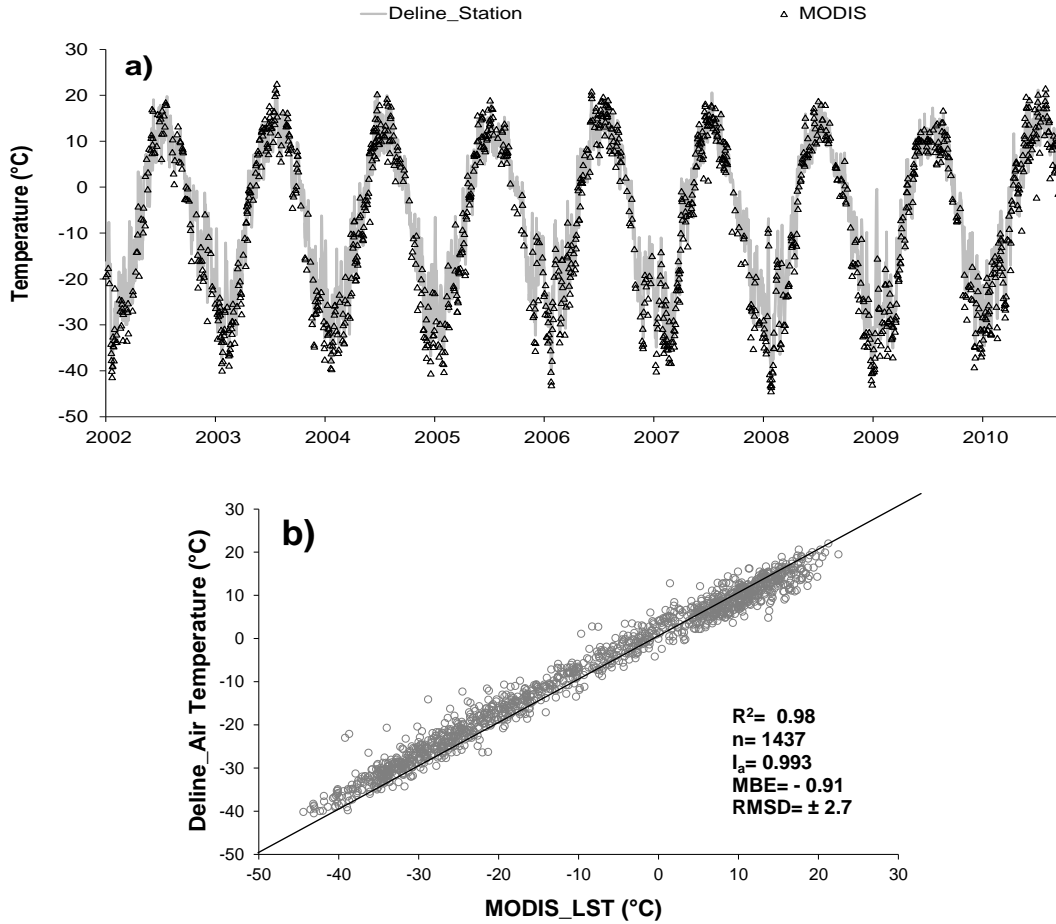


**Figure 4-4:** Time series comparison (a) and the relation (b) between  $LST_{land}$  -derived from MODIS and the air temperature at 2 m above the ground surface for Deline weather station.

### 4.3.2 Comparison of MODIS $LST_{lake}$ with In situ Lake Temperature

Figure 4.5 presents the comparison for all three mooring stations on GBL. The graphs show  $\Delta T$  (MODIS minus *in situ*), the temperature difference between these two sets of data. MODIS shows relatively colder temperatures compared to *in situ* with MBE of  $-0.10$  °C,  $-0.50$  °C, and  $-0.79$  °C for station1, 2, and 3. The RMSE, which provides a measure of non-systematic error, presents small deviations between MODIS and *in situ* (RMSE =  $1.23$  °C,  $1.27$  °C, and  $1.49$  °C for stations 1, 2, and 3, respectively). In spite of the small MBE and RMSE values,  $I_a$  presents a moderate performance. This is happening because satellite measures the skin temperature of the lake, which is under the direct influence of air

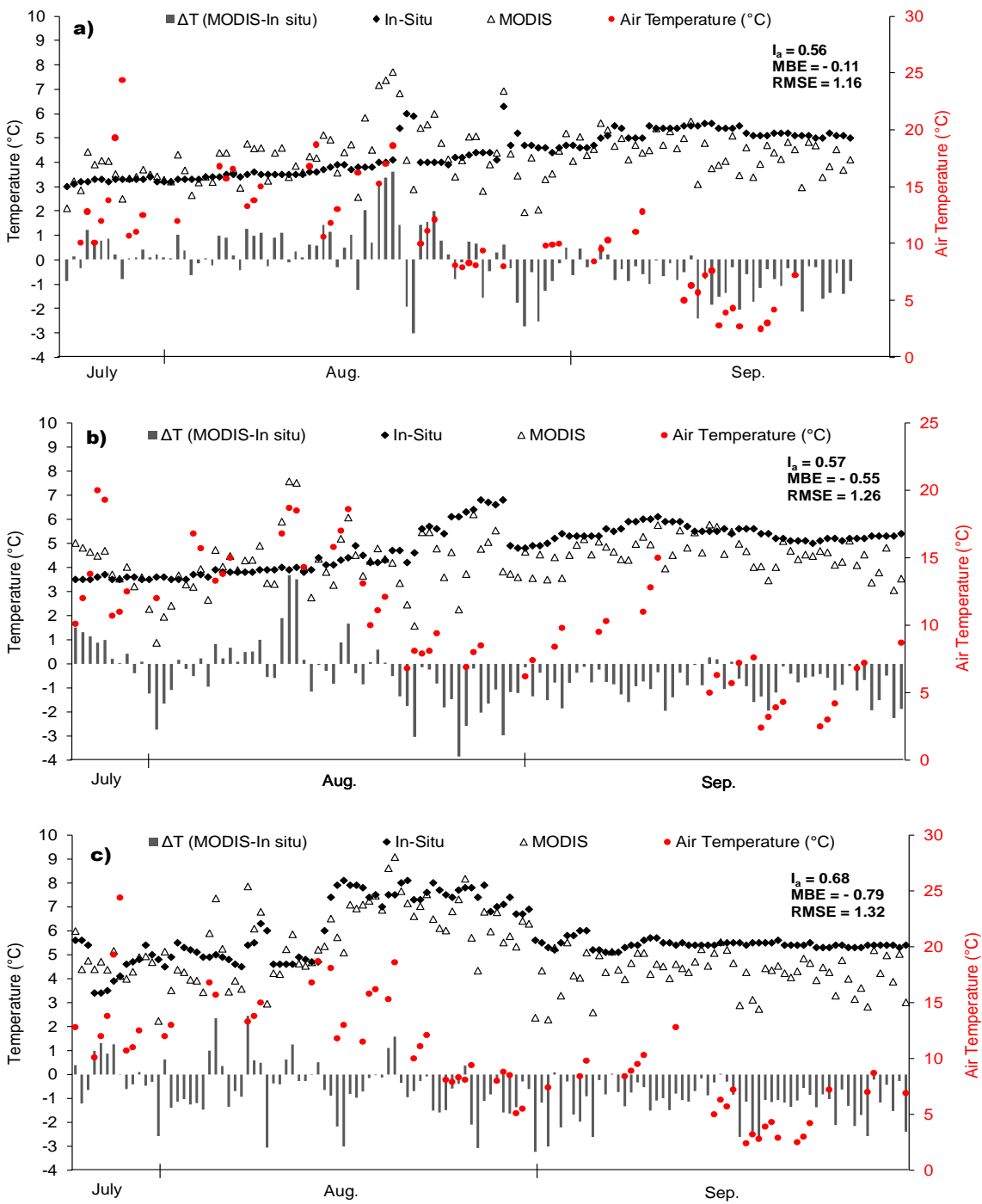


**Figure 4-5:** Comparison of hourly MODIS LST<sub>lake</sub> with hourly temperature mooring data over GBL on a) station 1, b) station 2, and c) station 3 (mid-July to September 2008).

temperature and wind. However, moorings give the temperature at a depth of 0.5 m. Red dots in Figure 4.5 display the hourly air temperatures from the weather stations within the hour of the satellite overpasses. As shown, air temperatures have a considerable effect on  $LST_{lake}$  variations. During the colder month of September,  $\Delta T$  shows negative values most of the time.

The MODIS sensors on the Terra and Aqua satellites overpass times are between 9 a.m. to 3 p.m. (day) and 7 p.m. to 3 a.m. (night) over GBL. Results show that satellite skin temperatures are usually colder than lake temperatures at 0.5 m during nighttime and warmer during daytimes (Appendix II-IV). This is due to the effect of radiative cooling/warming. The surface (skin) water temperature cools and warms faster than at 0.5 m.

### 4.3.3 Lake Depth versus Lake Surface Temperature

Figure 4.6 shows the monthly averaged surface temperature over GSL, GBL, and surrounding land for January to December 2003 from MODIS L3 observations. The maps illustrate that  $LST_{lake}$  varies with lake depth.  $LST_{lake}$  is very sensitive to depth, which controls the dynamical range of the lake temperature and its capacity to mix and freeze (Balsamo *et al.*, 2010). The maps show the water surface temperature over lakes in open-water season and snow/ice surface temperature during ice-cover season. Seasonality and air temperatures are the main factors of  $LST_{lake}$  variations over the whole year. Monthly averaged  $LST_{lake}$  data also show warmer temperatures near the shore (~ 8-13°C) and colder temperatures in the main basin of GSL (3-5°C) in July 2003. Leon *et al.* (2004) simulated the spatial variability of surface temperature in GSL using the hydrodynamic model ELCOM for four time periods in 2003 through the summer ice-free season (July 10<sup>th</sup>, July 20<sup>th</sup>, Aug 20<sup>th</sup>, and Sep 20<sup>th</sup>). In their simulation results, there was a comparable difference in temperature of about 6-12 °C in July near the shore compared to cooler mid-lake. Figure 4.6 indicates that GSL reaches a maximum temperature of about 15 °C in August and, in September; the lake starts to cool down. Cooling progresses more rapidly in the shallow near-shore than in the mid-lake areas. Large lakes mix (overturn) twice yearly when the surface water temperature reaches its maximum density (Schertzer, 1997). Schertzer *et al.* (2008) also mentioned that the large

variability in the onset dates of thermal stratifications for large lakes, such as GSL and GBL, is defined as the number of days between spring and fall overturn. They showed the large variability in the onset dates of thermal stratifications in GSL by June 27 (averaged of 1998 to 2002). Thermal stratifications happen earlier in warm years and later in cold years.

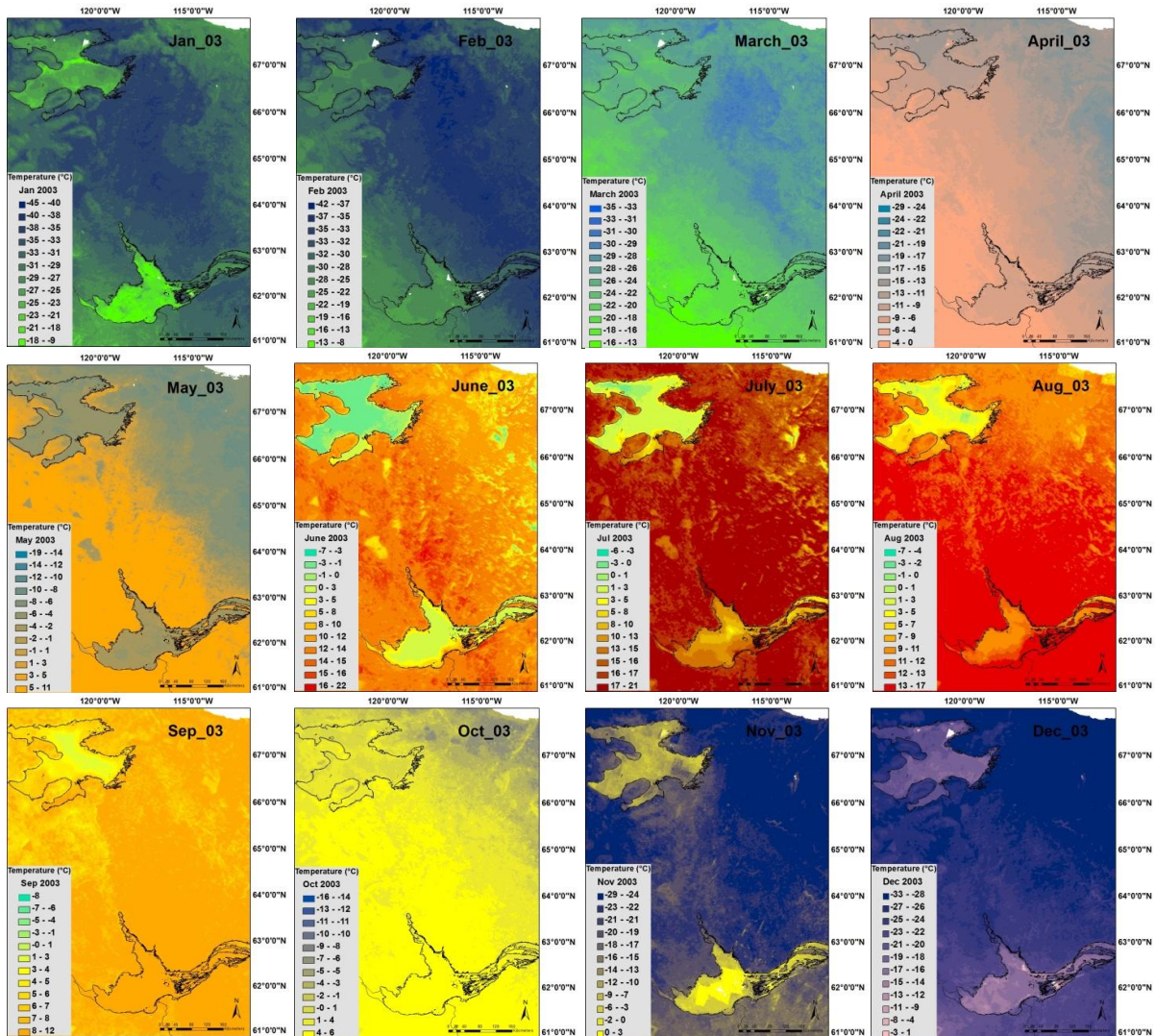


**Figure 4-6:** MODIS Land/Lake surface temperature in the Great Bear and Great Slave Lake region (January–December 2003).

Figure 4.7 compares the MODIS-derived monthly average  $LST_{lake}$  over GSL in July for the period of 2002-2010 at different depths from 10 to 120 m. The satellite data shows that temperature decreases as lake depth increases. This relation between depth and  $LST_{lake}$  has also been recently reported by Balsamon *et al.* (2010) using the FLake model for Lake Ladoga, Russia, which has a mean depth of 46.9 m. The minimum surface temperature variations between depths were found in years 2006, 2007 and 2010 (see Figure 4.7). This can be explained by higher air temperature in the GSL region in these years, as revealed by the Yellowknife weather station, located at the north part of GSL, which reported higher air temperatures in 2006 (16.27 °C in June), 2007 (18.63 °C in July), and 2010 (18.20 °C in July). Higher solar heating results in highly stratified and shallow mixed layers. As a result, the upper layer is warm (lighter) and thin over the whole area of the lake. Visualization of MODIS monthly average  $LST_{lake}$  for July of various years portrayed in Figure 4.8 also illustrates that the surface temperatures in 2006, 2007 and 2010 have the minimum  $LST_{lake}$  differences at dissimilar depths.

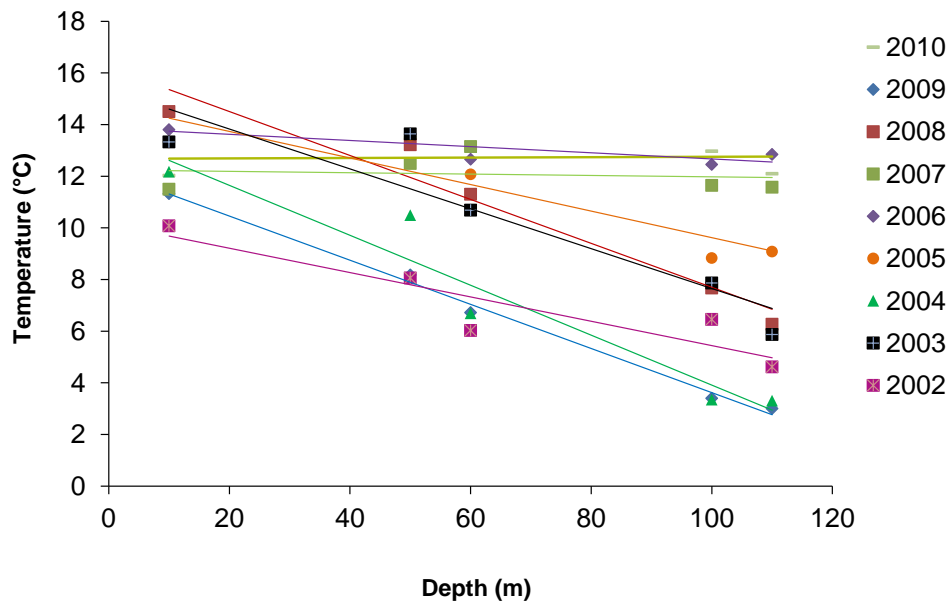


**Figure 4-7:** Monthly  $LST_{lake}$  average versus depth in GSL for July 2002-2010.

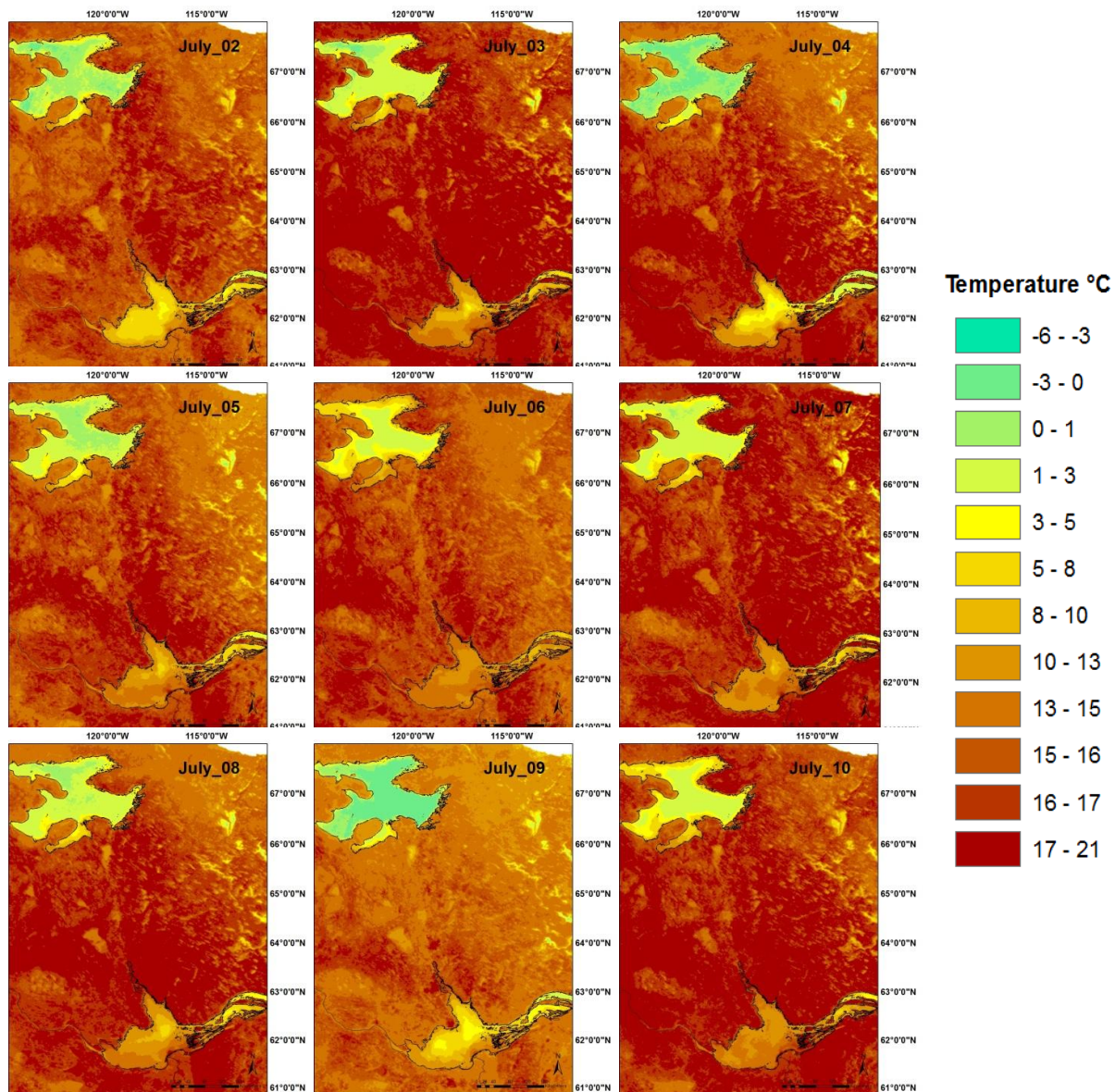


**Figure 4-8:** MODIS Land/Lake surface temperature in the Great Bear and Great Slave Lake region (July 2002-2010).

Characteristics of the seasonal thermal cycles vary among lakes of different physical dimensions and latitudinal locations (Schertzer, 1997). The latitudinal climatic gradients of greatest importance in limnology are related mainly to solar irradiance, which will affect the

water temperature and the layering and mixing of lakes (Lewis, 1996). Figure 4.8 shows the surface temperature differences of GSL and GBL mainly related to latitudinal differences. GBL, located at latitude 65.10 °N, has lower  $LST_{lake}$  compared to GSL (61.50 °N) over the full period of analysis (2002 to 2010). MODIS shows an average temperature 2.44 °C colder in the main basin of GBL compared to the main basin of GSL. This difference is much higher in July by 7.74 °C.

As lakes are covered with ice and snow in the winter period, the temperature differences at various depths are not as much as in summer. This is shown in Figure 4.9 where the relation between  $LST_{lake}$  at different depths in January is plotted for the period 2002-2010. One of the essential sources of heat in winter-time is the conductive heat flux through lake ice and snow cover. In winter-time, the conductive heat flux dominates the heat budget (Sturm *et al.*, 2001). The greater heat transfer occurs earlier in the winter (Jeffries *et al.*, 1999) because the snow and ice are not thick enough to block the heat transfer.

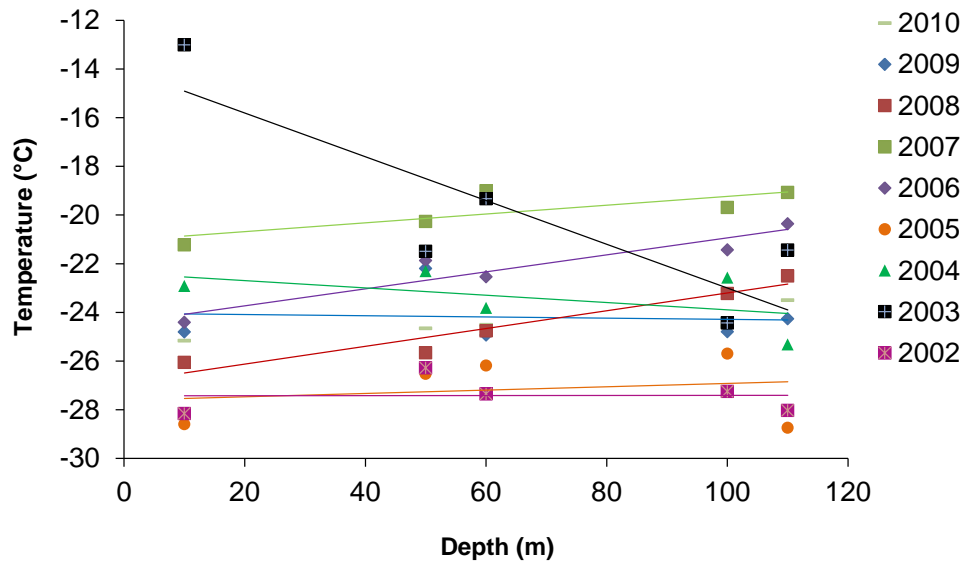


**Figure 4-9:** Monthly  $LST_{lake}$  average versus depth in GSL for January 2002-2010.

Figure 4.9 shows warmer  $LST_{lake}$  in 2003 in the shallow part of GSL. Visualization of the MODIS monthly average  $LST_{lake}$  for January mapped in Figure 4.10 also illustrates the warmest surface temperature over lakes in 2003. Warm surface temperature over lakes could be explained by higher thermal conductive heat flow through the ice and snow. To understand the amount of thermal conductivity over the lakes, the conductive heat fluxes calculated from the CLIMo were used. Simulated conducted heat fluxes show the highest amount of thermal conductivity over GSL in 2003 by  $26.06 \text{ W/m}^2\text{K}$  ( $5.12 \text{ W/m}^2\text{K}$  more than the average of 2002-2010). The heat flow decreases as the total thickness of snow and ice increase with time (Jeffries and Morris, 2006). Thermal conductivity is not only a function of snow depth or ice thickness, but also snow texture (e.g., grain size, shape, and bonding), and density (Sturm *et al.*, 1997), a topic beyond the scope of this paper.

#### **4.3.4 Lake and Land Surface Temperature Variations in the GSL region**

Figures 4.11 and 4.12 compare lake and surrounding land surface temperature of a medium sized lake (Duncan Lake) and large (GSL) during the ice-free and ice-cover seasons. Lake temperature colder than land temperature is observed from the beginning of April until August for both lakes using MODIS monthly average  $LST_{land/lake}$  (see Figure 4.11). Duncan Lake is smaller than GSL and, therefore, has smaller temperature differences between land and lake. The maximum temperature difference ( $\Delta T = T_{land} - T_{lake}$ ) between lake and land in summer occurs in June (Figure 4.11).  $\Delta T$  is larger for GSL than Duncan Lake in June by  $8.3^\circ\text{C}$  ( $\Delta T_{GSL} = 14.5^\circ\text{C}$ ,  $\Delta T_{Duncan} = 6.3^\circ\text{C}$ ). Lake size is one of the main factors that influence the seasonal cycle of lakes and has a detectable effect on the local climate. Water has a higher heat capacity than land and therefore requires more energy to heat up and cool down. As large and deep lakes have more volume compared to the small and shallow lakes, they display much greater time-lag in their heat and moisture cycle than the smaller ones and are able to store significant amount of heat. Therefore, medium lakes store less heat than bigger ones, hence lose heat much faster. It takes more time for GSL to lose the heats therefore stays warmer during this period of time compared to Duncan Lake or the surrounding land.

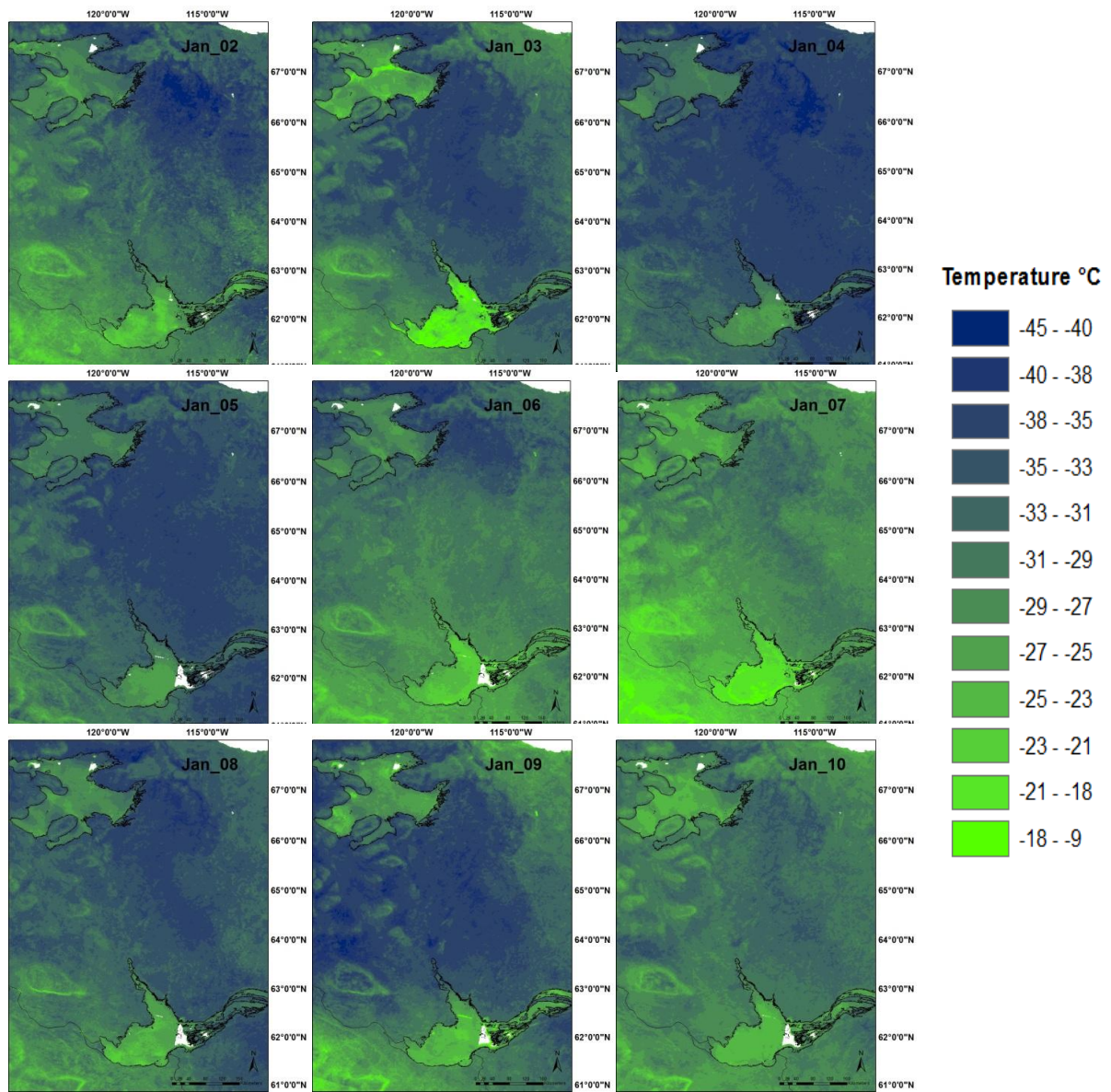


**Figure 4-10:** MODIS Land/Lake surface temperature in the Great Bear and Great Slave Lake region (January 2002-2010).

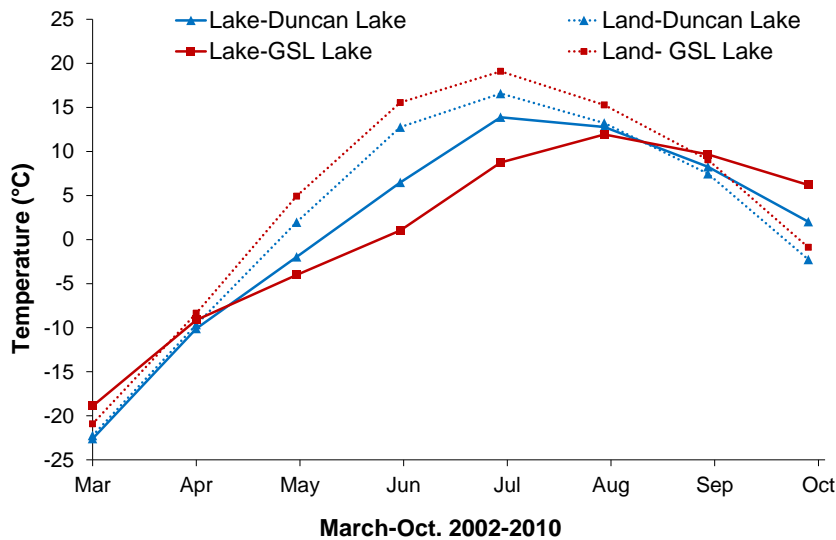


**Figure 4-11:** Monthly averaged LST <sub>land/lake</sub> in GSL and Duncan (March-October, 2002-2010).

The surface of a lake warms less rapidly than the air above so that temperature and vapour gradients are more moderate than the nearby terrestrial surface. This suppresses sensible and latent heat fluxes and they can have a net gain in heat storage (Rouse *et al.*, 2007b). The larger the lake size, the greater its heat gain. In the fall, chilly air temperatures cool the lake’s surface. Water cools less rapidly than the air above and the surrounding land surface, which enhances sensible and latent heat fluxes. When surface water cools to about 4°C, it becomes denser and sinks to the bottom. As the surface water cools even more, it becomes less dense and floats on top of the denser water, forming ice at 0 °C. As Figure 4.12 displays, the surface temperature of GSL stays warmer during the winter compare with Duncan Lake and the land around.

The ice-cover duration period varies between lakes based on their size. It has been reported to range from about 6 to 9 months for small lakes and 4 to 7 months for large lakes over the entire MRB (Rouse *et al.*, 2007b). The differences in ice-cover duration can be explained by the large heat capacity of the deep lakes, which freeze at the later date than shallow lakes (Ménard *et al.*, 2002). Consequently, deep lakes have thinner ice due to the late ice formation. During the winter ice growth season, lakes lose heat by conduction through the

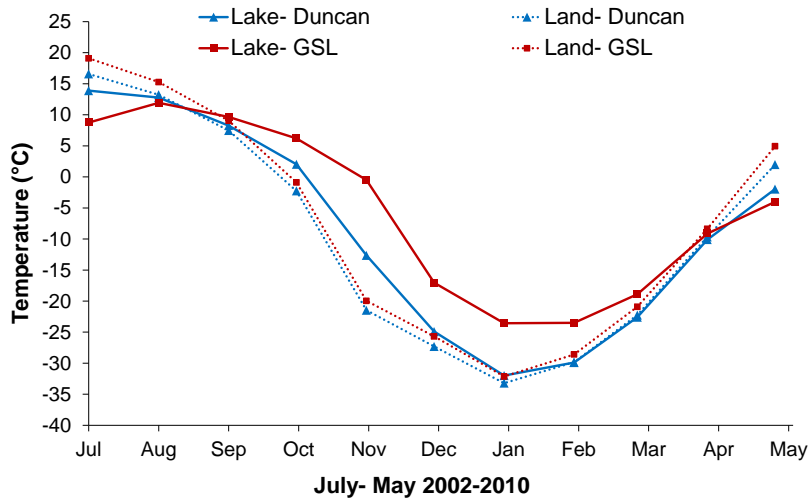


**Figure 4-12:** Monthly averaged LST<sub>land/lake</sub> in GSL and Duncan (July- May 2002-2010).

upper ice surface due to the gradient from the relatively warmer water below the ice and the colder air above the ice/snow interface (Jeffries and Morris, 2006). As a result, due to the thinner ice over GSL, more heat is released and therefore causes higher surface temperature during the ice-cover season. Maximum temperature difference between lake and land in winter occurs in November (Figure 4.13).  $\Delta T$  is larger for GSL than Duncan Lake in November by  $10.6^{\circ}\text{C}$  ( $\Delta T_{\text{GSL}}= 19.5^{\circ}\text{C}$ ,  $\Delta T_{\text{Duncan}}= 8.8^{\circ}\text{C}$ ).

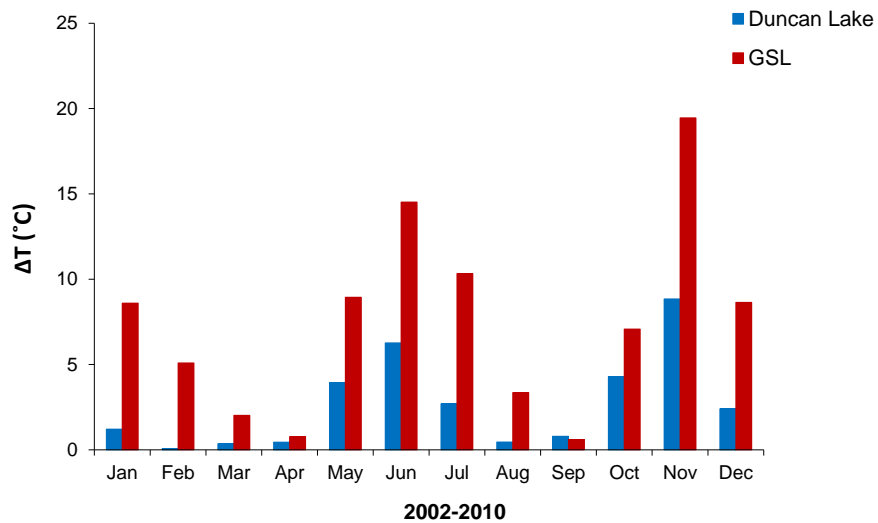


**Figure 4-13:** LST<sub>land/lake</sub> differences ( $\Delta T = T_{\text{land}} - T_{\text{lake}}$ ) in GSL and Duncan Lake (January–December 2002-2010).

#### 4.4 Summary and Conclusion

The spatial and temporal patterns in lake and land surface temperature in the GBL and GSL regions were investigated using MODIS satellite data. Research objectives were pursued into comparison of MODIS-derived  $LST_{land}$  with available meteorological station measurements, evaluating MODIS-derived  $LST_{lake}$  using *in situ* temperature moorings, and the analysis of the seasonal and inter-annual variations and spatial patterns in  $LST_{land/lake}$ . MODIS showed a good agreement compared to *in situ* station data with the higher agreements during the open-water season over land. The statistical differences in the open-water and ice-cover seasons are due to the fact that MODIS provides a skin surface temperature and stations measure air temperature at screen (about 2-m) height. As a result, skin temperature of ice/snow is colder than air temperature during winter. Results also indicate good agreement between MODIS hourly  $LST_{lake}$  and *in situ* data for GBL. Deviation between the two sets of measurements was because satellite measures the skin temperature of the lake, which is under the direct influence of air temperature and wind, but moorings provided the temperature at a depth of 0.5 m. The results demonstrated that lake depth, lake size and latitude are essential factors in the surface temperature of a lake. MODIS data indicated that GSL had its maximum temperature in August with  $\sim 15$  °C and then the lake started to cool afterwards. Maps of  $LST_{land/lake}$  showed that cooling progresses more rapidly in the shallow near-shore than in the mid-lake section. Large lakes influence their surrounding land surface by sinking heat during the summer and releasing heat in late fall and in winter.  $LST_{lake}$  is colder than the surrounding land during the open-water season (April-August) and warmer during the ice growth season (mid-September- mid-March). For GSL,  $LST_{lake}$  becomes close to that of land in September. Duncan Lake has a close temperature to land one month earlier (August). Then, lakes become warmer than surrounding land until spring thaw.

MODIS satellite data used in this research were found to be appropriate for studying the spatial and temporal variations in surface temperature of lakes and land. Such data provide frequent temperature measurements over large areas. The large spatial coverage at a

medium resolution (1 km) is a major advantage over *in situ* measurements. Furthermore, satellite data can be used for the assimilation into numerical weather prediction and also to validate land and lake surface schemes used in climate models.

### **Acknowledgements**

This research was supported by European Space Agency (ESA-ESRIN) Contract No. 4000101296/10/I-LG (Support to Science Element, North Hydrology Project) and a Discovery Grant from the Natural Sciences and Engineering Research Council of Canada (NSERC) to C. Duguay.

## Chapter 5

### General Conclusion

#### 5.1 Summary

This research examined the potential of using thermal satellite observations to understand the lakes thermal and hydrodynamic processes for two large and deep lakes located in northwestern Canada. Based on extensive previous studies in this region, lakes are known to control evaporation, runoff, and water storage and are responsible for essential transportation of energy and water into and through the basin. Collecting detailed and spatially systematic *in situ* data over large lakes such as GBL and GSL is a real challenge, both during the ice-free and ice-cover seasons. Satellite acquisitions provide the opportunity to collect continuous data over very large geographic areas, in remote regions, and during hazardous conditions for *in situ* measurements such as at the beginning of ice formation and the end of the melt period.

This study focused on examining surface temperature variations over land and lake (shown with  $LST_{lake}$  and  $LST_{land}$ ) using MODIS satellite data and numerical lake models. The two main objectives were to: a) analyze satellite-derived surface temperature against modeling using the CLIMo and FLake models and identify the uncertainties and limitations of the numerical models and the MODIS satellite data products [discussed in paper1, chapter 3], and b) compare and verify MODIS-derived surface temperature over land and lake with available meteorological station measurements and *in situ* observations and analyze the seasonal and inter-annual variations and spatial patterns in surface temperature over lakes and land [discussed in paper 2, chapter 4].

Chapter 3 presented results of two 1-D lake models (CLIMo and FLake) that were applied to simulate surface temperature, ice thickness and phenology on GBL and GSL for a nine-year period (2002-2010). Forcing data used to run the models were obtained from three weather stations (Yellowknife, Hay River and Deline) on shore of both lakes. Simulated  $LST_{lake}$  products, ice thickness, and freeze-up/break-up dates were compared with the ones

from MODIS-Terra/Aqua as well as *in situ* ice observations. The surface temperature results were first plotted for the full years (Jan.-Dec.) and then separately for the open-water season (June-Oct.) and ice-cover season (Nov.-May), as the physics of these two types of surfaces differ substantially. Results revealed a good performance of both models when compared against MODIS-derived  $LST_{lake}$  over complete years. Larger differences were observed when results were examined separately for the open-water and ice-cover seasons. The CLIMo showed a generally better performance than the FLake model, especially for ice-cover season. The absence of snow in the FLake model had a large effect on surface temperature of lakes during ice-cover season as well as ice growth and decay rates. Observed surface temperatures by MODIS were generally colder compared to models. This could be explained to some extent by erroneous measurements during cloudy conditions as undetected clouds and the time differences of the MODIS  $LST_{lake}$  used to calculate clear-sky daily averages, compared to the daily air temperatures from weather stations used as forcing data in models. Overall, MODIS presented a very good agreement with the model simulations.

Chapter 4 examined MODIS-derived Terra/Aqua  $LST_{land/lake}$  data for analyzing surface temperature patterns during the open-water and ice growth seasons (2002-2010) in the GBL and GSL regions. Daily  $LST_{land}$  from MODIS were compared to near-surface air temperature measurements obtained at three nearby weather stations and hourly  $LST_{lake}$  were also compared to *in situ* water temperatures obtained from temperature moorings installed on GBL. MODIS pixels, which were chosen close to the weather stations in open shrublands, showed a cold bias value between 0.91 and 2.34 for all three study sites. The reason of colder satellite data for land is because the MODIS presents skin temperature and the data from stations are the temperature at 2 m above the ground. Land surface lose and gain heat faster compared to the air and thus the results above zero °C temperature showed a better fit. Results also indicated a good agreement between MODIS  $LST_{lake}$  and *in situ* data taken within the same hour over GBL.

The outcomes demonstrated that lake depth, lake size and latitude play an essential role in the surface temperature of the lakes. Lake surface temperatures were found to be

colder than the surrounding land from April until mid-August and then became equivalent. Lake surface “skin” temperature was warmer starting in September and remained warmer than the land until spring break-up because during ice growth season, lakes lose heat by conduction through the upper ice surface.

Lake investigations in high latitude regions are important as they contribute to a better understanding of the role and response of lakes to recent climate warming. There is a need to supplement more traditional *in situ* measurement methods and a better spatially continuous coverage possible with satellite remote sensing. In particular,  $LST_{land/lake}$  retrieved from satellite sensors offer the opportunity to apply remote sensing technology for obtaining a consistent coverage of a key parameter for climate and hydrological research. Based on the results of this study, the MODIS sensor aboard the Terra and Aqua satellite platforms offered the potential to provide spatial estimates of surface temperature values.

## 5.2 Limitations

Some limitations were identified, particularly with the availability of *in situ* measurements. There were not sufficient *in situ* data points for a rigorous evaluation of the MODIS temperature measurements. To validate the satellite thermal observations, there is a need of a dataset of surface temperature for both land and lake.  $LST_{land/lake}$  obtained from thermal cameras would be the best dataset for validation, which were not available for this research. Temperature moorings provided measurements at 0.5 m in the water column that explained the deviation between two methods (satellite and *in situ*), because the skin temperatures of lake are under the direct influence of air temperature and wind. Another limitation in the *in situ* measurements was the absence of measurements for ice thickness and freeze-up/break-up dates for GBL and also there was a gap in ice thickness observations for Back Bay (Yellowknife) between 1996 and 2002, and the freeze-up dates for the same station between 1981 and 1985.

MODIS provides data with 1 km spatial resolution, which allows the Earth’s surface to be covered in 1 day with a frequency of acquisition of as much as 4 times per day (combining Terra and Aqua data). In addition, MODIS acquires data in 36 channels that

calculates surface temperatures with thermal infrared reflectivity and calculates atmospheric water contents with short infrared, reducing errors in surface temperature and cloud cover. Despite these advantages, there are some limitations using MODIS-derived surface temperature especially in the fall and early winter. Large lakes like GBL and GSL cool more slowly than the air during these seasons. As a result, this source of heat and moisture causes the local destabilization of the lower atmosphere resulting in enhanced clouds and precipitation downwind of the lakes (Niziol, 1995). When the lakes are covered with cloud, the MODIS data might not be updated for several days or, on occasion, clouds may not be detected by the MODIS surface temperature algorithm, resulting in anomalous cold temperatures (i.e. top of cloud instead of lake surface).

### **5.3 Future Work**

There is a great potential for future research regarding satellite remote sensing of lake surface temperature. One potential research area is to validate MODIS surface temperature products over varied lakes of different sizes in Europe especially in Finland, where an important source of *in situ* measurements data is available. Another research avenue is the comparison of MODIS surface temperature products with the same type of products derived from the Envisat AATSR (thermal) sensor. Moreover, there are other products generated from sensors on board of Terra and Aqua satellite such as ice thickness and albedo. It would be interesting to combine these products with  $LST_{lake}$  to improve our understanding of the response and role of ice-cover of high latitude lakes during the ice growth season.

$LST_{lake}$  data from MODIS or other thermal infrared satellite sensors are a useful data source for calibrating/evaluating lake models. Moreover, they can potentially be used for data assimilation into NWP models since  $LST_{lake}$  *in situ* observations are either not available or very limited for operational NWP. Data from MODIS are available over large lakes due to the wide swath possible with such satellite sensors. Therefore, further work is proposed to explore methods for assimilation of MODIS sensor observations into NWP models.

Last, but not least, is the possible improvement that can be made to the CLIMo regarding the calculation of the mixed layer depth (prognostic) rather than specified as a constant value, as well as improvement of the snow module in the Flake model.

## References

- Adams, W.P. (1976). Diversity of lake cover and its implications, *Musk-Ox Journal*, **18**, 86-98.
- Adams, W.P., and N.T. Roulet. (1980). Illustration of the roles of snow in the evolution of the winter cover of a lake. *Arctic*, **33**(1), 100-116.
- Arnell, N., B. Bates, H. Lang, J. Magnuson, and P. Mulholland. (1996). Hydrology and freshwater ecology, *Climate Change 1995: Impacts, Adaptations, and Mitigation—Scientific-Technical Analysis*, 325 – 363, Cambridge Univ. Press, New York.
- Bengtsson, L. (1986). Spatial variability of lake ice-covers, *Geographiska Annaler*, **68A**(1-2), 113-121.
- Blanken, P. (2003). Enhancement of Evaporation from a Large Northern Lake by the Entrainment of Warm, Dry Air. *J. Hydrometeorol*, **4**, 680- 693.
- Blanken, P., W.R. Rouse, W.M. Schertzer. (2008). The time scales of evaporation from Great Slave Lake. Chapter 10 in *Cold Region Atmospheric and Hydrologic Studies: The Mackenzie GEWEX Experience, Volume 2: Hydrologic Processes*. Springer-Verlag, 181-196.
- Blasamon, G., E. Dutra, V. M. Sepanenko, P. Viterbo, P. M. A. Miranda, D. Mironov. (2010). Deriving an effective lake depth from satellite lake surface temperature data: a feasibility study with MODIS Data. *Boreal Environment Research*, **15**, 178-190.
- Bluteau C.E. (2006). *Mixing in Brackish Lakes due to Surface Ice: A Physical Model*, Master thesis, University of British Columbia.
- Brewer, M. (1958). The thermal regime of an arctic lake: Transactions, American Geophysical Union, **39**, 278-284.
- Brown, L.C. and C.R. Duguay, 2011. A comparison of simulated and measured lake ice thickness using a Shallow Water Ice Profiler. *Hydrological Processes*, **25**, DOI: 10.1002/hyp.8087.
- Brown, L.C., and Duguay, C.R. (2010). The response and role of ice cover in lake-climate interactions. *Progress in Physical Geography*, **34**(5) 671–704
- Bussi eres N., D. Verseghy, and J.I. MacPherson. (2002). The evolution of AVHRR-derived water temperatures over boreal lakes. *Remote Sensing of Environment*, **80**, 373–384.
- Chen, C. T., and F. J. Millero. (1986). Precise thermodynamic properties for natural waters covering only the limnological range, *Limnol. Oceanogr.*, **31** , 657–662.
- Coll, C., V. Caselles, J.M. Galve, E. Valor, R. Niclos, J.M. Sanchez, and R. Rivas. (2005). Ground measurements for the validation of land surface temperatures derived from AATSR and MODIS data, *Remote Sens. Environ.*, **97**, 288–300.
- Coll, C., S.J. Hook, and J.M. Galve. (2009). Land surface temperature from the Advanced Along-Track Scanning Radiometer: Validation over inland waters and vegetated surfaces. *IEEE Transactions on Geoscience and Remote Sensing*, **47**, 350-360.
- Crosman, E.T., and J.D. Horel. (2009). MODIS-derived surface temperature of the Great Salt Lake. *Remote Sensing of Environment*, **113**, 73–81.
- Duguay, C.R., T. Pultz, P.M. Lafleur, and D. Drac. (2002). RADARSAT backscatter characteristics of ice growing on shallow sub-Arctic lakes, Churchill, Manitoba, Canada. *Hydrological Processes*, **16**, 1631-1644.

- Duguay, C.R., G.M. Flato, M.O. Jeffries, P. Ménard, K. Morris, and W.R. Rouse. (2003). Ice covers variability on shallow lakes at high latitudes: model simulation and observations. *Hydrological Processes*, **17**, 3465–3483.
- Duguay, C., J. Green, C. Derksen, M. English, A. Rees, M. Sturm, and A. Walker. (2005). preliminary assessment of the impact of lakes on passive microwave snow retrieval algorithms in the Arctic. *62nd Eastern Snow Conference Proceedings*, Waterloo Ontario Canada.
- Dutra, E., V.M. Stepanenko, G. Balsamo, P. Viterbo, P.M.A. Miranda, D. Mironov, and C. Schaer. (2010). An Offline Study of the Impact of Lakes on the Performance of the ECMWF Surface Scheme, *Boreal Environment Research*, **15**, 100-112.
- Eerola, K., L. Rontu, E. Kourzeneva, and E. Shcherbak. (2010). A study on effects of lake temperature and ice cover in HIRLAM. *Boreal Environment Research*, **15**, 130-142.
- Galve, J. M., C. Coll, V. Caselles, E. Valor, R. Niclos, J.M. Sanchez, and M. Mira. (2007). Simulation and validation of land surface temperature algorithms for MODIS and AATSR data, *Tethys*, **54**, 27–32.
- Hinzman, L.D., D.J. Goering, D.L. Kane. (1998). A distributed thermal model for calculating soil temperature profiles and depth of thaw in permafrost regions. *Journal of Geophysical Research*, **103**(D22), 28 975–28 991.
- Hook, S. J., R.G. Vaughan, H. Tonooka, and S.G. Schladow. (2007). Absolute radiometric inflight validation of mid infrared and thermal infrared data from ASTER and MODIS on the Terra Spacecraft using the Lake Tahoe, CA/NV, USA, automated validation site, *IEEE T. Geosci. Remote.*, **45**, 1798–1807.
- Howell, S.E.L., L.C. Brown, K.K. Kang, and C.R. Duguay. (2009). Monitoring lake ice phenology variability on Great Bear Lake and Great Slave Lake, Northwest Territories, Canada, from SeaWinds/QuikSCAT: 2000-2006. *Remote Sensing of Environment*, **113**(4), 816-834.
- Jeffries M.O, K. Morris, G.E. Liston. (1996). A method to determine lake depth and water availability on the North Slope of Alaska with spaceborne imaging radar and numerical ice growth modelling. *Arctic* **49**, 367–374.
- Jeffries, M.O., T. Zhang, K. Frey, N. Kozlenko. (1999). Estimating late winter heat flow to the atmosphere from the lake-dominated Alaskan North Slope. *Journal of Glaciology* **45**(150), 315–324.
- Jeffries, M.O., K. Morris, and C.R. Duguay. (2005). Lake ice growth and decay in central Alaska, USA: observations and computer simulations compared. *Annals of Glaciology*, **40**, 195-199.
- Jeffries, M.O., K. Morris. (2006). Instantaneous daytime conductive heat flow through snow on lake ice in Alaska. *Hydrological Processes*, **20**, 803-815.
- Kheyrollah Pour, H., C.R. Duguay, A. Martynov, and L.C. Brown (accepted). Simulation of surface temperature and ice cover of large northern lakes with 1-D models: A comparison with MODIS satellite data and *in situ* measurements. *Tellus Series A: Dynamic Meteorology and Oceanography*.

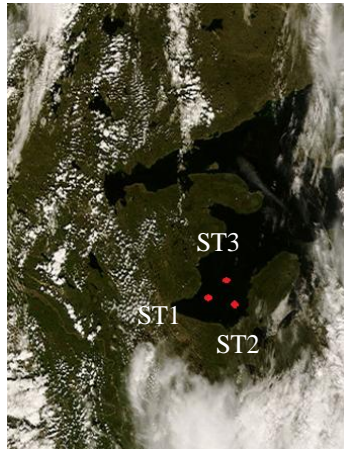
- Ledley, T.S. (1991). Snow on sea ice: competing effect in shaping climate. *F. Geophys. Res*, **96** (D9), 17195-17208.
- Lenormand, F., C.R. Duguay, R. Gauthier. (2002). Development of a historical ice database for the study of climate change in Canada. *Hydrological Processes*, **16**, 3709–3724.
- Lewis W. M. (1996). Tropical Lake: how Latitude makes a difference, *Tropical Limnology*, 43-64.
- León, L.F, D.C.L. Lam, W.M. Schertzer, D.A. Swayne. (2005). Lake and climate models linkage: a 3-D hydrodynamic contribution. *Advances in Geoscience*, **3**, 1-6.
- León, L.F, D.C.L. Lam, W.M. Schertzer, D.A. Swayne and J. Imberger. (2007). Towards coupling a 3D hydrodynamic lake model with the Canadian regional climate model: Simulation on Great Slave Lake. *Environmental Modelling Software*, **22**, 787-796.
- Livingstone, D. M., and M. T. Dokulil. (2001). Eighty years of spatially coherent Austrian lake surface temperatures and their relationship to regional air temperature and the North Atlantic Oscillation, *Limnol. Oceanogr.*, **46**, 1220– 1227.
- Livingstone, D. M. (2003). Impact of secular climate change on the thermal structure of large temperate central European lake. *Climatic Change*, **57**, 205–225.
- Liston, G. E. and M. Sturm. (2002). Winter precipitation patterns in arctic Alaska determined from a blowing snow model and snow depth observations. *J. of HydroMeteorology*, **3**(5), 646-659.
- Ljungemyr, P., N. Gustafsson, and A. Omstedt. (1996). Parameterization of lake thermodynamics in a high-resolution weather forecasting model. *Tellus*, **48A**, 608-621.
- Lofgren B. M., and Y. Zhu. (2000). Surface energy fluxes on the Great Lakes based on satellite-observed surface temperatures 1992 to 1995. *J. Great Lakes Res.*, **26**, 305–314.
- Long, Z., W. Perrie, J. Gyakum, D. Caya, and R. Laprise. (2007). Northern Lake impacts on local seasonal Climate. *J. Hydrometeor*, **8**, 881- 896.
- Longer, M., S. Westermann, J. Boike. (2010). Spatial and temporal variations of summer surface temperatures of wet polygonal tundra in Siberia - implications for MODIS LST based permafrost monitoring. *Remote Sensing of Environment*, **114**, 2059–2069.
- Martynov, A., L. Sushama, and R. Laprise. (2010). Simulation of temperate freezing lakes by one-dimensional lake models: Performance assessment for interactive coupling with regional climate models. *Boreal Environment Research*, **15**, 143–164.
- Maykut GA, N. Untersteiner. (1971). Some results from a time-dependent thermodynamic model of sea ice. *Journal of Geophysical Research*, **76**, 1550–1575.
- Ménard, P., C.R. Duguay, G.M. Flato, and W.R. Rouse. (2002). Simulation of ice phenology on Great Slave Lake, Northwest Territories, Canada. *Hydrological Processes*, **16**, 3691–3706.
- Mironov, D.V. (2008). *Parameterization of lakes in numerical weather prediction. Description of a lake model*. COSMO Technical Report, Deutscher Wetterdienst, Offenbach am Main, Germany, **11**, 41.

- Mironov, D., E. Heise, E. Kourzeneva, B. Ritter, N. Schneider, and A. Terzhevik.(2010). Implementation of the lake parameterisation scheme FLake into the numerical weather prediction model, COSMO. *Boreal Environment Research*, **15**, 218-230.
- Morris, K., M. Jeffries, C.R. Duguay. (2005). Model simulation of the effects of climate variability and change on lake ice in central Alaska, USA. *Annals of Glaciology*, **40**, 113-118.
- Niziol, T.A., W.R. Snyder, and J.S. Waldstreicher. (1995). Winter Weather Forecasting throughout the Eastern United States: Part IV: Lake Effect Snow. *Wea. Forecasting.*, **10**, 61-77.
- Oesch, D. C., J.-M. Jaquet, A. Hauser, and S. Wunderle. (2005). Lake surface water temperature retrieval using advanced very high resolution radiometer and Moderate Resolution Imaging Spectroradiometer data: Validation and feasibility study, *Journal of Geophysical Research*, **110**, C12014.
- Oswald C. M., and W. R. Rouse. (2004). Thermal characteristics and energy balance of various-size Canadian Shield lakes in the Mackenzie River Basin. *J. Hydrometeor.*, **5**, 129–144.
- Price, J. C. (1983). Estimating surface temperature from satellite thermal infrared data-A simple formulation for the atmospheric effect. *Remote Sensing Environ.*, **13**, 353-361.
- Price, J. C. (1984). Land surface temperature measurements from the split window channels of the NOAA-7 AVHRR, *J. Geophys. Res.*, **79**, 5039-5044.
- Rind, D., R. Healy, C. Parkinson and D. Martinson. (1995). The role of sea ice thickness and extent. *F. Geophys. Res.*, **8** (3), 449-463.
- Rouse, W. R., M. S. V. Douglas, R. E. Hecky, A. E. Hershey, G. W. Kling, L. Lesack, P. Marsh, M. McDonald, B. J. Nicholson, N. T. Roulet, and J. P. Smol. (1997). Effects of Climate Change on the Freshwaters of Arctic and Subarctic North America. *Hydrological Processes*, **11**(8), 873-902.
- Rouse, W.R., J. Binyamin, P.D. Blanken, N. Bussi eres, C.R. Duguay, C.J. Oswald, M.W. Schertzer, and C. Spence. (2007a). The Influence of lakes on the regional heat and water balance of the central Mackenzie River Basin. Chapter 18 in *Cold Region Atmospheric and Hydrologic Studies: The Mackenzie GEWEX Experience*, Volume 1: Atmospheric Dynamics. Springer-Verlag, 309-325.
- Rouse, W.R., P.D. Blanken, C.R. Duguay, C.J. Oswald, and W.M. Schertzer. (2007b). Climate-lake interactions. Chapter 8 in *Cold Region Atmospheric and Hydrologic Studies: The Mackenzie GEWEX Experience*, Volume 2: Hydrologic Processes. Springer-Verlag, 139-160.
- Rouse, W.R., P.D. Blanken, N. Bussi eres, C.J. Oswald, W.M. Schertzer, and C. Spence, and A.E. Walker. (2008). An investigation of the thermal and energy balance regimes of Great Slave and Great Bear Lakes. *Journal of Hydrometeorology*, **9**, 1318-1333.
- Samuelsson, P., E. Kourzeneva, and D. Mironov. (2010). The impact of lakes on the European climate as simulated by a regional climate model. *Boreal Env. Res.*, **15**, 113-129.

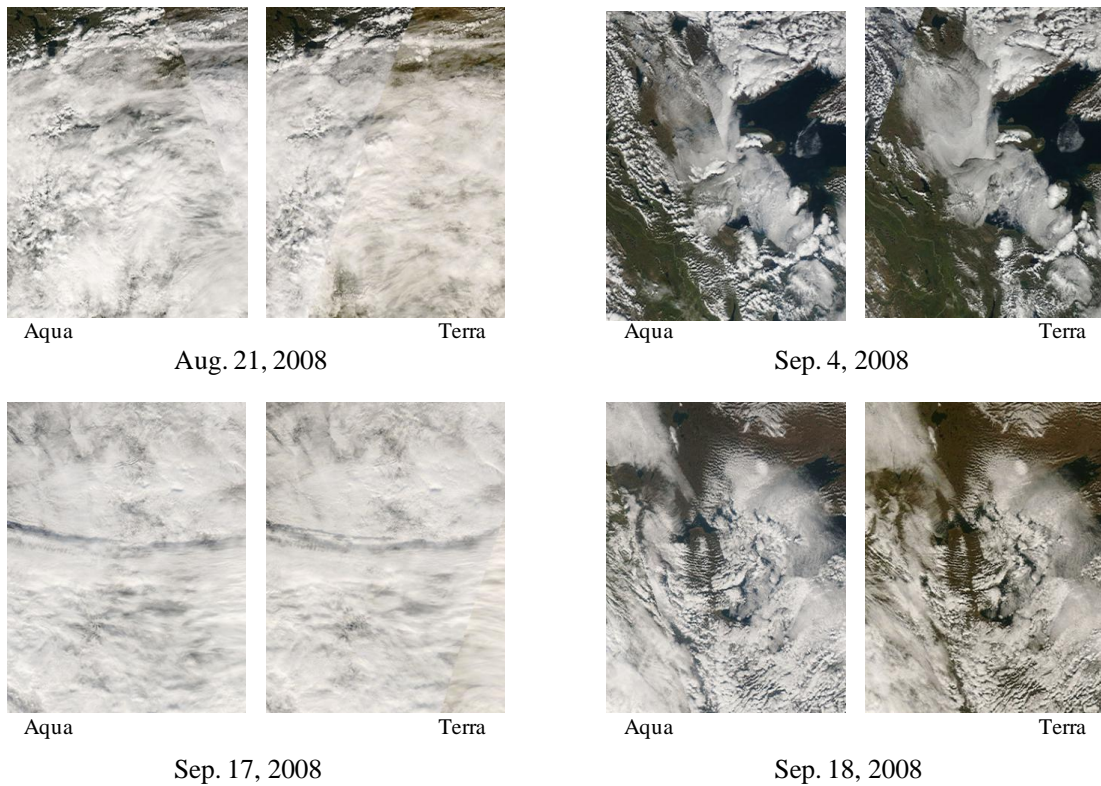
- Schertzer W. M. (1997). Freshwater Lakes. Chapter 6 in *The Surface Climates of Canada*. McGill-Queen's University Press, 124-148.
- Schertzer W. M. (2000). Digital bathymetry of Great Slave Lake, NWRI contrib. No 00-257, National Water research Institute, Burlington, ON, Canada.
- Schertzer W. M., W. R. Rouse, P. D. Blanken, A. E. Walker. (2003). Over-Lake Meteorology and Estimated Bulk Heat Exchange of Great Slave Lake in 1998 and 1999. *American Meteorological Society*, **4**, 649-659.
- Schertzer, W.M., W.R. Rouse, P.D. Blanken, A.E. Walker, D.C.L. Lam, and L. León. (2008). Interannual Variability of Thermal Components and Bulk Heat Exchange of Great Slave Lake. *Cold Region Atmospheric and Hydrologic Studies. The Mackenzie GEWEX Experience*, Volume 2: Hydrologic Processes, 197-219.
- Schneider, P., S.J. Hook, R.G. Radocinski, G.K. Corlett, G.C. Hulley, S.G. Schladow, and T.E. Steissberg. (2009). Satellite observations indicate rapid warming trend for lakes in California and Nevada. *Geophysical Research Letters*, **36**, L22402.
- Sturm, M., J. Holmgren, and G. E. Liston. (1995). A seasonal snow cover classification system for local to global applications. *Journal of Climate*, **8**(5), 1261-1283.
- Sturm, M., J. Holmgren, M. König, and K. Morris. (1997). The thermal conductivity of seasonal snow, *J. Glaciol*, **43**, 26-41.
- Sturm, M., J. Holmgren, D.K. Perovich. (2001). Spatial variations in the winter heat flux at SHEBA: estimates from snow-ice interface temperatures. *Annals of Glaciology*, **33**, 213-220.
- Sturm, M., and G.E. Liston. (2003). The Snow Cover on Lakes of the Arctic Coastal Plain of Alaska, U.S.A. *J. of Glaciology*, **49** (166), 370-380.
- Susskind J., J. Rosenfield, D. Reuter, and M. T. Chahine. (1984). Remote sensing of weather and climate parameters from HIRS2MSU on TIROS-N. *J. Geophys. Res.*, **89**, D3, 4677-4697.
- Taras, B., M. Sturm, and G. E. Liston. (2002). Snow-ground interface temperatures in the Kuparuk River Basin, Arctic Alaska: Measurements and Model: *J. of Hydrometeorology*, **3**, 377-394.
- Wan, Z., and J. Dozier. (1996). A generalized split-window algorithm for retrieving landsurface temperature from space. *IEEE Transactions on Geoscience and Remote Sensing*, **34**, 892-905.
- Wan, Z., and Z.-L. Li. (1997). A physics-based algorithm for retrieving land-surface emissivity and temperature from EOS/MODIS data. *IEEE Transactions on Geoscience and Remote Sensing*, **35**, 980-996.
- Wan, Z., Y. Zhang, Z.-L. Li, R. Wang, V. V. Salomonson, A. Yves, R. Bosseno, and J. F. Hanocq. (2002a). Preliminary estimate of calibration of the Moderate Resolution Imaging Spectroradiometer thermal infrared data using Lake Titicaca, *Remote Sens. Environ.*, **80**, 497-515.
- Wan, Z., Y. Zhang, Q. Zhang, and Z.-L. Li. (2002b). Validation of the land-surface temperature products retrieved from Terra Moderate Resolution Imaging Spectroradiometer data, *Remote Sens. Environ.*, **83**, 163-180.

- Wan, Z., Y. Zhang, Q. Zhang, and Z.-L. Li. (2004). Quality assessment and validation of the MODIS global land surface temperature, *Int. J. Remote Sens.*, **25**, 261–274.
- Wan, Z. (2005). *Refinements of the MODIS Land-Surface Temperature Products*. Technical Progress Report Submitted to the National Aeronautics and Space Administration.
- Wan, Z. (2007). *Collection-5 MODIS Land Surface Temperature Products Users' Guide*. ICESS, University of California, Santa Barbara.
- Wan, Z. and Z-L. Li, (2008). Radiance-based validation of the V5 MODIS land-surface temperature product, *Int. J. Remote Sens.*, **29**, 5373–5395.
- Westermann, S., M. Langer, and J. Boike. (2011). Spatial and temporal variations of summer surface temperatures of high-arctic tundra on Svalbard-Implications for MODIS LST based permafrost monitoring, *Remote Sens. Environ.*, **115**, 908–922.
- Wilmott, C.J., D.E. Wicks. (1980). An empirical method for the spatial interpolation of monthly precipitation within California. *Physical Geography*, **1**, 59–73.
- Woo, M., & Heron, R. (1989). *Freeze-up and break-up of ice-cover on small Arctic lakes*. *Journal of Northern Lakes and Rivers*, W.C. Mackay, 56-62.
- Yuan D. (2009). *Sea Surface Temperature Measurements of the MODIS and AIRS Instruments Onboard of Aqua Satellite*. NASA Goddard Earth Sciences Data and Information Services Center. Code 610.2.

## Appendix I

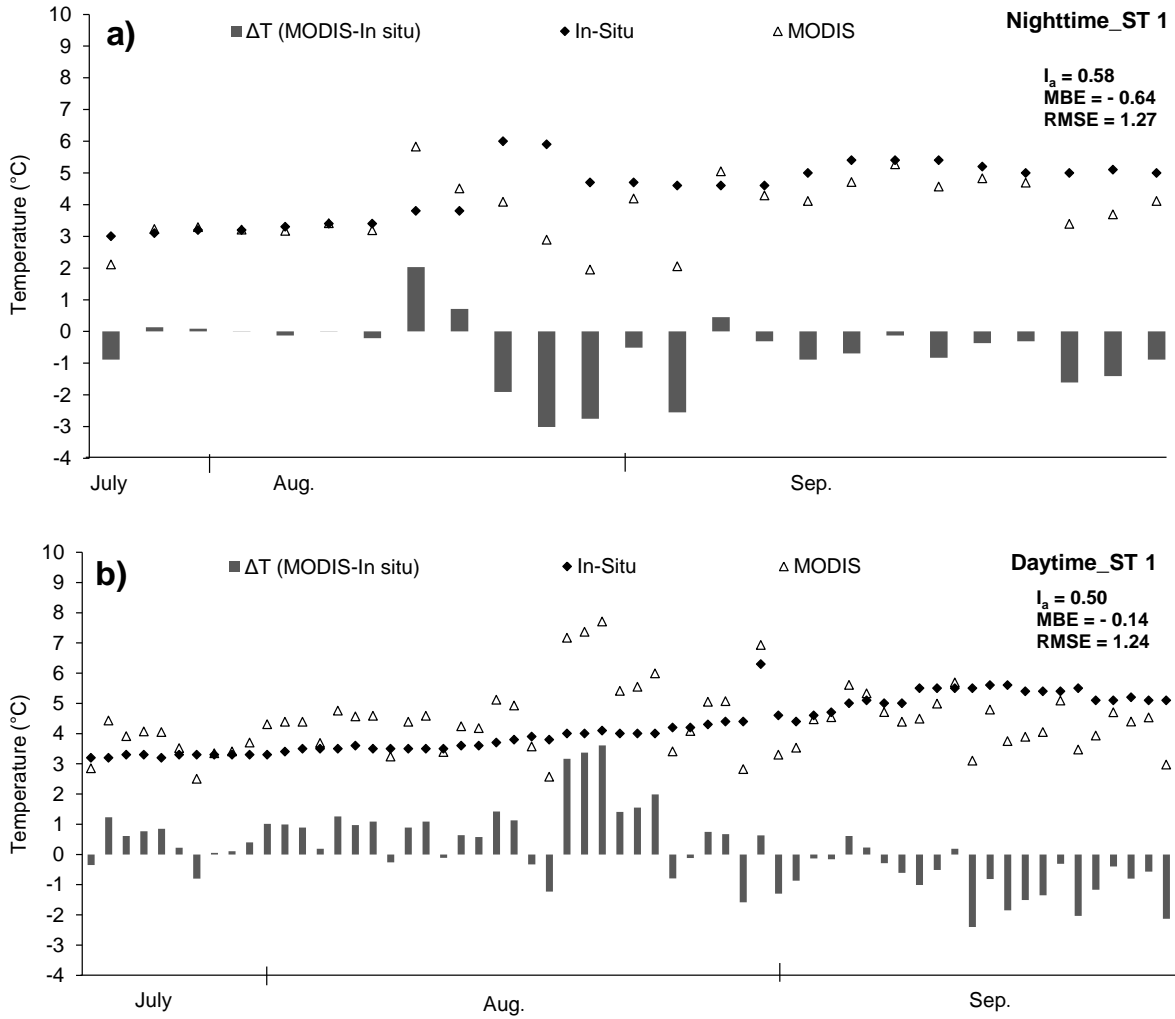


**Appendix I- 1:** MODIS-Terra visible image of GBL at clear sky condition (September 1, 2008). Red dots show location of temperature mooring stations.



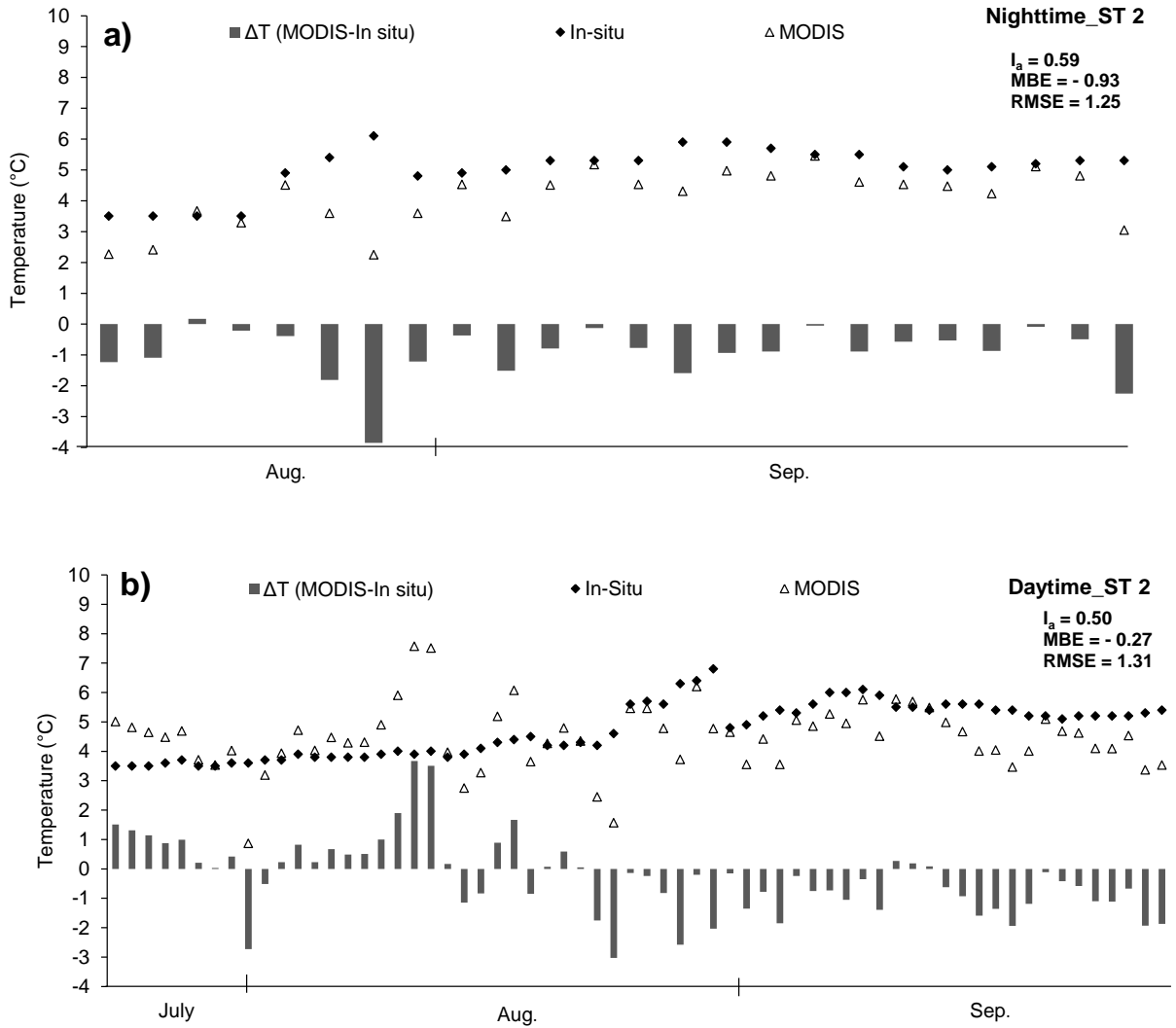
**Appendix I- 2:** MODIS visible image of GBL from both Aqua and Terra satellites in cloud cover conditions.

## Appendix II



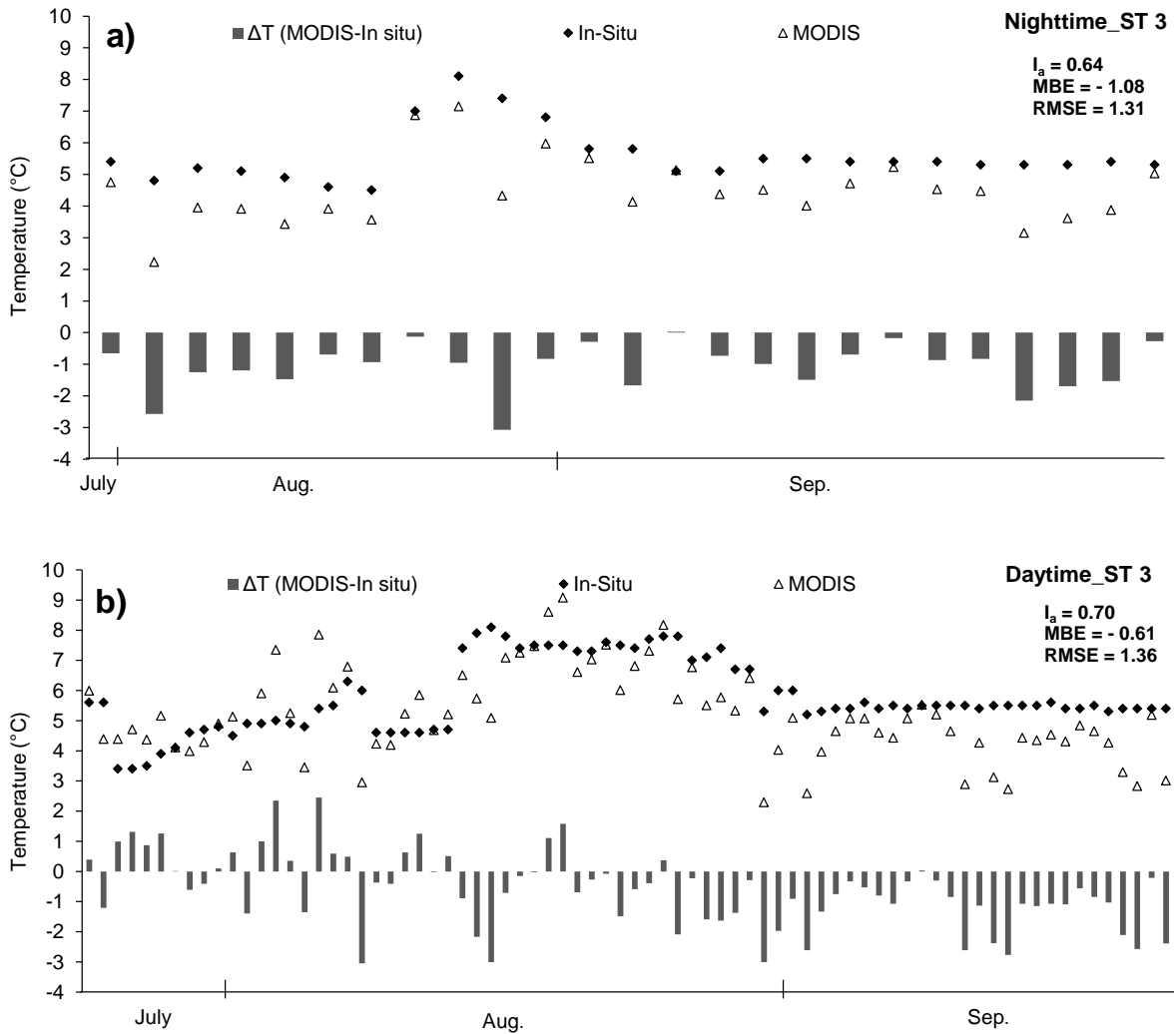
**Appendix II:** Comparison of hourly MODIS  $LST_{lake}$  with hourly temperature mooring data over GBL on a) nighttime, b) daytime on station 1 (mid-July to September 2008).

### Appendix III



**Appendix III:** Comparison of hourly MODIS  $LST_{lake}$  with hourly temperature mooring data over GBL on a) nighttime, b) daytime on station 2 (mid-July to September 2008).

## Appendix IV



**Appendix IV:** Comparison of hourly MODIS  $LST_{lake}$  with hourly temperature mooring data over GBL on a) nighttime, b) daytime on station 3 (mid-July to September 2008).